Chemical Engineering Department , Faculty of Engineering, Universitas Negeri Semarang

Jurnal Bahan Alam Terbarukan

Vegetable Oil and Essential Oil, Renewable Energy,
Bio-process and Bio-product
Thermochemical Processes for Biomass Conversion
Waste Treatment

Indexed by:
Google Scholar Crossref DOAJ DIRECTORY OF OPEN ACCESS JOURNALS GARUDA GARBA RUJUKAN DIGITAL
sinta ASEAN CITATION INDEX

Address:
Jurusan Teknik Kimia, Fakultas Teknik
Universitas Negeri Semarang
Kampus Sekaran, Gunungpati, Semarang 50229
Phone/Fax: (024) 850 8101 ext 110

Email : jurnal.bat@mail.unnes.ac.id
website : http://journal.unnes.ac.id/nju/index.php/jbat

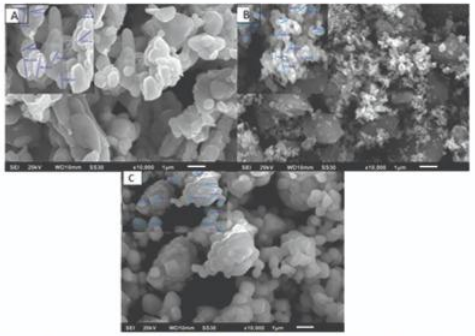

SEM Image of ZnO, WO_3 and ZnO-WO_3

Accredited SINTA 2 by Ministry of Research and Technology/National Research and Innovation Agency
SK No. 200/M/KPT/2020

JBAT	Volume11	Number 1	1 - 67	June 2022	p-ISSN 2303-0623 e-ISSN 2407-2370

Address

Jurusan Teknik Kimia, Fakultas Teknik
Universitas Negeri Semarang
Kampus Sekaran, Gunungpati, Semarang 50229
Phone/Fax: (024) 8508101 ext 114
Email: jbat@unnes.ac.id
Web Site: http://journal.unnes.ac.id/nju/index.php/jbat

INTRODUCTION

Industrial developments that continue to escalate as economic growth, causes more natural resources that are exploited continuously without considering the impact. Resources available in nature are divided into two groups, which are non-renewable and renewable natural resources. The exaggerated exploitation of non-renewable natural resources to support human life causes the depletion of such resource reserves in nature.
Therefore, renewable natural resources and processing technology turns out to be an interesting field to be analyzed and researched in order to a sustainable life.

In addition, the increase of industries causing a lot of environmental pollution either on wastewater, soil or air. Environmental pollution by industrial activities is caused by factors contained in raw materials, outdated technology, and waste treatment process. To solve the various problems are the responsibility of chemical engineers; a great challenge for us to find the latest innovations to reduce that aftermath.

This Journal presents articles on Renewable Natural Materials that include vegetable oils and essential oils, new and renewable energy, renewable products and processes, biomass, thermochemical processes for biomass conversion, waste utilization and treatment.

Hopefully this journal will be advantageous and may boost our insight into the latest innovations in technology and engineering. We realize that there are still deficiencies in the representation of this journal; therefore we are very open with suggestions and criticism. Thank you

Editor in Chief

TABLE OF CONTENT
JBAT Vol. 11 No. 1 June 2022

.....

JBAT 11(1) (2022) 1 – 7

Jurnal Bahan Alam Terbarukan

Accredited SINTA 2 by Ministry of Research and Technology/National Research and Innovation Agency
SK No. 200/M/KPT/2020
http://journal.unnes.ac.id/nju/index.php/jbat

p-ISSN 2303 0623
e-ISSN 2407 2370

Detoxification of Distillery Wastewater by AOP Fenton for the Enhancement of Biogas Production

Dhias Cahya Hakika[1,✉], Sarto[2], Aswati Mindaryani[2], Muslikhin Hidayat[2], Zahrul Mufrodi[1]

DOI: https://doi.org/10.15294/jbat.v11i1.35844

[1]Department of Chemical Engineering, Faculty of Industrial Technology, Universitas Ahmad Dahlan, Jl. Jend. Ahmad Yani Banguntapan Bantul 55191, Indonesia
[2]Department of Chemical Engineering, Faculty of Engineering, Universitas Gadjah Mada, Jl. Grafika 2 Yogyakarta 55281, Indonesia

Article Info

Article history:
Received
April 2022
Accepted
June 2022
Published
June 2022

Keywords:
biogas; COD; Distillery wastewater; Fenton reaction; Phenol; Sulfate

Abstract

Distillery wastewater from the bioethanol industry contains a high level of organic content which can be converted into biogas. However, the presence of toxic compounds in this wastewater could inhibit biogas production. Therefore, prior detoxification of distillery wastewater is required. Fenton, one of the Advanced Oxidation Process (AOP) methods, was selected due to its high performance to degrade organic pollutants, short reaction time, and the process is simple and easy. Additionally, this method can also be used as a pretreatment for biogas production. This paper aims to study the improvement of biogas production from distillery wastewater by applying AOP Fenton as a pretreatment method. The experiment consists of two stages, the first was application of AOP Fenton to the distillery wastewater in order to determine its effect on the concentration of COD and some toxic compounds such as phenol and sulfate. The second stage was biogas production through anaerobic digestion process, which was carried out under two conditions of raw materials: (i) distillery wastewater without pretreatment of AOP Fenton as a control and (ii) distillery wastewater that has been treated with AOP Fenton as pretreatment. Results show a remarkable decrease in COD concentration by 45%, phenol (63%), and sulfate (18,6%) from distillery wastewater after applying AOP Fenton. It implies that the application of AOP Fenton significantly detoxified distillery wastewater. As a biogas pretreatment, this method also increased biogas production by 33% higher, from 2.399 mL (without pretreatment) to 3.191 mL (with pretreatment). It indicates that AOP Fenton increased the biodegradability of distillery wastewater. Thus, it was easier to be converted into biogas.

INTRODUCTION

Along with the global outbreak of the coronavirus (Covid-19), there has been a significant surge in demand for alcohol in order to meet the needs of sterilization or sanitation. Alcohol or ethanol, as a raw material used in the manufacture of alcohol-based hand sanitizers, disinfectants, and antiseptics, is one of the essential compounds in handling the Covid-19 pandemic. This condition causes several ethanol industries to increase their production capacity, especially in Indonesia. Most of the bioethanol factories in Indonesia use molasses (sugarcane molasses) as raw material because the production costs are considerably low (Setyawati et al., 2015). On the other hand, the bioethanol industry from molasses produces liquid waste that can harm the environment if disposed directly into the water body. This liquid waste, also known as distillery wastewater or vinasse, has high organic matter content with the value of chemical oxygen demand (COD) concentration is more than 150,000 mg/L. It is also acidic (pH 3.5–5) with dark brown color and unpleasant odor. The volume of

✉ Corresponding author:
E-mail: dhias.hakika@che.uad.ac.id

liquid waste generated from bioethanol industry is also one of the challenging factors in processing this wastewater because the production of 1 liter of bioethanol will produce 8–15 liters of wastewater (España-Gamboa et al., 2011; Janke et al., 2015; Rodrigues Reis and Hu, 2017).

Based on its characteristics, distillery wastewater is potential to be converted into biogas through the anaerobic digestion process as it is a biodegradable waste and contains high organic compounds. However, the biodegradability index (BOD_5/COD ratio) of this wastewater is considerably low (0.2–0.4) because the COD concentration is too high. In order to be easily broken down biologically, the recommended value of biodegradability index should be more than 0.4 (Rodriguez-Couto et al., 2021). The presence of toxic compounds in distillery wastewater such as phenol and sulfate can also inhibit the anaerobic digestion process. In addition, the value of the Carbon/Nitrogen (C/N) ratio of distillery wastewater is relatively low. The ratio of C/N of organic compounds is one of the crucial parameters during anaerobic digestion process in order to maintain nutrients balance and stability (Damayanti et al., 2019; Moset et al., 2012; Syaichurrozi and Rusdi, 2020). Therefore, it is necessary to detoxify the distillery wastewater prior to being used as biogas raw material so that biogas production can be successfully carried out.

Distillery wastewater can be detoxified using physical, biological, and chemical treatment. Several options of chemical methods have been implemented to treat this wastewater, including Fenton, which is one of the advanced oxidation processes (AOP) methods. AOP Fenton is a catalytic oxidation process using a mixture of hydrogen peroxide (H_2O_2) and ferrous (Fe^{2+}) or ferric ions (Fe^{3+}) to produce hydroxyl radicals (•OH) (Neyens and Baeyens, 2003). Hydroxyl radicals are free radicals that are highly reactive and have high oxidation-reduction potential (+2.33 V), higher than ozone (+2.07 V) and H_2O_2 itself (+1.36 V) (Bacardit et al., 2007; Pilli and Tyagi, 2015). These hydroxyl radicals would attack and destroy the organic pollutants and toxic compounds in wastewater.

In this study, AOP Fenton is selected to detoxify distillery wastewater because this method has been known as an effective technology and has been proven to degrade organic pollutants in various kinds of wastewater successfully. It has the main advantage of degenerating contaminants into simpler and safer compounds such as CO_2, H_2O, and inorganic salts. Other benefits of this method are that the reaction time is short, no additional external energy is needed, and the application is simple and convenient. Despite its advantages, Fenton has some shortcomings, including the potential for sludge generated after the reaction and the narrow working pH range. Several studies have reported that Fenton reaction is working optimally under acidic conditions, specifically in the pH range of 3–5 (Amelia et al., 2021; Rossi, 2014). However, the specific range is beneficial to this study because the pH of distillery wastewater is also acidic (3–4), so there is no need to do any pH adjustment during the application of AOP Fenton treatment to this wastewater. Therefore, this method is considered suitable to be implemented as a detoxification treatment for distillery wastewater (Hakika et al., 2019).

This research aims to study the effect of AOP Fenton to detoxify distillery wastewater and investigate its result during biogas production. The experiment consisted of two stages; the first stage was the application of AOP Fenton to the distillery wastewater in order to detoxify the toxic compounds, especially sulfate and phenol. The next stage is biogas production from distillery wastewater which was conducted by comparing two conditions of distillery wastewater: (i) without AOP Fenton pretreatment and (ii) with AOP Fenton pretreatment to examine the effect of AOP Fenton as a pretreatment method on the biogas production.

MATERIALS AND METHODS

Materials

Distillery wastewater as raw material was obtained from one of the bioethanol industries in Yogyakarta with characteristics as shown in Table 1.

Table 1. Characteristics of distillery wastewater.

No	Parameter	Value
1	COD (mg/L)	150,840
2	BOD_5 (mg/L)	31,250
3	pH	3.80
4	Sulfate (mg/L)	3.27
5	Phenol (mg/L)	4.65

The inoculum was taken directly from an active biogas reactor treating cow dung in Boyong Village, Pakem, Sleman Yogyakarta. The characteristics of the inoculum are shown in Table 2.

Table 2. Characteristics of inoculum.

No	Parameter	Value
1	Total solid (TS) (mg/L)	75,665
2	Volatile solid (VS) (mg/L)	56,000
3	pH	6.90

The chemicals used as reagents in this study were Hydrogen peroxide (H_2O_2) 30%wt (PT Peroksida Indonesia Pratama), $Fe(NO_3)_3.9H_2O$ 98% (Sigma Aldrich), Sodium hydroxide (NaOH) flake 97% (Sigma Aldrich), and aquadest.

Methods

AOP Fenton

The first stage of the experiment was run in batch operation. One liter of distillery wastewater was poured into the reactor followed by 3.62 grams of $Fe(NO_3)_3.9H_2O$. The solution was mixed until the iron salt dissolved. H_2O_2 with a ratio of COD:H_2O_2=0.5 (g/g) was added afterward. Fenton reaction was carried out for 60 minutes with constant stirring (200 rpm). After 60 minutes, the pH of the solution was increased to 7 using NaOH to stop the reaction.

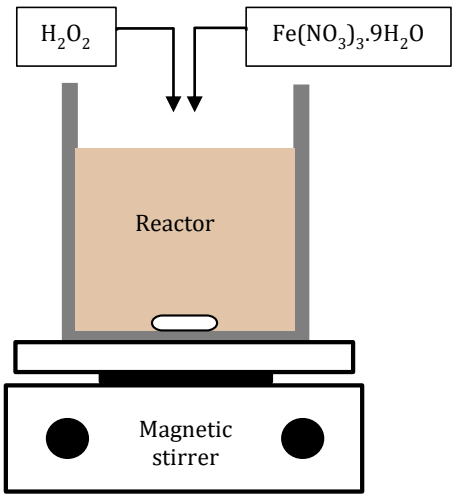

Figure 1. Experimental setup of detoxification of distillery wastewater by AOP Fenton.

Biogas Production

The experiment in the second stage was carried out using two (2) batch digesters. The first digester was filled with substrate from distillery wastewater without AOP Fenton as a control, and the second digester was filled with substrate from distillery wastewater with AOP Fenton. Distillery wastewater as a substrate was mixed with inoculum with a ratio of substrate:inoculum (RSI) 2:1. The pH of the mixture was then adjusted to neutral conditions (pH 7) using NaOH. Anaerobic digestion was carried out at room temperature for approximately 32 days (until biogas production stopped).

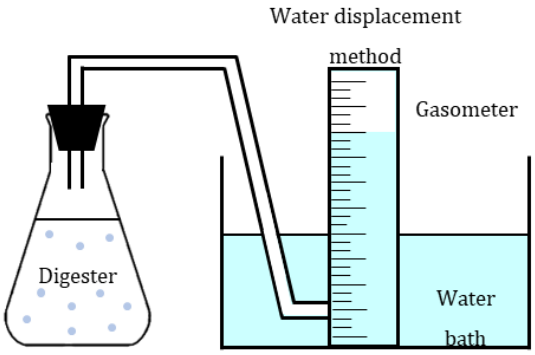

Figure 2. Experimental setup of biogas production from distillery wastewater.

Data Analysis

The sampling point of AOP Fenton (first stage) was taken at the beginning (t=0) and the end of the reaction (t=60 minutes). The samples were collected and several parameters were measured: pH, the concentration of COD, sulfate, phenol, Total Carbon, and Total Nitrogen. In the second stage, biogas volume was measured every two (2) days using water displacement method.

RESULTS AND DISCUSSION

Detoxification of Distillery Wastewater Using AOP Fenton Method

In this study, the COD parameter was chosen to represent the concentration of organic matter in distillery wastewater. The concentration of phenol and sulfate compounds in distillery wastewater before and after AOP Fenton treatment was also measured.

Figure 3 shows that AOP Fenton was able to detoxify distillery wastewater from bioethanol industry. This is indicated by the decrease in COD

concentration by as much as 45% and the reduced concentration of toxic compounds, in this case are

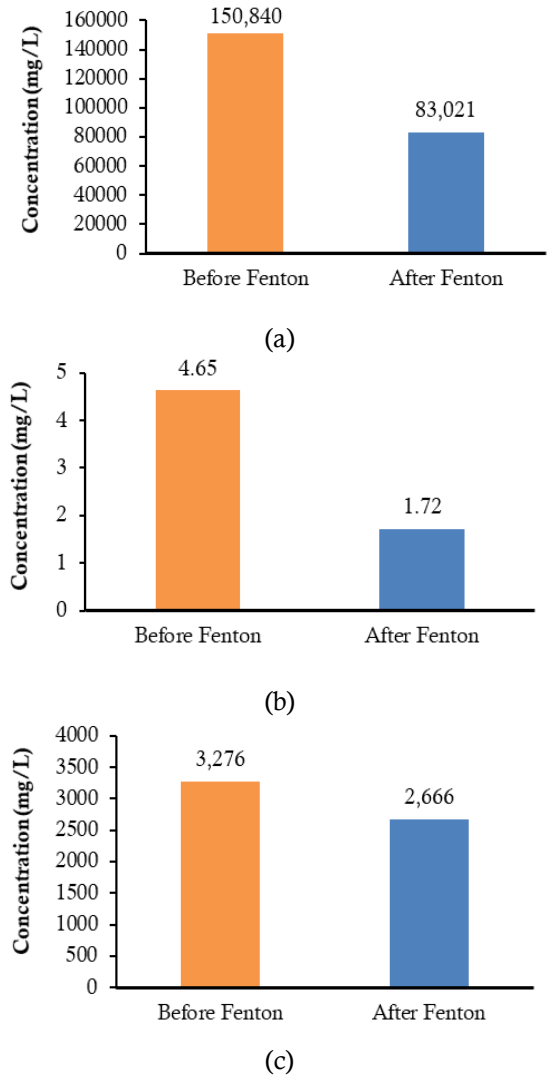

Figure 3. The concentration of: (a) COD, (b) phenol, and (c) sulfate in distillery wastewater before and after AOP Fenton.

wastewater after AOP Fenton was applied. During the Fenton reaction, equations (1) and (2) occur as follows:

$$Fe^{3+} + H_2O_2 \rightarrow Fe^{2+} + HO_2\bullet + H^+ \quad (1)$$

$$Fe^{2+} + H_2O_2 \rightarrow Fe^{3+} + \bullet OH + OH^- \quad (2)$$

Equation (1) occur first followed by Equation (2) to produce hydroxyl radical (•OH) quickly. At the beginning of the reaction, the presence of Fe^{3+} and Fe^{2+} ions in the solution will immediately decompose H_2O_2 into •OH. Subsequently, •OH reacts with organic compounds in solution and degrades these compounds. The decrease in COD, phenol, and sulfate concentration phenol (63%) and sulfate (18.6%) in distillery

of distillery wastewater in this study occurred as a result of further oxidation process of hydroxyl radicals that attack these organic materials and toxic compounds, so that they are broken down into simpler compounds (Chen et al., 2020; Pérez et al., 2002).

In addition, the effect of AOP Fenton treatment on the value of C/N ratio of distillery wastewater was also observed. The C/N ratio of distillery wastewater before and after AOP Fenton treatment can be seen in Figure 4.

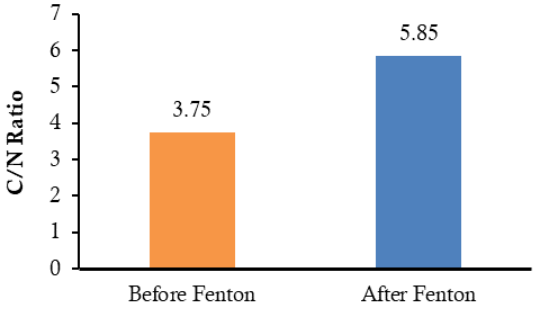

Figure 4. C/N ratio of distillery wastewater before and after AOP Fenton.

The ratio of C/N of distillery wastewater increased by 56% (from 3.75 to 5.85) after being treated by AOP. The C/N ratio indicates the ratio of carbon and nitrogen content in substrate as an important source of nutrients required by microorganisms during anaerobic digestion process. Carbon is the primary energy source for microbial activities, while nitrogen is needed by microbes for the growth and development of cell structures. If carbon and nitrogen content in the substrate is low, the process of anaerobic digestion will run slowly (Khanal et al., 2019). Therefore, the value of the C/N ratio in distillery wastewater is essential and has to be considered because the distillery wastewater will be used as a biogas substrate after being treated by AOP Fenton.

Biogas Production from Distillery Wastewater

After being treated by AOP Fenton, distillery wastewater proceeded to the next stage, which was biogas production through anaerobic digestion. To compare the effect of AOP Fenton treatment on biogas production, the anaerobic digestion process from distillery wastewater as a raw material was carried out under two conditions: (i) distillery wastewater without AOP Fenton (as a

control), and (ii) distillery wastewater which has been pretreated using AOP Fenton. The volume of daily and cumulative biogas production from these two conditions were observed for 32 days (until there was no gas production) as shown in Figure 5.

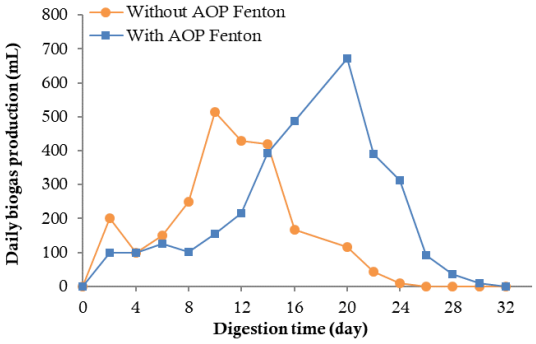

(a)

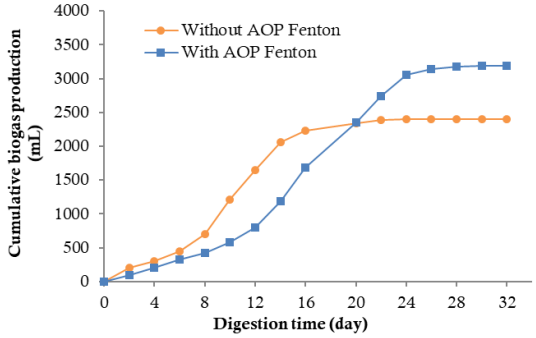

(b)

Figure 5. Profile of: (a) daily volume and (b) cumulative volume biogas production from distillery wastewater.

Experiment results showed that digester with distillery wastewater which has been treated using AOP Fenton generated 3,191 mL of biogas. This result is 33% higher than biogas production from distillery wastewater without AOP Fenton treatment which only produced 2,399 mL of biogas. This low gas production was due to the concentration of organic matter (represented by COD) in distillery wastewater without AOP Fenton treatment was too high and causing the digester overload. Thus, the process of anaerobic digestion was hindered and could not occur in optimal conditions (Hallaji et al., 2018; Widyastuti et al., 2021). On the other hand, digester with substrate from distillery wastewater which has been pretreated using AOP Fenton yielded more biogas. Higher biogas production from this substrate indicated that detoxification method using AOP Fenton increased the biodegradability of distillery wastewater. As a result, the distillery wastewater became easier to be biologically degraded through anaerobic digestion process. This led to better conditions for anaerobic digestion so that more substrate could be converted into biogas than the one without AOP Fenton treatment.

Based on the value of the C/N ratio obtained from this study, distillery wastewater that has been pretreated with AOP Fenton has a higher C/N ratio than distillery wastewater without pretreatment. The C/N ratio is one of the critical parameters that can determine the amount of biogas produced. In general, increasing the C/N ratio until its optimum condition during anaerobic digestion positively affects the volume of biogas. According to Cerón (2019), a high C/N ratio can encourage an increase in microbial activity during the anaerobic digestion process, thereby the volume of biogas produced also increases.

Results achieved in this study are in agreement with previous findings from Nagarajan & Ranade (2020) which applied physical treatment by hydrodynamic cavitation to detoxify distillery wastewater before being utilized into biogas. Hydrodynamic cavitation pretreatment helped in breaking down the recalcitrant compounds from distillery wastewater such as phenol and melanoidins. This pretreatment led to more digestible COD and enhanced higher biomethane yield (10 – 22%) from the treated wastewater. Other than physical treatment, biological treatment also provided successful method to detoxify distillery wastewater by using white rot fungi (*Trametes versicolor*) to eliminate the phenolic compounds and melanoidins (España-Gamboa et al., 2017). It mentioned that the removal of phenols presents on distillery wastewater resulted higher biogas flow (from 1,102 mL to 2,370 mL) and methane content (from 65% to 74%) in the biogas.

CONCLUSION

AOP Fenton successfully detoxified distillery wastewater. The COD concentration of distillery wastewater after AOP Fenton treatment was reduced by 45%. The concentrations of other toxic compounds that can inhibit biogas production through anaerobic digestion, which are phenol and sulfate, were also reduced by 63% and 18.6%, respectively. The ratio of C/N in distillery wastewater also increased from 3.75 to 5.85. The application of AOP Fenton as a pretreatment method for biogas production from distillery wastewater enhanced biogas production by increasing 33% biogas produced from 2,399 mL

(without AOP Fenton) to 3,191 mL (with AOP Fenton). It indicates that AOP Fenton degraded organic matter in distillery wastewater into more easily biodegradable compounds.

REFERENCES

Amelia, S., Muflikhah, R.S., Ustinah. 2021. Role of The Concentration of Fe/C Catalysts on Heterogeneous Fenton Degradation Remazol Yellow FG. IOP Conference Series: Materials Science and Engineering 1053: 012054.

Bacardit, J., Stötzner, J., Chamarro, E., Esplugas, S. 2007. Effect of Salinity on the Photo-Fenton Process. Industrial & Engineering Chemistry Research. 46: 7615–7619.

Cerón, A., Cáceres, K.T., Rincón, A., Cajigas, A. 2019. Influence of pH and the C/N ratio on the biogas production of wastewater. Revista Facultad de Ingeniería Universidad de Antioquia. 92.

Chen, Y.J., Fan, T.Y., Wang, L.P., Cheng, T.W., Chen, S.S., Yuan, M.H., Cheng, S. 2020. Application of fenton method for the removal of organic matter in sewage sludge at room temperature. Sustainability. 12: 1–10.

Damayanti, S.I., Astiti, D.F., Purnomo, C.W., Sarto, S., Budhijanto, W. 2019. Inoculum Selection and Micro-Aeration for Biogas Production in Two-Stage Anaerobic Digestion of Palm Oil Mill Effluent (POME). Jurnal Bahan Alam Terbarukan 8: 14–21.

España-Gamboa, E., Mijangos-Cortes, J., Barahona-Perez, L., Dominguez-Maldonado, J., Hernández-Zarate, G., Alzate-Gaviria, L. 2011. Vinasses: Characterization and treatments. Waste Management and Research. 29: 1235–1250.

España-Gamboa, E., Vicent, T., Font, X., Dominguez-Maldonado, J., Canto-Canché, B., Alzate-Gaviria, L. 2017. Pretreatment of vinasse from the sugar refinery industry under non-sterile conditions by Trametes versicolor in a fluidized bed bioreactor and its effect when coupled to an UASB reactor. Journal of Biological Engineering. 11: 1–11.

Hakika, D.C., Sarto, S., Mindaryani, A., Hidayat, M. 2019. Decreasing COD in sugarcane vinasse using the fenton reaction: The effect of processing parameters. Catalysts 9: 12.

Hallaji, S.M., Torabian, A., Aminzadeh, B., Zahedi, S., Eshtiaghi, N. 2018. Improvement of anaerobic digestion of sewage mixed sludge using free nitrous acid and Fenton pre-treatment. Biotechnology for Biofuels. 11: 1–12.

Janke, L., Leite, A., Nikolausz, M., Schmidt, T., Liebetrau, J., Nelles, M., Stinner, W. 2015. Biogas Production from Sugarcane Waste: Assessment on Kinetic Challenges for Process Designing. International journal of molecular sciences. 16: 20685–20703.

Khanal, S.K., Nindhia, T.G.T., Nitayavardhana, S. 2019. Biogas from Wastes: Processes and Applications, in: Taherzadeh, M.J., Bolton, K., Wong, J., Pandey, A. (Eds.), Sustainable Resource Recovery and Zero Waste Approaches. Elsevier. pp. 165–174.

Moset, V., Cambra-Lopez, M., Moller, H.B. 2012. The inhibiting effect of sulfate on thermophilic anaerobic digestion of cattle and pig waste slurry. Transactions of the ASABE. 55: 2309–2317.

Nagarajan, S., Ranade, V.V. 2020. Pre-treatment of distillery spent wash (vinasse) with vortex based cavitation and its influence on biogas generation. Bioresource Technology Reports. 11: 100480.

Neyens, E., Baeyens, J., 2003. A review of classic Fenton's peroxidation as an advanced oxidation technique. Journal of Hazardous Materials B98, 33–50.

Pérez, M., Torrades, F., Garcıa-Hortal, J.A., Domènech, X., Peral, J. 2002. Removal of organic contaminants in paper pulp treatment effluents under Fenton and photo-Fenton conditions. Applied Catalysis B: Environmental. 36: 63–74.

Pilli, S., Tyagi, S.Y.R.D. 2015. Overview of Fenton pre-treatment of sludge aiming to enhance anaerobic digestion. Reviews in Environmental Science and Biotechnology. 14: 453–472.

Rodrigues Reis, C.E., Hu, B. 2017. Vinasse from Sugarcane Ethanol Production: Better Treatment or Better Utilization?. Frontiers in Energy Research. 5: 1–7.

Rodriguez-Couto, S., Shah, M.P., Biswas, J.K. 2021. Development in Wastewater Treatment Research and Processes: Removal of Emerging Contaminants from Wastewater through Bio-nanotechnology. Elsevier Science.

Rossi, A.F. 2014. Fenton's Process Applied to Wastewater Treatment: Heterogeneous and Homogeneous Catalytic Operation Modes. University of Coimbra.

Setyawati, I., Ambarsari, L., Nur'aeni, S., Suryani, S., Puspita, P.J., Kurniatin, P.A., Nurcholis, W. 2015. Bioethanol Production by Using Detoxified Sugarcane Bagasse Hydrolysate and Adapted Culture of Candida tropicalis. Current Biochemistry. 2(1): 1-12.

Syaichurrozi, I., Rusdi, R. 2020. Development of Simple Kinetic Model on Biogas Production from Co-Digestion of Vinasse Waste and Tofu Residue at Variation of C/N Ratio. World Chemical Engineering Journal. 4(1): 18–28.

Widyastuti, N., Hidayat, M., Purnomo, C.W., 2021. Enhanced Biogas Production from Sugarcane Vinasse using Electro-Fenton as Pre-treatment Method. IOP Conference Series: Earth and Environmental Science. 830.

JBAT 11(1) (2022) 8 – 16

Jurnal Bahan Alam Terbarukan

Accredited SINTA 2 by Ministry of Research and Technology/National Research and Innovation Agency
SK No. 200/M/KPT/2020
http://journal.unnes.ac.id/nju/index.php/jbat

p-ISSN 2303 0623
e-ISSN 2407 2370

Optimization of Drying Process for Production Red Ginger Granulated Palm Sugar Using Response Surface Methodology

Prima Astuti Handayani ✉, Idama Kusuma Dewi, Ady Prasetyo

DOI: https://doi.org/10.15294/jbat.v11i1.36124

Chemical Engineering Department, Faculty of Engineering, Semarang State University (UNNES), Indonesia

Article Info

Article history:
Received
April 2022
Accepted
May 2022
Published
June 2022

Keywords:
Granulated Palm Sugar;
Red Ginger;
Water Content;
Optimum;
Response Surface Methodology

Abstract

Palm sugar is used as a natural sweetener that is added to food and beverages. The nutritional content in palm sugar can be enriched with the addition of antioxidants derived from red ginger (Zingiber *officinale var. rubrum).* The antioxidant activity of red ginger is 75.61% higher than that of emprit ginger and elephant ginger. The problem that arises during the production process of granulated palm sugar is the drying process that has not considered chemical characteristics, especially water content. The requirement for water content of palm sugar according to SNI 01-3743-1995 is a maximum of 3%. Moisture content is the main parameter that determines the quality of granulated palm sugar to long shelf life. Water content can affect other chemical characteristics such as sucrose, reducing sugar, ash content, calories, protein, fat, and carbohydrates. This optimization is using RSM (Response Surface Methodology) CCD model (Central Composite Design) on Software Statistica 10 with 20 treatments. The independent variables used were time (4-6 hours), material weight (100-300) grams, and material size (10-26 mesh). Data processing with Statistica 10 software resulted in the optimum water content condition of 2.9019%, with the drying process conditions covering 6.68 hours, material weight 368.18 grams, and material size 31.45 mesh. Validation was carried out to test the accuracy of the optimization results from Statistica 10 Software. The validation of the moisture content results obtained a value of 2.9016%, with an error percentage of 0.0003%. The chemical characteristic test was applied to the granulated palm sugar as a result of optimization so that the value of sucrose (96.5967%) was obtained, reducing sugar (6.0434%), ash content (1.8660%), calories (379.93%), protein (2,4268%), fat (0.3972%), and carbohydrates (91,5379%).

INTRODUCTION

Granulated palm sugar is one of the natural sweeteners that is rich in benefits and is consumed by the community as a food or drink sweetener (Pratama, et al., 2020). Granulated palm sugar has a lower glycemic index value than cane sugar, which is 35% (Wilberta et al., 2021). In addition, granulated palm sugar also contains several compounds useful for the body, such as calories, carbohydrates, fat, protein, and calcium (Fatriani et al., 2019). The content of beneficial compounds in granulated palm sugar can be enriched by adding antioxidants obtained from spices, one of which is red ginger (Zingiber officinale var. rubrum) (Wulandari et al., 2021). Red ginger can increase the body's response to fighting viruses. Including the chikungunya virus, pharyngitis, and COVID-19 (Assegaf et al., 2020; Kaushik et al., 2020; Sinamo & Hutabarat, 2021).

Granulated palm sugar has a shelf life of 1 year, longer than jaggery sugar, lasting for two weeks. The shelf life of granulated palm sugar is influenced by the water content (Ritonga et al., 2020). The drying process is an essential part of the production of granulated palm sugar to obtain a minimum water content. Optimum drying operating conditions will produce granulated palm

✉ Corresponding author:
E-mail: prima@mail.unnes.ac.id

sugar with minimum moisture content (Meldayanoor et al., 2019).

In general, the conventional drying process of granulated palm sugar still use the sunlight. The disadvantages of this drying method are the poor physical quality of sugar and high water content (Muhandri et al., 2020). These weaknesses can be overcome by determining the optimum operating conditions of the granulated palm sugar drying process. Parameters that are considered to produce granulated palm sugar water content according to SNI 01-3743-1995 standards are drying time, material weight, and material size using the Response Surface Methodology (RSM) method. So that, it fulfill the water content standard according to SNI 01-3743-1995, which is a maximum of 3 %. The purpose of this study was to determine the effect of optimum drying operating conditions on granulated palm sugar.

MATERIALS AND METHODS

Materials

The materials used in this study were palm sugar obtained from the Palm Sugar Production Center Limbangan and red ginger obtained from the Karang Ayu Market, Semarang. Materials used for analysis include 30% HCl (Merck), 45% NaOH (Merck), 30% NaOH (Merck), Luff's reagent, aquades, 20% KI (Merck), Na-thio 0.1 N, H_2SO_4 26 ,5%(Merck), starch indicator, arsenomolybdate reagent, concentrated H_2SO_4(Merck), 2% boric acid, 0.01 N HCl (Merck), 30% HCl (Merck).

The tools used in this study were oven, thermometer, analytical scale, wooden stirrer, frying pan, stove, coconut shell, sieve, baking sheet, grater, measuring cup, filter cloth, mesh sieve, brush, and spoon. The tools used for analysis include vochdoos, 100 mL Erlenmeyer, 100 mL volumetric flask spectrophotometer (UV Vis Shimadzu), test tube, water bath, furnace (Thermolyne 1000), and a cup.

Methods

This research was conducted in several stages, namely the production of red ginger granulated palm sugar, optimization with RSM (Response Surface Methodology) using Statistica 10 software, and testing the chemical characteristics of red ginger granulated palm sugar.

Red Ginger Granulated Palm Sugar Production

The red ginger that was cleaned is grated using a grater to extract the juice. Red ginger juice is separated from starch deposits through a filtering process. The red ginger juice is then cooked until it boils. The boiling red ginger juice is added with palm sugar that has been cut into pieces. Cooking is done until the sugar crystallizes. The granulated palm sugar that has been formed is sieved using a sieve to obtain granulated palm sugar based on material size. The palm sugar that passed the filter then dried using an oven to fullfil water content standard set by SNI, a maximum of 3%.

Optimization With RSM (Response Surface Methodology)

Optimization with RSM is based on research that has been done by (Mariana 2017). The RSM method is used to obtain data based on time, material weight, and material size so the water content of granulated palm sugar samples fulfill the SNI standards is a maximum of 3% (SNI, 1995).). The experimental design was carried out using the Central Composite Design (CCD) with 20 trials using the Statistica 10 software.

Moisture Test

The water content during drying of granulated palm sugar is calculated based on the following gravimetric equation (Normilawati et al., 2019).

$$\%\text{moisture level} = \frac{(W1 + W) - W2}{W} \text{x } 100\% \qquad (1)$$

Where, W is the weight of granulated palm sugar sample before drying (grams), W1 is the weight of vochdoos after drying (grams) and W2 is the weight of vochdoos + granulated palm sugar sample after drying (grams).

Sucrose Test

50 ml of the sample filtrate was put into an Erlenmeyer added with 25 ml of distilled water and 10 ml of 30% HCl. Heat the solution on a water bath at 200℃. The solution is neutralized with 45% NaOH then diluted to a specific volume so that the solution contains 15-60 mg of reducing sugar. A total of 25 ml of the solution was taken and put into an Erlenmeyer, then added 25 ml of Luff Schoorl's solution. The solution in the Erlenmeyer was

cooled rapidly, and 15 ml of 20% KI was added, then carefully added 25 ml of 26.5% H2SO4 solution. The iodine is titrated with a 0.1 N Na-thiosulfate solution using 2-3 ml starch indicator. Calculation of sucrose level using the Eq. (2)

$$\text{Sucrose level} = (\text{Reducing sugar content after inversion} - \text{Reducing sugar content after inversion}) \times 0.95 \quad (2)$$

Reducing Sugar Test

Testing for reducing sugar was carried out using the Nelson Somogyi method (Haryanti, 2020). A total of 1 ml of a solution containing 0.02-0.08 mg/mL of glucose solution and 1 ml of Nelson's reagent was put into a test tube. Heated in a water bath for 20 minutes and then cooled. The solution that has been cooled is added with 1 mL of Arsenomolybdate reagent, then shaken until the Cu2O precipitate dissolves. After the precipitate dissolves, add 7 mL of distilled water, then shake until homogeneous. Optical Density (OD) was read by spectrophotometry at 540 nm wavelength.

Ash Level Test

Testing the ash content is carried out at temperatures above 450 ℃ (Yenrina et al., 2015). 3 - 5 grams of the sample is placed on a cup and put into an ashing furnace. The heating temperature is carried out in the first stages of 400 ℃ then the second stage is heated to 550 ℃. The sample which has become ash is cooled in a desiccator. Ash content is calculated based on the Eq. (3).

$$\text{Ash level} = \frac{\text{C} - \text{A}}{\text{B} - \text{A}} \text{x } 100\% \quad (3)$$

Where, A is the weight of empty cup, B is the weight of cup + sample and C is the weight of cup + sample (after ashing)

Calorie Value Test

The caloric value is calculated using the bomb calorimeter test (Sogandi, 2019). Calculation of heat of combustion based on the Eq. (4).

$$\Delta U_T = \frac{C\Delta T - \Delta U_1 - \Delta U_2}{m} \quad (4)$$

Where, ΔU_T is heat of combustion of the sample (cal/g) and C is heat capacity of the calorimeter (cal/°C).

Protein Level Test

Protein level test using Kjeldahl method to determine protein levels (Siska & Apri, 2021). 0.4 grams of granulated palm sugar sample was put into a 100 ml Kjeldahl flask, added 25 ml of concentrated H_2SO_4, and heated for 2 hours. Then cooled and diluted with a 100 ml volumetric flask to the limit. 5 mL of the solution was put into a distillation and added 5 mL of 30% NaOH with a few drops of phenolphthalein indicator and distilled for 10 minutes. 10 ml of the distillation solution was added with 10 ml of 2% boric acid and then titrated with 0.01N HCl solution. The protein content is calculated based on the Eq. (5)

$$\text{Protein level} = \frac{(V_1 - V_2) \times N \times 0{,}014 \times fk \times 100}{\text{w}} \quad (5)$$

Where V_1 and V_2 are the volume of HCl used for titration of sample and blank solutions, W is the sample weight, N is the normality of HCl and fk is the conversion factor.

Fat Level Test

1-2 grams of sample is weighed and put into a beaker glass. 30 ml of 25% HCl and 20 ml of water were put into a beaker glass, and then some boiling stones were added. The beaker glass was covered with a watch glass and boiled for 15 minutes. After that, the liquid is filtered in hot conditions by washing using hot water to prevent the acid reaction from occurring again. The filter paper and its contents were dried in an oven at 100-105 degrees.

The dried samples were extracted with hexane solvent for 5-6 hours at 80℃. The extracted solution was then distilled to separate the fat extract from the hexane solvent. The fat extract was dried in an oven at 100-105, then cooled and weighed. Calculation of fat content based on the Eq. (6).

$$\%\text{fat} = \frac{\text{mass of extract}}{\text{mass of sample}} \text{x } 100\% \quad (6)$$

Carbohydrate Test

1 mL of the sample filtrate was added with 25 mL of distilled water. The filtrate and distilled water mixture were heated with a water bath for 1 hour. After that, the sample was dripped with three drops of PP and NaOH with 50% to neutral pH concentration. The neutral solution was diluted into

a 100 mL volumetric flask, shaken, and filtered to obtain the filtrate. The filtrate formed was taken 0.05 mL with a pipette and then added 0.45 mL of distilled water and 0.5 mL of Nelson's reagent. The solution was then heated for 10 minutes and cooled. The cooled solution was added with 4 mL of arsenomolybdate reagent, then vortexed and incubated for 30 minutes to read the absorbance. The absorbance value will be used to calculate the carbohydrate content. Calculation of carbohydrate content with Eq. (7)

$$\%\text{Carbohydrate} = \frac{X\left(\frac{\text{mg}}{\text{L}}\right) \times \text{fp} \times \text{Total Volume (L)}}{w \times 100} \times 100\% \quad (7)$$

Where, X is the concentration (mg/L), fp is the dilution factor and w is the initial sample weight (kg).

RESULTS AND DISCUSSION

The influence between variables consisting of time, material weight, and material size was used to determine the optimum moisture content of the red ginger granulated palm sugar drying process. The data processing results with statistical software 10 to obtain a relationship between the observed value and predicted value.

The results of the percentage error that obtained were analyzed by MAPE (Mean Absolute Percentage Error). So that a value of 2.58% was obtained. This value indicates that the experiments carried out are very accurate. The value of the data accuracy category on MAPE is as follows:

< 10% = very accurate
10-20% = good
20-50% = reasonable
>50% = inaccurate
(Maricar, 2019)

Based on Table 1. the values have shown the accuracy between the predicted and observed so it can be analyzed to know equations of the mathematical model. The data that were obtained as shown in Table 2.

Based on Table 2, the R^2 value is 0.956. It shows that the model used is accurate because it is close to 1. Adjust R^2 of 0.917 indicates that the relationship between the independent and response variables is getting stronger. The p-value for the time factor (X_1) is 0.8892, and the weight of the material (X_2) is 0.4193, which shows no significant effect on the water content response because the p-value is > 0.05. Based on the interaction effect and significance, the response equation is shown in Eq. (8).

$$\begin{aligned} Y = {} & 2.02379 + 0.00629X_1 + 0.03774X_2 \\ & -0.136877X_3 - 0.18784{X_1}^2 + 0.31622{X_2}^2 \\ & + 0.13226{X_3}^2 + 0.46205X_1X_2 \\ & +0.48250X_1X_3 + 0.30515X_2X_3 \end{aligned} \quad (8)$$

Equation 8 is mathematical modeling in a polynomial equation of order 2 with significant coefficients on the model as in Table 2. The above equation is not the final equation because there are still insignificant effects. The linear factors of time (X_1) and weight of the material (X_2) must be neglected so that Eq. (8) is simplified to Eq. (9)

$$\begin{aligned} Y = {} & 2.02379 - 0.136877X_3 - 0.18784{X_1}^2 \\ & +0.31622{X_2}^2 + 0.13226{X_3}^2 + 0.46205X_1X_2 \\ & +0.48250X_1X_3 + 0.30515X_2X_3 \end{aligned} \quad (8)$$

The interaction effect between the variables obtained was validated using ANOVA, as shown in Table 3.

ANOVA determines the significance value of the independent variables that affect the dependent variable. The error tolerance limit (α) used is 5% or 0.05 so that the confidence level (1-0.05) = 0.95 or 95%. Based on Table 3, the time factor (X_1) and material weight (X_2) have a significance value of 0.88917 and 0.41932. So, these two factors do not affect the value of the optimum water level. However, the quadratic factor of time (X_1^2) and weight of material (X_2^2) had a significant effect on the optimum moisture content because it had a p-value of <0.05, namely 0.00642 and 0.00064. The interaction factor between time variables on the weight of material (X_1X_2), time on the size of the material (X_1X_3), and weight of the material on the size of the material (X_2X_3) has a significant effect on the optimum water level because it has a p-value <0.05, which is 0.00043; 0.00035; and 0.00284.

In addition to the significance test, it is necessary to do a model fit test (Lack of Fit). Lack of fit means a discrepancy so that if H_0 is accepted, then there is no discrepancy in the model, so it means that the model is appropriate (Pertiwi, 2018)

The hypothesis used in this test is as follows:

H_0= There is no lack of fit in the model
H_1 = There is a lack of fit in the model

Table 1. Value of Observed and Predicted Moisture Content

Run	Value			*Response Observed*	*Response Predicted*	*% Error*
	X_1(hour)	X_2(grams)	X_3(mesh)			
1	4	100	10	2.90	2.83	2.56
2	4	100	26	1.91	1.90	0.33
3	4	300	10	2.05	2.10	2.13
4	4	300	26	1.83	1.78	2.62
5	6	100	10	1.81	1.89	4.13
6	6	100	26	1.94	1.93	0.86
7	6	300	10	2.05	2.08	1.62
8	6	300	26	2.63	2.73	3.85
9	3.32	200	18	1.69	1.75	3.75
10	6.68	200	18	1.87	1.76	5.45
11	5	31.82	18	2.41	2.44	1.09
12	5	368.18	18	2.57	2.50	2.51
13	5	200	4.55	2.36	2.33	1.41
14	5	200	31.45	2.10	2.10	0.24
15	5	200	18	2.10	2.02	3.72
16	5	200	18	2.02	2.02	0.34
17	5	200	18	2.14	2.02	5.26
18	5	200	18	1.96	2.02	3.30
19	5	200	18	1.94	2.02	4.14
20	5	200	18	1.98	2.02	2.28

Table 2. Effect Estimation for Polynomial Equations of Order 2

Factor	*Effect*	*Std.Err.*	t	p
Mean/Interc.	2.0238	0.0323	62.5862	0.00000
X_1	0.0063	0.0429	0.1466	0.8892 (p>0.05)
X_1^2	-0.1878	0.0418	-4.4971	0.0064
X_2	0.0377	0.0429	0.8796	0.4193 (p>0.05)
X_2^2	0.3162	0.0418	7.5704	0.0006
X_3	-0.1369	0.0429	-3.1898	0.0243
X_3^2	0.1323	0.0418	3.1665	0.0249
X_1X_2	0.4621	0.0561	8.2417	0.0004
X_1X_3	0.4825	0.0561	8.6064	0.0003
X_2X_3	0.3052	0.0561	5.443	0.0028
R^2	0.95662	Adjust R^2	0.91758	

For the model to fit, it is necessary to reject H_1 so that H_0 is accepted. In Table 3, the F table value is 1.50524 < F count is 4.77247, and the p table value is 0.33228, which is greater than 0.05, so the conditions for H_0 are accepted. It means that the model is appropriate and there is no model discrepancy so that the second-order polynomial equation model can be accepted.

Determination of Optimum Conditions

The profile and desirability determine the optimum conditions for the drying process. We used it to predict the optimum condition of the process to obtain valuable data for the validation process. The interaction of the three variables is known for its optimum condition by drawing a straight line vertically. The optimum conditions for

Table 3. Results of ANOVA Analysis with Statistica 10 Software

Factor	SS	df	MS	F	p
X_1	0.00014	1	0.00014	0.02149	0.88917 (p>0.05)
X_1^2	0.12713	1	0.12713	20.22358	0.00642
X_2	0.00486	1	0.00486	0.77377	0.41932 (p>0.05)
X_2^2	0.36026	1	0.36026	57.31085	0.00064
X_3	0.06396	1	0.06396	10.17489	0.02427
X_3^2	0.06303	1	0.06303	10.02642	0.02491
X_1X_2	0.42698	1	0.42698	67.92509	0.00043
X_1X_3	0.46561	1	0.46561	74.07078	0.00035
X_2X_3	0.18623	1	0.18623	29.62641	0.00284
Lack of Fit	0.04731	5	0.00946	1.50524	0.33228
Pure Error	0.03143	5	0.00629		
Total SS	18.151	19			
R^2	0.95662	Adjust R^2	0.91758		

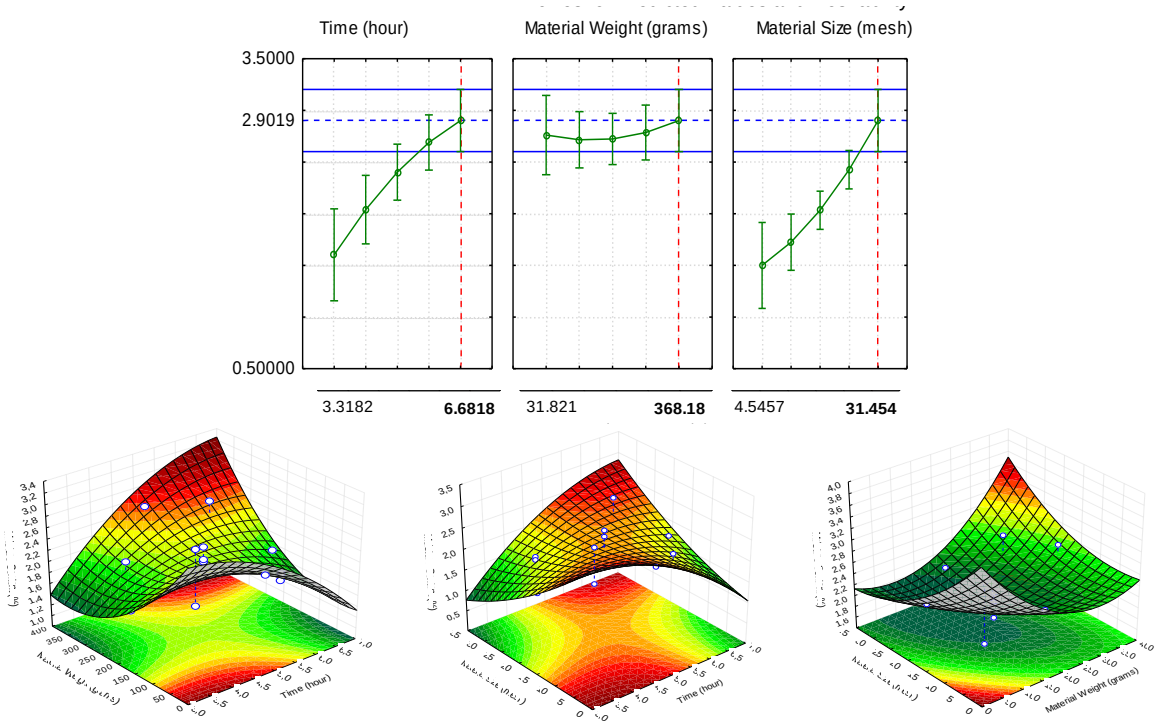

Figure 1. Optimum Condition of Drying Process on Moisture Level

the drying process of granulated palm sugar are shown in Figure 1.

A desirability value of 1 indicates that the goal solution has been fulfilled. While a desirability value of 0 indicates that the response must be discarded (Nurmiah et al., 2013). The prediction model produces a moisture response of 2.9019% with an optimum condition of 6.68 hours, material weight 368.18 grams, and material size 31.45 mesh. The surface plot shows that the optimization of time, material size and material weight can affect the moisture content of granulated palm sugar.

Validation of Optimum Conditions for Drying Process Optimization Results

The optimum condition of granulated palm sugar was validated by running process and testing the water level. It aims to determine the

Table 4 Validation Results of Predicted Value and Observed Value of Software Statistics

Variable	Optimum Value Based on Statistica 10 Software	Water Level of Granulated palm Sugar	
		Predicted value	Observed value
X_1	6.68 hour		
X_2	368.18 gram	2.9019%	2.9016%
X_3	31.45 mesh		
	% Error	0.0003%	

Table 5. Chemical Characteristics of Red Ginger Granulated Palm Sugar Test Results

Chemical Characteristics	Test Results	Quality qualification SNI 01-3743-1995	Information
Sucrose	96.5967%	Minimum 90%	Fulfilled
Sugar reduction	6.0434%	Minimum 6%	Fulfilled
Ash level	1.8660%	Maximum 2%	Fulfilled
Caloric	379.8951 kcal	379.93 kkal	Fulfilled
Protein	2.4268%	2.45%	Fulfilled
Fat	0.3972%	0.41%	Fulfilled
Carbohydrate	91.5379%	91.61%	Fulfilled

match between the observed values from running validation and the predicted values from optimization with RSM. The validation value of the optimization results is shown in Table 4.

Based on the data in Table 4, the difference in the response value between the prediction software and the actual data is 0.0003%. The difference in value is less than 5% so that the validation results can be accepted. It proves that the test results' water content matches the program's predicted value (Mariana, 2017).

Chemical Characteristics of Red Ginger Granulated Palm Sugar Optimum Validation Results

The chemical characteristics observed include sucrose, sugar reduction, ash level, calories, protein, fat, and carbohydrates are presented in Table 5.

The sucrose level of the test results showed a value of 96.5967%. This value is under the quality requirements of SNI 01-3743-1995, which is at least 90%. A significant sucrose value affects the durability of granulated palm sugar because it is associated with a low content of reducing sugar, so it is more durable during storage (Zuliana et al., 2016). It is appropriate because the reducing sugar content in palm sugar ant optimization results shows a low value of 6.0434%. This value is close to the minimum condition stated in SNI 01-3743-1995, at least 6%.

Low reducing sugar levels indicate the quality of the granulated palm sugar produced is good, because the sugar becomes stable and does not melt quickly (Indahyanti et al., 2014). The ash content of the test results shows a value of 1.8660%. It follows the quality requirements of SNI 01-3743-1995, which is a maximum of 2%. The ash level is related to the preservative level added in palm sugar. The higher the ash level in palm sugar, indicates the presence of mineral additives, one of which is preservatives added during the cooking process (Haryanti, 2020). Other chemical characteristics that are not a quality requirement for palm sugar in accordance with SNI 01-3743-1995 include calories, protein, fat, and carbohydrates. The results of the test on these characteristics are calories (379.8951 kcal), protein (2.4268%), fat (0.3972%), and carbohydrates (91.5379%). This value has met the quality of the Banten Agricultural Technology Assessment Agency (Heryani, 2016).

CONCLUSION

The second order polynomial equation with RSM has an R^2 value of 0.95662 with the simplified equation. The optimum operating condition of the drying results showed a response of water content of 2.9016% with a percentage error of 0.0003%, affecting the chemical characteristics of granulated palm sugar so that it fulfill the quality requirements of SNI SNI 01-3743-1995, sucrose (96.5967%), sugar reduction (6.0434%), ash level

(1.8660%), calories (379.8951 kcal), protein (2.4268%), fat (0.3972 %) and carbohydrates (91.5379%).

REFERENCES

Assegaf, S., Kawilarang, A. P., Handajani, R. 2020. Antibacterial Activity Test of Red Ginger Extract (*Zingiber officinale var. Rubrum*) Against Streptococcus pyogenes In vitro. Biomolecular and Health Science Journal. 3(1): 24–27.

Fatriani. 2019. Karakteristik Gula Semut dari Pengaron Sebagai Pemanis Pangan Alternatif. Prosiding Seminar Nasional Lingkungan Lahan Basah. 4(1): 34–37.

Haryanti, P. 2020. Evaluasi Mutu Gula Kelapa Kristal (Gula Semut) Di Kawasan Home Industri Gula Kelapa Kabupaten Banyumas. Jurnal Agroteknologi. 5(1): 48–61.

Heryani, H. 2016. Keutamaan Gula Aren dan Strategi Pengembangan Produk. (Edisi Pertama). Lambung Mangkurat Universit Press, pp. 1-157.

Indahyanti, E., Kamulyan, B. Ismuyanto, B. 2014. Optimasi Konsentrasi Garam Bisulfit pada Pengendalian Kualitas Nira Kelapa. Jurnal Penelitian Saintek. 19(1): 1–8.

Kaushik, S., Jangra, G., Kundu, V., Yadav, J. P., Kaushik, S. 2020. Anti-viral Activity of Zingiber officinale (Ginger) Ingredients Against the Chikungunya Virus. Virus Disease. 31(3): 270–276.

Mariana. 2017. Optimasi Formulasi dan Karakterisasi Fisikokimia dalam Pembuatan Daging Restrukturisasi Menggunakan Response Surface Methodology (Konsentrasi Jamur Tiram Serta Gel Porang dan Karagenan). Jurnal Pangan dan Agroindustri. 5(4): 83–91.

Maricar, A. 2019. Analisa Perbandingan Nilai Akurasi Moving Average dan Exponential Smoothing untuk Sistem Peramalan Pendapatan pada Perusahaan XYZ. Jurnal Sistem dan Informatika. 13(2): 36–45.

Meldayanoor, M., Ilmannafian, A. G., Wulandari, F. 2019. Pengaruh Suhu Pengeringan Terhadap Kualitas Produk Gula Semut dari Nira. Jurnal Teknologi Agro-Industri. 6(1): 1.

Muhandri, T., Rifqi, D. M., Lestari, T., Widodo, S. 2020. Pelatihan Teknis dalam Rangka Perbaikan Mutu Gula Semut di Kabupaten Tasikamaya. Agrokreatif: Jurnal Ilmiah Pengabdian kepada Masyarakat. 6(3): 276–280.

Normilawati, N., Fadlilaturrahmah, F., Hadi, S., Normaidah, N. 2019. Penetapan Kadar Air dan Kadar Abu pada Biskuit Yang Beredar Di Pasar Banjarbaru. Jurnal Ilmu Farmasi. 10(2): 51–55.

Nurmiah, S., Syarief, R., Sukarno, S., Peranginangin, R., Nurmata, B. 2013. Aplikasi Response Surface Methodology pada Optimalisasi Kondisi Proses Pengolahan Alkali Treated Cottonii (ATC). Jurnal Pascapanen dan Bioteknologi Kelautan dan Perikanan. 8(1): 9.

Pertiwi, P. 2018. Aplikasi Response Surface Methodology (RSM) untuk Meningkatkan Kuat Tekan Paving Block dengan Campuran Abu Ampas Tebu. Teknik Sipil Universitas Mataran. 2(1): 1–10.

Pratama, A., Wisdaningrum, O., Nugrahani, M. P. 2020. Pendampingan dan Penerapan Teknologi untuk Peningkatan Produktivitas Usaha Mikro Gula Semut. Dinamisia : Jurnal Pengabdian Kepada Masyarakat. 4(2): 275–284.

Ritonga, A. M., Masrukhi, S. 2020. Pendugaan Umur Simpan Gula Kelapa Kristal Menggunakan Metode Akselerasi Berdasarkan Pendekatan Kadar Air Kritis. Jurnal Teknologi Pertanian. 21(1): 11–18.

Sinamo, K. N., Hutabarat, N. D. M. R. 2021. Red Ginger Wedang to Strengthen Immune System Against Covid-19 of Children Living in an Orphanage. ABDIMAS TALENTA: Jurnal Pengabdian Kepada Masyarakat. 6(1): 60–67.

SNI. 1995. *SNI 01-3743-1995 Gula Palma*. Badan Standar Nasional.

Sogandi, S. 2019. Identifikasi Kandungan Gizi dan Profil Asam Amino dari Ikan Seluang (Rasbora Sp). The Journal of Nutrition and Food Research. 42(2): 73–80.

Wilberta, N., Sonya, N. T., Lydia, S. H. R. 2021. Analisis Kandungan Gula Reduksi Pada Gula Semut dari Nira Aren yang Dipengaruhi pH dan Kadar Air.

BIOEDUKASI (Jurnal Pendidikan Biologi). 12(1): 101–107.

Wulandari, T. S. H., Nurhaniefa, A. M., Lestari, W. A. 2021. The Content Effectiveness in Red Ginger (Zingiber officinale Rosc.) Variety to Increase Immunity. 1st International Conference In Education, Science And Technology. 1(1): 459–463.

Yenrina, I. R. 2015. Metode Analisis Bahan Pangan dan Komponen Bioaktif (Edisi Pertama). Andalas University Press. Padang, Indonesia.

Zuliana, C., Widyastuti, E., Susanto, W. H. 2016. Pembuatan Gula Semut Kelapa (Kajian pH Gula Kelapa dan Konsentrasi Natrium Bikarbonat). Jurnal Pangan dan Agroindustri. 4(1): 109–119.

JBAT 11(1) (2022) 17 – 22

Jurnal Bahan Alam Terbarukan

Accredited SINTA 2 by Ministry of Research and Technology/National Research and Innovation Agency
SK No. 200/M/KPT/2020
http://journal.unnes.ac.id/nju/index.php/jbat

p-ISSN 2303 0623
e-ISSN 2407 2370

The Effect of Solvent Ratio and Extraction Time on Antioxidant Activity and Flavonoid Concentration of Kedawung Leaf (*Parkia Biglobosa*) Through Microwave-Assisted Extraction

Ferika Indrasari✉, Buanasari

DOI: https://doi.org/10.15294/jbat.v11i1.33426

Nusaputera College of Pharmacy Semarang, Indonesia

Article Info

Article history:
Received
November 2021
Accepted
April 2022
Published
June 2022

Keywords:
antioxidant; DPPH; *kedawung;* Microwave-Assisted Extraction

Abstract

Kedawung (*Parkia biglobosa*) contains various ingredients such as alkaloids, saponins, tannins, flavonoids, and terpenoids. The flavonoid content in Kedawung is thought to have an antioxidant effect. Antioxidants are able to counteract free radicals that enter the body by donating electrons and binding them. Currently, the microwave-assisted extraction (MAE) method is widely used because the solute mass transfer from the sample matrix into the solvent is higher than the Soxhlet method. The following study aimed to know the effect of solvent ratio and extraction time on the extraction yield, flavonoid concentration, and antioxidant activity of kedawung leaf through microwave-assisted extraction. In this method, we used 40% ethanol to make the varied solute: solvent ratio such as 1:20, 1:30, 1:40, and 1:50. The extraction time used in this method was 4-7 minutes respectively. Microwave-assisted extraction has good performance to extract the active substance in Kedawung leaves. The highest yield 16.36%, total flavonoid content (57.32±2,2 mg QE/g extract), and DPPH scavenging activity (88.87±1.062%) was obtained in the extraction with a solids-solvent ratio of 1:40 g/mL, at an extraction time of 6 minutes. This method promises to take the active substance in a short time.

INTRODUCTION

Indonesia is well-known for plants with pharmacological effects or healing effects on various diseases (Sholikhah, 2016). Many plants contain antioxidant compounds such as phenolic compounds, flavonoids, and xanthones. These compounds can be used as a natural antioxidant (Panche et al., 2016). Antioxidants are able to counteract free radicals that enter the body by donating electrons and binding them (Halliwell, 2012). Antioxidants function as an antidote against free radicals in the body to prevent cell damage (Kurutas, 2016).

Kedawung (*Parkia biglobosa*) has various pharmacological activities such as antibacterial, antifungal, and antioxidant activity. The microwave-assisted extraction (MAE) method is widely used because it can increase the solute's mass transfer rate from the sample matrix into the solvent faster than that of the Soxhlet extraction method (Kataoka, 2019). Besides, the time required for extraction is relatively short, and the obtained yield is higher than other extraction methods, such as maceration, soxhlet extraction, and ultrasonic.

One of the factors that influence the extraction yield is the extraction time studied in research conducted by Shuncheng et al. (2013) on the extraction of corn's husk using 4, 5, and 6 minutes time variation. The study has revealed that the best yield was obtained from the 6 minutes extraction time. The following study aimed to know the effect of solvent ratio and extraction time on the extraction yield, flavonoid concentration, and antioxidant activity of kedawung leaf through microwave-assisted extraction.

✉ Corresponding author:
E-mail: ferikaindrasari89@gmail.com

MATERIALS AND METHODS

Materials

The materials used in this research were kedawung leaf (*Parkia biglobosa*) from Semarang, Central Java. Other materials which used: methanol (Merck, 98% purity 1060092500), 1,1 Diphenyl 2-Picryl Hydrazyl/DPPH (Sigma-Aldrich, 90% purity, D9132), quercetin hydrate (Sigma-Aldrich, 95% purity, 337951), ethanol (Merck, 96% purity), $AlCl_3$ (Merck) and distilled water.

The tools which used in this study are microwave (Samsung), analytical balances (Sartorius), oven (Memmert), moisture analyser (Radwag MAC50), UV-Vis spectrophotometer (Shimadzu 2480), and rotary evaporator (Scilogex).

Methods

This experimental study evaluated the solute effect: solvent ratio and the extraction time on the extraction yield, the flavonoid concentration, and the antioxidant activity of kedawung leaf (*Parkia biglobosa*) extract obtained through microwave-assisted extraction.

Raw Material Preparation

This research used a random sampling method. The kedawung leaf sample was randomly collected and processed by using the microwave-assisted extraction method. Preparation of raw materials is carried out like the previous research method.

Microwave Assisted Extraction (MAE)

The raw materials were extracted by microwave-assisted extraction with a time variation of 4-7 minutes (fixed condition were ratio of solid to solvent 1:30 g/mL, temperature of 40°C, ethanol concentration of 40%v and power of 300 Watt) and variation of the ratio of solid to solvent 1:20, 1:30, 1:40 and 1:50 g/mL, at fixed time conditions (best results from variations in extraction time), temperature of 40°C, ethanol concentration of 40%v and power of 300Watt. The extracts were filtered, and stored at room temperature before being examined.

Analysis of Total Flavonoid Content (TFC)

The modified aluminum chloride colorimetric method was used (Buanasari et al., 2021), 0.5 mL of the standard solution was diluted and each extract was mixed separately with 1.5 mL of ethanol (95%), 0.1 mL of aluminum chloride (10%), 0.1 mL of potassium acetate (1M) and 2.8 mL of distilled water. After incubation at room temperature for 30 min, the absorbance of the reaction mixture was measured at 426 nm by spectrophotometer. The results are expressed as percent by weight of flavonoids.

DPPH Scavenging Activity (DPPH-SA)

Antioxidant activity testing was carried out using the DPPH method. 1.0 ml of the extract sample solution was added with 3.0 m of the newly prepared 0.1 mM DPPH solution. The absorbance was measured with a spectrophotometer (Shimadzu Japan) at a wavelength of 514 nm. The extract activity at DPPH is expressed as shown in Eq. (1).

$$DPPH\ Scavenging\ activity = x\ 100\% \qquad (1)$$

RESULTS AND DISCUSSION

The results obtained that leaves's moisture content were 4.70%. It met the requirement for the standard moisture content of simplicia (<10%) (Sulasmi et al., 2016). The characteristics of the sample are listed in Table 1.

Table 1. The characteristic of raw material.

Properties	Leaf
Shape	Powder
Color	Green
Smell	Specific
Taste	Bitter
Texture	Smooth
Moisture Content	4.70%

The phytochemical screening aimed to identify the bioactive compounds of the extract. The results are listed in Table 2.

The test results showed that kedawung leaf contained bioactive compounds of flavonoids, saponins, and tannins. The test tubes that were carried out included alkaloids, flavonoids, saponins, and tannins. One indicator of the reaction in the test tube was a color change. The test results showed that kedawung (*Parkia biglobosa*) contained bioactive compounds of flavonoids, saponins, and tannins.

Table 2. The screening of Kedawung extract.

Bioactive Compound	Reagent	Result	Standard
Alkaloid	Dragendroff	-	Red or orange sediment
	Mayer	-	Sediment
	Wagner	-	Brown Sediment
Flavonoid	HCl + $MgSO_4$	+	Colored
Saponin	+ Aquadest + 2N HCl → Unremoved Foam	+	Foamed
Tannin	10% $FeCl_3$	+	Black, blue or green color

The Effect of Extraction Time and The Solid to Solvent Ratio on The Yield of Kedawung Leaf Extract

The effect of extraction time on percent yield is presented in Figure 1. The longer the extraction time increases the yield value to 6 minutes, after that it decreases.

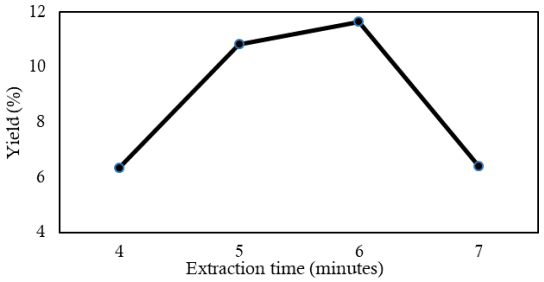

Figure 1. The effect of extraction time on the yield of kedawung extract.

Figure 1 shows that the amount of extract obtained is proportionate with the time needed during the extraction process. It means that the more time added, the higher the amount of section which is then obtained. The extraction time used in this research was 4-7 minutes. The highest extract yield is obtained from the extraction process using 6 minutes of extraction time, 11.66%. The 6 minute of the extraction time seems to be optimum. It means, after the 7 minute, the rise of the time extraction doesn't influence the amount of extract which is then obtained because all the solute particles have gotten good contact with all the solvent molecules (Mandal et al., 2007; Chen et al., 2007; Wang et al., 2010).

To determine the effect of the ratio of solvent solids on the percent yield, an extraction time of 6 minutes was used from the previous experiment. The amount of solvent was an essential factor that should be taken into account during the extraction process to ensure that all solute particle was in contact with the solvent molecules (Zhang et al., 2018).

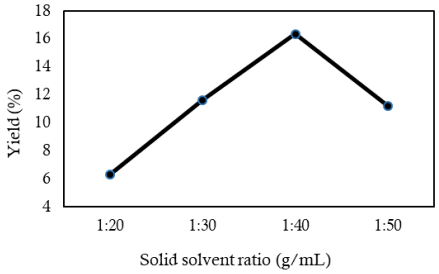

Figure 2. The effect of solid to solvent ratio on the yield of kedawung extract.

Figure 2 showed that the increase in the solvent amount is proportionate with the extract obtained during the extraction process. It means the more solvent added, the higher the obtained extract. The solute : solvent ratios used were 1:20, 1:30, 1:40 and 1:50, and the extract yields obtained were 6.3; 11.3; 16.36; and 11.2% respectively. The highest extract yield is obtained from the extraction process using a 1:40 ratio, 16.36%. It's also showed that the extraction yield decreases by 11.2% on the 1:50 ratio. The 1:40 ratio seems to be the optimum solute: solvent ratio. It means, after that concentration, the rise of the solvent doesn't influence the amount of extract, which is then obtained because all the solute particles have gotten good contact with all the solvent molecules. The higher solute: solvent ratio will increase the extract obtained in the general conventional extraction process. However, the higher solute: solvent ratio in microwave-assisted extraction will decrease the extract yield (Zhang et al., 2018). The heat radiation emitted by the tool cannot reach all solute particles with higher solvent amounts. Therefore, the extraction process doesn't function well (Kamaludin et al., 2014).

The Effect of Extraction Time and The Solid to Solvent Ratio on The Total Flavonoid Concentration (TFC) of Kedawung Leaf Extract

The effect of extraction time on TFC is presented in Figure 3. The longer the extraction

time increases the TPC value. At six minutes it gives the highest TFC value. This is similar to the yield gain.

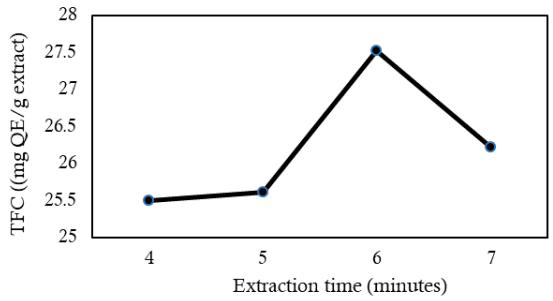

Figure 3. The effect of time extraction on the total flavonoid concentration.

Figure 3 showed that the highest total flavonoid concentration is obtained from the 6 minute of extraction time, the optimum extraction time. According to research conducted by Miollogo et al. (2009), kedawung leaf (*Parkia biglobosa*) has higher flavonoid content than its bark. It is in line with this research, in which the concentration of total flavonoid obtained was about 27.52 mg QE/g extract on the leaf.

Analysis results revealed that the solute: solvent ratio had different impacts on the total flavonoid content. Flavonoid has some unsubstituted hydroxy groups. Some polar molecules such as ethanol, methanol, ethyl acetate, or combination can be used for flavonoid extraction (Hidayati et al., 2019).

Figure 4 shows that increasing the solute:solvent ratio can increase the amount of flavonoids to a solid solvent ratio of 1:40 g/mL, then increasing the ratio further decreases the TFC value. The largest total flavonoid concentration at a ratio of 1:40 was 57.32 ± 2.2 mg QE/g extract. The heat exposure that occurred during the extraction process caused the degradation of the compound.

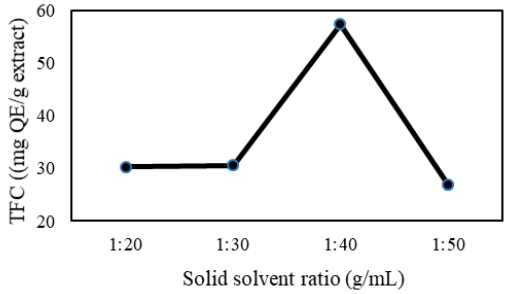

Figure 4. The effect of solid to solvent ratio on TFC of kedawung leaf extract.

Therefore the concentration found was lacking. According to the research conducted by Kusnadi *et al.* (2017), which used microwave-assisted extraction using a 1:15 ratio, the 1:15 ratio gave a lower concentration than that of the 1:10 ratio. This is in line with this study, where the total flavonoid concentration decreased after reaching the maximum ratio of 1:40.

The Effect of Extraction Time and The Solid to Solvent Ratio on The Antioxidant Activity of Kedawung Leaf

The longer the time increases the TFC value and also increases the antioxidant activity of the extract. This shows that the greater the TFC, the greater the antioxidant activity.

Figure 5 shows that the extraction time of 6 minutes resulted in an extract with the highest antioxidant activity of 86.40%. This is in accordance with the flavonoid content obtained at the extraction time of 6 minutes giving the largest flavonoid content.

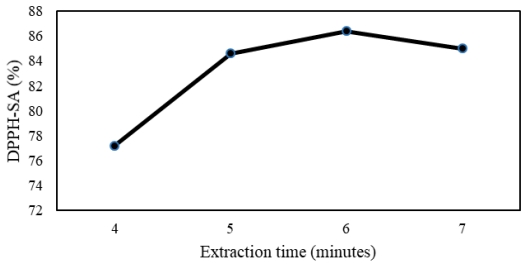

Figure 5. The effect of extraction time on the antioxidant activity of kedawung leaf.

When the DPPH was added to the kedawung (*Parkia biglobosa*) sample, the sample color changed from purple to yellow. The decrease of color intensity was measured at the wavelength of 515.4 nm, in which the maximum absorbance was given. The reduction of the absorbance showed the extract's potency to catch free radicals.

Figure 6 shows that the solute: solvent ratio increase can influence the flavonoid amount and thus the antioxidant activity. The total flavonoid concentration found in the leaf was 88.87 ± 1.06 % . However, the total flavonoid concentration had no significant influence on antioxidant activity because the bioactive compounds obtained had complex and various bioactive compounds with their antioxidant and prooxidant activity. For example, other than flavonoids, tannin can also function as an antioxidant that interferes with the assay of the

flavonoid's antioxidant activity (Komolafe et al., 2016).

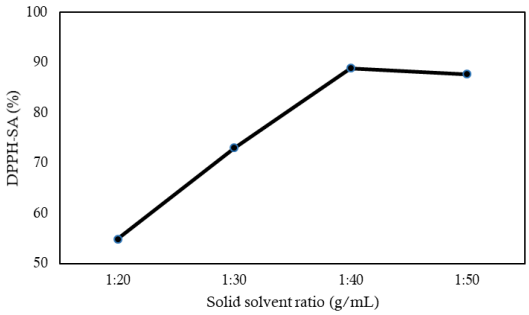

Figure 6. The effect of solid to solvent ratio on the antioxidant activity of kedawung leaf.

CONCLUSION

Microwave-assisted extraction has good performance to extract the active substance in Kedawung leaves. The highest yield 16.36%, total flavonoid content (57.32±2,2 mg QE/g extract), and DPPH scavenging activity (88.87±1.062%) was obtained in the extraction with a solids-solvent ratio of 1:40 g/mL, at an extraction time of 6 minutes. This method promises to take the active substance in a short time.

ACKNOWLEDGEMENT

The authors would like to thank the *Indonesian Education Minister Research* Fund for financial support which enabled the development of our research. We also express our deepest gratitude to the Chemical Laboratory of the Sekolah Tinggi Ilmu Farmasi Nusaputera Semarang, for the provision of equipment and support for this research.

REFERENCES

Buanasari, B., Sugiyo, W., Rustaman, H. 2021. Effect of Ultrasonic Assisted on The Degree of Deacetylation of Chitosan Extracted from Portunus Pelagicus. 10(1):17-23.

Chen, K. H, Miyazaki, T., Tsai, H. F., Bennett, J. E. 2007. The bZip transcription factor Cgap1p is involved in multidrug resistance and required for activation of multidrug transporter gene CgFLR1 in Candida glabrata. Gene. 386(1-2):63-72.

Kamaludin, H., Lihan, T., Ali Rahman, Z., Mustapha, M. A., Idris, W. M. R., Rahim, S. A. 2014. Integration of remote sensing, RUSLE and GIS to model potential soil loss and sediment yield (SY). Hydrology and Earth System Sciences Discussions. 10: 4567–4596.

Kataoka, H. 2019. Microwave Assisted Extraction (MAE). Science Direct: Encyclopedia of Analytical Science (Third Edition). 231-255

Komolafe, K., Akinmoladun, A., Olaleye, M. 2016. Methanolic Leaf Extract of Parkia biglobosa Protect against Doxorubicin-in ducet Cardiotoxicity in Rats. International Journal of Applied Research in Natural Products. 6(3): 39-47.

Kurutas, E. B. 2016. The Importance of Antioxidants Which Play the Role in cellular Response Against Oxidative/Nitrosative Stress: Current State. Nutrition Journal. 15(71):1-22.

Kusnadi, K., Dedi, D., Yunianta, Y., Arumingtyas, E. L. 2017. Extraction of Phenol Compounds and Antioxidant Activity from Cayenne Pepper Fruit by Microwave Assisted Extraction. Jurnal Teknologi Pertanian. 18(3): 181-190.

Halliwell, B. 2012. How to characterize an antioxidant- An update. Biochemical Social Symposia. 61:73–101

Hidayati J. R., Yudiati, E., Pringgenies, D., Arifin, A., Oktaviyanti, D. T. 2019. Antioxidant Activities, Total Phenolic Compound And Pigment Contents of Tropical Sargassum sp. Extract, Macerated In Different Solvents Polarity. Jurnal Kelautan Tropis. 22(1):73-80

Mandal, V., Mohan, Y., Hemalatha, S. 2007. Microwave-Assisted Extraction-An Innovative and Promoting Extraction Tool for Medical Plant Research. Pharmacognosy Reviews. 1 (1): 7-18.

Miollogo-Kone, H., Lompo, M., Kini, F., Asimi, S., Guissou, I. P., Nacoulma, O. 2009. Evaluation of Flavonoids and Total Phenolic Content of Stem Bark and Leaves of Parkia bigobosa (Jacq) Bent (Mimosaceae)-Free Radical Scavenging

and Antimicrobial Activities. Research Journal of Medical Sciences. 3(2):70-74.

Panche, A. N., Diwan, A. D., Chandra, S. R. 2016. Flavonoids: an overview. Journal of Nutritional Science. 5: 47.

Sholikhah, E. N. 2016. Indonesian Medicinal Plants as Sources of Secondary Metabolites for Pharmaceutical Industry. Journal of Medical Science. 48(4):226-239.

Shuncheng, R., Yani, C., Suyun, H., Yiwei, C. 2013. Study on the Simultaneous Extraction of Total Flavonoid and Total Sponins from Corn Silks by Microwave-Assisted Technology. Medicinal Plant. 4(8):68-73.

Sulasmi, E. S., Indriwati, S. E., Suarsini, E. 2016. Preparation of Various Type of Medicinal Plants Simplicia as Material of Jamu Herbal. International Conference on Education in the 21th.21:1014-1024

Wang, Y., O'Leary, L.A., Rickard, R.S., Mason, C.A. 2010.. Geocoding capacity of birth defects surveillance programs: Results from the National Birth Defects Prevention Network Geocoding Survey. Journal of Registry Management. 37: 22-26.

Zhang, Q. W., Lin, L. G., Ye, W. C. 2018. Techniques for Extraction and Isolation of Natural Product: a Comprehensive review. Chinese Medicine. 13:1-26.

JBAT 11(1) (2022) 23 – 32

Jurnal Bahan Alam Terbarukan

Accredited SINTA 2 by Ministry of Research and Technology/National Research and Innovation Agency
SK No. 200/M/KPT/2020
http://journal.unnes.ac.id/nju/index.php/jbat

p-ISSN 2303 0623
e-ISSN 2407 2370

The Carbon of *Swietenia Machrophylla* Fruit Peel and Coal Fly Ash as Bio-Composite Brake Ingredients

Sutikno Madnasri✉, Muhammad Zakaria, Sukiswo Supeni Edi, Putut Marwoto

DOI: https://doi.org/10.15294/jbat.v11i1.35527

[1]Physics Department, Faculty of Mathematics and Natural Sciences, Universitas Negeri Semarang, Buliding D7 2nd Floor, Sekaran Campus, Unnes, Gunungpati, Semarang, Indonesia, 50229

Article Info

Article history:
Received
March 2022
Accepted
May 2022
Published
June 2022

Keywords:
Brake friction material;
Carbon;
Coal fly ash;
Composite;
Swietenia Machrophylla

Abstract

The eco-friendly brake composite has been still an interesting issue in the development of brake friction materials. Wastes of *S. Macrophylla* (mahogany) fruit skin and coal fly ash are available as organic ingredients of bio-composite brakes. In this research, we investigated the effects of both ingredients on the brake composite properties which were fabricated using hot isostatic pressing at temperature 200 °C and pressure 5 kN for 3 h. The specimens were prepared in some volume fractions of carbon (2 vol% - 12 vol%). As a result, several tested specimens containing mahogany fruit skin carbon revealed maximum Rockwell hardness 69 HRB, wear 2.49×10^{-4} mm^2/kg, and water absorption 2.72 %, while specimens containing coal fly ash showed 78 HRB, 1.1×10^{-3} mm^2/kg, and 3.5 %, respectively. The brake composites containing coal fly ash performed better than ones containing mahogany fruit skin carbon. The hardness and wear of these two types of brake composite friction materials meet the minimum criteria required by SAE, JA661, and are close to the quality of the brake pads of two commercial brake composite materials. Water absorption in the brake lining specimens with mahogany leather carbon showed that the addition of the volume fraction caused an increase in water absorption, while the specimen containing coal fly ash showed that the increase in the carbon volume fraction caused a decrease in water absorption.

INTRODUCTION

The brake composites are multiphase materials that serve to stop the rotor movements of vehicles and should have standard characteristics namely stable friction, low wear rate, noise resistance, ecofriendly, and high thermal stability. In the fabrication process, the superiority of these material properties could be achieved by the usage of about 7-15 ingredients (Singaravelu et al., 2019; Maleque & Atiqah, 2013). Meanwhile, the uniform materials could not meet the minimum requirements of a commercial brake friction material because the parameters like safety and comfort of brake performance were not achieved (Pujari & Srikiran, 2019). In recent years, many organics ingredients and recyclable wastes were used to manufacture green brakes in avoiding the use of asbestos material (Pujari and Srikiran, 2019; Singh et al., 2017). The bio-composite brake was selected as an alternative in recent years to substitute the conventional brake because it is lighter, stronger, higher wear resistance, higher corrosion resistance, higher durability so that it has been still attracting the interest of researchers to develop it (Wasilewski, 2017). In this research, the mahogany fruit skin carbon and the coal fly ash were selected as brake composite ingredients. because of their abundances in nature and its recyclability. Based on the data in the Indonesian Central Bureau of Statistics, Indonesia's forest area is around 144 million hectares, and 1.3 million hectares of land are in the form of industrial forest plantations. In detail, eight percent of industrial plantations are sources of mahogany. The carbon either in fiber or powder form is one of the

✉ Corresponding author:
E-mail: sutiknomadnasri@mail.unnes.ac.id

important ingredients in bio-composite brake and it plays a role as a lubricant in the friction mechanism (Ahmadijokani et al, 2019). In the previously published work, the carbon of coconut chars was used as one ingredient of brake composite (Sutikno et al., 2010). Th carbon fiber can enhance the wear resistance drastically in comparison with aramid fiber (Ahmadijokani et al., 2020) and the chopped carbon fibers are used as reinforcement material for brake composite (Dang et al. 2018). The carbon is also available to make composites for integrated electrodes as electrochemical detectors in microchips (Arvinte et al., 2020; Adam et al., 2012). Some amazing characteristics in the carbon-based brake composites such as low density, high thermal capacity, low thermal expansion, and outstanding friction property are found in recent years by many researchers (Hao et al., 2014). To produce a stable friction coefficient and low wear loss, the content and dimension of carbon in the brake lining composite need to be adjusted (Hao et al, 2014; Wasilewski 2017). The shape of ingredients influences the tribological properties (Singh et al., 2017) and for example, the hardness and flexural strength of brake composites are improved steadily by increasing the carbon fiber content (Ahmadijokani et al., 2019).

The usage of wastes such as metals, glasses, and organic materials to fabricate brake friction material has been developed by the material society around the world (Sutikno et al., 2013). Coal fly ash is a result of the industry which is using coal as a fuel for energy-generating such as electricity, metallurgy, cement, and ceramic industries. These waste abundances have not recyclable and give a negative impact on society and environmental health. It contains a high content of alumina and silica and available as reinforcement particles for polymer matrics composite to replace ceramics materials for example MgO and Al_2O_3 (Chen et al., 2005). Coal fly ash fulfills the criteria as pozzolanic materials because it has cylindrical particles and very smooth (Külaots et al., 2004), it is appropriate used as one of brake composite ingredients. Another application is as solid sorbent to reduce sulfur dioxide. The tribo-study proved that the fly ash significantly increased the friction coefficient of brake composite specimens (Ahlawat et al., 2020; Ahlawat et al., 2019).

Their contents of mahogany fruit skin and coal fly ash were optimized at each specimen and their effects on the water absorption, mechanical properties, and thermal properties were investigated. The wear resistance and hardness of brake composite specimens are performance parameters of brake composite that must be fulfilled following the minimum criteria. Based on the Indonesian National Standard (SNI), good brake linings have hardness specifications (68-105 HRB), wear ($5x10^{-4}$ - $5x10^{-3}$ mm^2/kg), friction coefficient (0.14 - 0.27), and fracture strength (480 - 1500 N/cm^2).

MATERIALS AND METHODS

Materials

This fabrication process of specimens included the preparation of mahogany fruit skin and coal fly ash preparation. The mahogany rind was taken from a plantation in Gunungpati Sub-district, Semarang City, Indonesia, while coal fly ash was supplied from the waste of the Cilacap steam power plant, Central Java, Indonesia. The other ingredients consisted of epoxy, magnesium oxide, calcium carbonate, metal mix, zinc oxide, stearic acid, glass powder, bagasse, bakelite, and sulfur. These materials were technical grade materials taken from the local market. The used materials were calculated based on their volume fractions, initiated by determining the total volume of the mixture as a basis of calculation. In detail, the fabrication route included sequential dry mixing, pre-forming, hot pressing (curing process, post-curing), and finishing (Singh & Patnaik, 2015; Sugözü, 2018).

The basic composition of brake composite was fixed the same as in the previous article (Sutikno et al., 2012; Madnasri et al., 2013) by adding new ingredients as listed in Table 1 that including carbon mahogany rind and coal fly ash. Meanwhile, the rubber material was not used. All ingredients were mixed and ignored in a petri dish up to homogeneous. A mixing variation of carbon content and coal fly ash in the specimen was made in 2 vol% - 12 vol% and it was pressed by hot isostatic pressing method at 200 °C, for 3 h, and pressure 5 kN (Shojaei et al., 2007).

The testing of specimens was done to determine the effects of carbon volume fraction of mahogany fruit peel or coal fly ash on the hardness, wear resistance, water absorption, thermal resistance, and to observe the microstructures of the composite brakes. Additionally, the hardness testing was done using Rockwell hardness tester

with load 981 N and ball indentor 2.5 mm. The scratch diameter of the indentation trace was observed using a microscope in magnification of 100x (1 strip = 38 microns) and used to determine Rockwell hardness using Eqs. (1) .

$$HRB = 100 - \frac{t}{0{,}002} \quad (1)$$

$$t = D - \sqrt{D^2 - d^2} \quad (2)$$

Where, HRB is the Rockwell hardness number, t is the indentation depth (mm), D is the diameter of indentor (mm) and d is the indentation diameter on the specimen (mm). Their hardness values of both specimens were compared to study the effects of carbons.

Table 1. The composition of developed brake composites.

Ingredient	Volume fraction (vol%)	
	Mahogany fruit skin	Coal fly ash
Epoxy	8.50	8.50
Metal powder	38.30	38.30
Carbon	2.84	2.84
Magnesium oxide	7.80	7.80
Calcium carbonate	7.80	7.80
Zinc oxide	2.13	2.13
Stearic acid	2.13	2.13
Glass powder	11.35	11.35
Bakelite	17.02	17.02
Sulfur	2.13	2.13

The specimen wear resistances were tested using Ogoshi High-Speed Universal Testing Machine (Type OAT-U) with load (P_0) of 6.36 kg, wearing distance (L_0) 200 mm, wearing plate length (B) of 3 mm, radius length of wearing plate (r) of 14 mm, and wearing time for 60 s. Scratches of revolving disc friction were measured by using an optical microscope in magnification of 100x (1 strip = 38 microns). Next, the wear resistance of both brake composite specimens was calculated using Eq. (3) and compared,

$$W_s = \frac{B\ (B_0)^3}{8r\ P_0 L_0} \quad (3)$$

where W_s is the wear resistance (mm^2/kg) and B_0 is the indentation length on the specimen (mm).

In this study, three brands of commercially available brake linings (Asmoto, Honda genuine part, and Indopart) were tested for their mechanical properties. These three types of commercial brake pads are original disc brakes for 125 cc class motorcycles. The testing of the mechanical properties of the three commercial brake linings includes the Rockwell hardness test, wear test, and tensile strength test. In the Rockwell hardness testing, some indentation loads were adjusted in adaptation with the specification of the test specimens. The results of testing the mechanical properties of commercial brake pads were compared with the test results of brake pads made of fly ash and brake pads made of carbon mahogany fruit skin.

Next, the water absorptions on both specimens were determined to obey their applicabilities in the wet environment. The specimens were sliced into 1 cm x 1 cm and their masses were weighed before and after the drying process at 50 °C for 2 h. After the specimens dried, we soaked it in a beaker glass filled with 100 mL water for 10 mins, and then it was taken to be re-weighed. The percentages of water absorption were calculated using Eq. (4) and then it was compared and analyzed,

$$Water\ Absorption = \frac{m_{wet} - m_{dry}}{m_{dry}} \quad (4)$$

where m_{dry} is mass of specimen before soaked (g) and m_{wet} is mass of specimen after soaked (g). We observed the microstructures of specimens (1 cm x 1 cm) surfaces and the chemical elements using a Scanning Electron Microscope (SEM) integrated with Energy Dispersive X-ray Spectroscopy (EDS).

To study the thermal properties and phase change of composite brake due to enthalpy change, the specimens were tested using differential thermal analysis (DTA). Several thermogravimetric analysis (TGA) parameters for different brake composites were set up at temperatures (T_{onset}) 0 °C - 450 °C, delta temperature (ΔT) 25 °C, and operation duration 120 mins. Many samples for TGA analysis were prepared of 1 g powders and the TGA instrument was operated in the temperature range of 25 °C – 425 °C for 2 h. Finally, a maximum operating temperature (T_{max}) was achieved at 425 °C.

RESULTS AND DISCUSSION

Several data on physical and mechanical properties are reported and analyzed in some tables and graphs. The brake composites containing mahogany fruit peel seem black and have an average density of 0.419 g/mL, while those containing coal fly ash were brown and have a mean density of 1.1915 g/mL. Figure 1 exhibits some Rockwell Hardness numbers scale B. The brake friction material containing mahogany peel has Rockwell hardness between 51 HRB - 69 HRB. On the other hand, brake friction material containing coal fly ash has Rockwell hardness in the range of 66 HRB - 78 HRB. It is found that the coal fly ash contributes to the hardness of friction material more dominant than the mahogany carbon shell. Both materials can produce brake linings that meet Rockwell hardness standards, namely greater than 68 HRB.

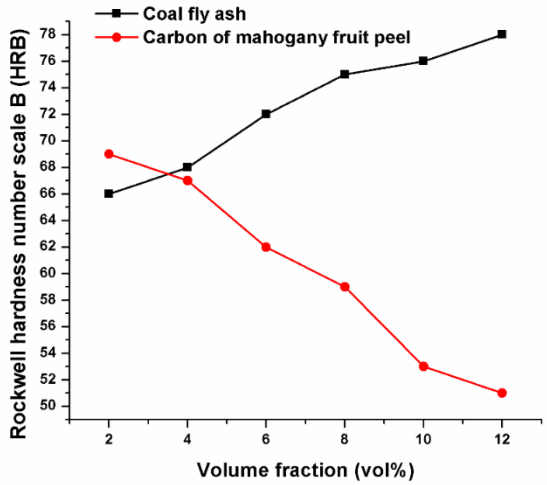

Figure 1. Rockwell hardness number of composite brake to the increase of volume fraction: (a) Mahogany fruit skin carbon and (b) coal fly ash.

At the testing of specimens containing mahogany rind carbon, the increase of volume fraction of mahogany rind carbon has decreased the hardness number. Inversely, at the testing of specimens containing coal fly ash, the increase of volume fraction of coal fly ash has improved the hardness number. The composite brake pads containing mahogany rind carbon have an optimum hardness number of 69 HRB, found in samples with 2 vol%, while those containing coal fly ash have an optimum hardness number of 78 HRB, found in samples with 12 vol%. This is because the size of coal fly ash particles (about 7.44 μm) is greater than that of the carbon particles of mahogany skin (about 3.53 μm). Large particles contribute to the nature of the material in resisting the movement of deformed structures. Coal fly ash particles have a denser structure and have stronger bonding between particles so they can withstand deformation during hardness testing. The addition of coal fly ash increases the hardness of the composite material of the brake lining due to the increased bonding strength (polymer) against plastic deformation. The smaller particles caused the density of the material to become higher and it plays a significant role in increasing the hardness of composite friction material. The carbon density of mahogany rind equals 35 % of the density of coal fly ash.

For the wear test of the brake lining composites, its results are plotted in Figure 2 and getting information that the addition of the volume fraction of the mahogany skin carbon causes the wear value increases as well, whereas the addition of the coal fly ash ingredient leads to a smaller wear value of the composite brake lining. The increasing trend in the wear of brake friction composites is proportional to the rising content of coal fly ash in the composite, it is consistent with the results of Dadkar et al's study in 2009 (Dadkar et al., 2009). Carbon-based brake composites provide excellent wear resistance and braking performance at high-energy braking conditions, larger than 5 MJ (Prabhu, 2016). The brake lining from coal fly ash has better wear resistance than the brake lining of the material of mahogany rind carbon. This is because coal fly ash has a specific gravity greater than carbon of the skin of mahogany so that composite samples containing coal fly ash have given a significant contribution to the densification process of the brake pad composite. The sample becomes harder and higher wear resistance. On the other hand, the composite of brake lining containing carbon of mahogany rind, the process of densification (compaction) of its constituent materials when mixing is not evenly distributed so that the sample is softer and has low wear resistance. It is thought a breaking process of a little coal fly ash particles is the cause.

A comparison of water absorption characteristics for two brake composites is exhibited in Figure 3. The addition of a volume fraction of coal fly ash causes a decrease in water absorption, in contrast to the addition of a volume fraction of the mahogany rind carbon causing an increase in

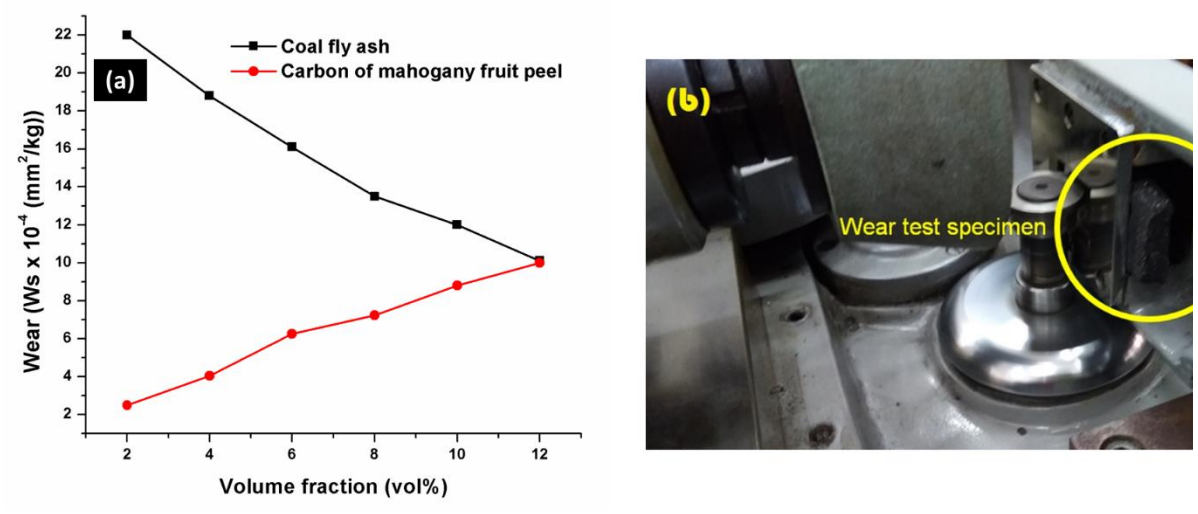

(a) (b)

Figure 2. (a) Wear of brake friction composite versus volume fraction increase of (i) mahogany rind carbon, and (ii) coal fly ash; and (b) picture of wear testing instrument of brake composite.

Table 2. Data on water absorption of specimen containing mahogany rind carbon.

The volume fraction of carbon (vol%)	Specimen immersion (10 min)		Water absorption of the specimen (%)
	The initial mass of specimen (g)	End mass of specimen (g)	
2	1.10	1.13	2.72
4	1.20	1.24	3.33
6	1.29	1.35	4.65
8	1.34	1.41	5.22
10	1.35	1.43	5.92
12	1.68	1.78	5.95

Table 3. Water absorption test data of specimens containing coal fly ash.

The volume fraction of coal fly ash (vol%)	Composite immersion (10 mins)		Water absorption (%)
	Initial mass (g)	End mass (g)	
2	1.30	1.40	7. 69
4	1.47	1.57	6.80
6	1.50	1.58	5.33
8	1.59	1.66	4.40
10	1.95	2.03	4.10
12	2.00	2.07	3.50

the water absorption rate. This is because coal fly ash has a smaller particle size so that it can fill smaller pores compared to carbon made of the mahogany rind. Thus, the produced composites of coal fly ash seem denser and solid. According to (Erol et al., 2008), the finer shapes of coal fly ash particles can reduce the composite porosities. The porosity at various sintered temperatures has shown a decrease due to the increase in the weight fraction of coal fly ash up to 5 %, where at the weight fraction of coal fly ash above of 5 wt%, the composite porosity with aluminum matrix material tended to be constant. Low porosity (relatively high density) was found in composites with a weight fraction of coal fly ash lower or equal to 5 wt%. The porosity is influenced by the weight fraction and the distribution of coal fly ash particles in the matrix. If the weight fraction of coal fly ash on the composite is low (less than or equal to 5 wt%), the distribution is evenly distributed. This makes the interaction or

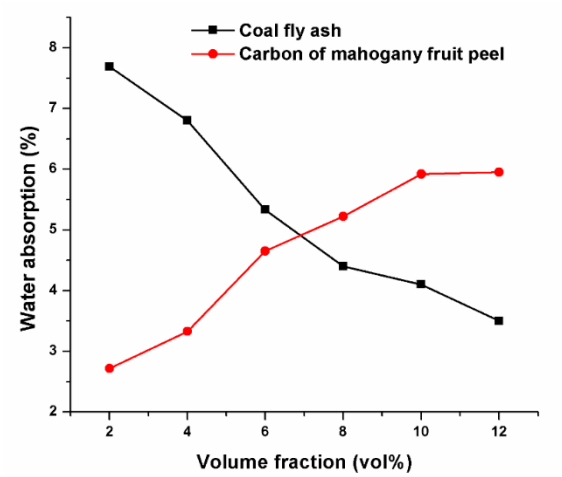

Figure 3. Water absorption for each composite brake linings on the different volume fraction: (a) Mahogany rind carbon and (b) coal fly ash.

bond between the coal fly ash particles and the matrix very good. Conversely, if the weight fraction of coal fly ash on the composite is more than 5 wt%, then some coal fly ash particles coincide or group together, so the bond between the coal fly ash particles and the matrix is imperfect. This will bring up the cavity so that its porosity increases. A previously published research result stated that the use of coal fly ash in composites can increase the compressive strength and water absorption rate (Ilic et al., 2003). The impact strength increases in the brake composite containing coal fly ash with smaller particle sizes which confirms that vacuum has existed in the composite with the larger particles of coal fly ash. This composite brake is better used in wet conditions because it can absorb water well.

Figure 4 shows some microstructures of composite brake lining containing mahogany leather and that of coal fly ash. The SEM images of composite brake pads containing carbon mahogany rind where the particle shapes are not clearly visible and very small while containing coal fly ash materials have the round particle shape and look very clear. Many pores found on the surfaces are in the separated positions because of the uneven mixing process and the particle size of each material is different.

The EDX curves of the composite brake linings are revealed in Figure 5. Table 4 exhibits the results of the weight percentages of chemical elements contained in the composite brake lining. The composite sample of brake lining with one of the ingredients of mahogany rind and coal fly ash has the same elemental content, but the amount of weight percentage of each chemical element contained is different. This can be seen in the carbon content of mahogany rind of 58.9 wt%, while the carbon content of coal fly ash material is 66.2 wt%. It is known that the specimen of brake composite made using mahogany fruit skin as one of the ingredients, containing carbon less than that of coal fly ash for the same formula mixing.

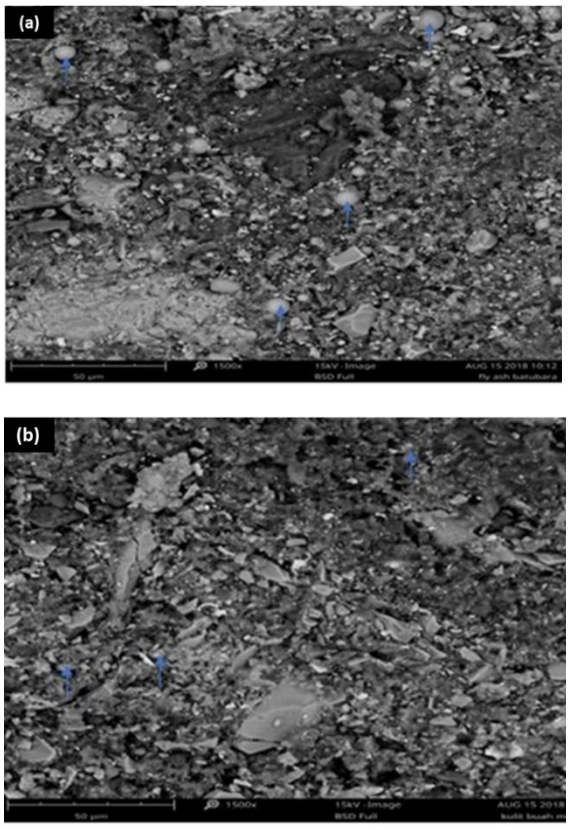

Figure 4. SEM images in magnification of 1500X of brake composite containing: (a) Mahogany rind carbon and (b) coal fly ash.

As a result of thermal characterization using Differential Thermal Analysis (DTA), its properties of composite materials from the carbon of mahogany rind and coal fly ash can be seen in Figure 6. The composite brake pads with mahogany rind carbon as one of its ingredients begin to experience enthalpy changes (delta m) of 1.75 mg when the temperature reached 3000 °C, whereas composite brake linings containing the coal fly ash material begin to suffer enthalpy changes (delta m) of 2.50 mg when the temperature reached 2500 °C. Meanwhile, the results of thermal testing revealed a difference in enthalpy change, which for brake lining with coal fly ash material has a greater enthalpy change (delta m) compared to that of with mahogany rind carbon material. A weight loss of

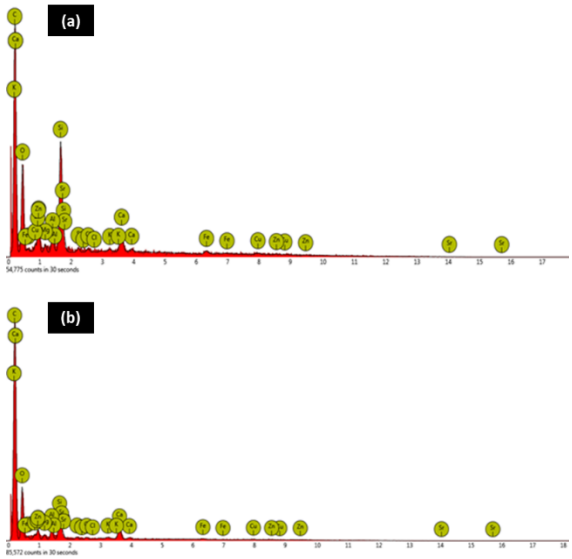

Figure 5. EDX curves of samples containing: (a) Mahogany rind carbon and (b) coal fly ash.

Table 4. Chemical elements in brake composite based on the EDX spectra.

Element	Weight in percentage (wt%)	
	Mahogany rind carbon	Coal fly ash
C	58.9	66.2
Si	3.6	1.3
Sr	3.3	1.5
O	25.9	26.2
Ca	1.8	1.4
Na	2.0	1.1
Al	0.9	0.8
Mg	0.4	0.4
S	0.2	0.1
Fe	0.9	0.3
Cl	0.2	0.1
K	0.2	0.1
Cu	1.0	0.3
Zn	0.6	0.3

mahogany rind carbon-based brake composite occurs at 400 – 125 °C as much as 1.75 mg, on the other hand, a weight loss of coal fly ash-based brake composites several 2.5 mg significantly occur at 325 – 150 °C. The weight loss characteristics of composite brake linings with different materials have been reported by Cong et al. in 2012 (Cong et al., 2012). Jeganmohan and Sugozu reported that heat treatment could improve both the physical properties and the friction properties of the composite brake pads (Jeganmohan & Sugozu, 2020). The DTA data are available to study the thermal properties of brake composite. In the real condition, the braking temperature for a motorcycle can achieve about 315 °C. Here, we simulate the real temperature of braking will increase up to 415 °C. It is expected, the brake material has been still good working at that temperature. The maximum temperature, 425 °C, is achieved after 23 mins.

The results of testing the mechanical properties of three types of commercial brake pads, namely Asmoto, Honda, and Indopart brands are shown in Table 5. These values are also compared with the brake pads made of coal fly ash and the brake pads made of charcoal mahogany fruit peel and Society American Engineers (SAE) Standard, J661. The three reported mechanical properties of brake lining to consist of material hardness, strength, and wear. Based on Table 5, the Asmoto brand brake pads show the most superior mechanical properties, namely hardness 134.2 HRB, tensile strength 1227 N/mm^2, and material wear 2.86x10^{-4} mm^2/kg. These values are compared with the experimental results of two types of fabricated brake lining specimens namely coal fly ash-based brake composite and mahogany fruit peel-based brake composite. Based on the superiority of its mechanical properties, it can be ranked from the most superior to the lowest as follows Asmoto brake composite, Honda brake composite, coal fly ash-based brake composite, mahogany fruit peel-based brake composite, and Indopart brake composite. The hardness values of the two types of brake lining composites of this study, coal fly ash-based brake composite (66 - 78 HRB) and MFP (51 - 69 HRB) meet SAE Standard J661, namely 68 - 105 HRB. Another fact is that the hardness value of Indopart brake pads is around 61 HRB, still below the minimum value set by SAE. In general, all tested specimens meet the wear requirements under SAE, J661 (5x10^{-4} – 5x10^{-3}mm^2/kg). Both coal fly ash-based brake pads and mahogany fruit peel-based brake pads meet the minimum wear requirements of the SAE, J661. Asmoto brake linings and Honda genuine parts also demonstrate superior tensile strength and meet SAE standards. The tensile strength of the Indopart brake pads (approximate 379 N/mm^2) is still below the SAE minimum standard (480 N/mm^2) and that of the coal fly ash-based brake composite specimen, 480 N/mm^2, is close to the minimum value of tensile strength according to SAE. Meanwhile, the tensile strength of the mahogany fruit peel-based

Table 5. Comparison of the assessed characteristics of fabricated brake composites with commercially available brake linings.

Test Specimen (TS)	Rockwell hardness number scale B (HRB)	Strength (N/mm^2)	Wear (mm^2/kg)
Asmoto	134.2	1227	$2.86x10^{-4}$
Honda genuine part	98.4	776.43	$1.06x10^{-3}$
Coal fly ash	66 – 78	385 - 480	$1x10^{-3} – 2.2x10^{-3}$
Mahogany fruit peel	51 – 69	300 - 400.33	$2.49x10^{-4} – 1x10^{-3}$
Indopart	61	379	$1.18x10^{-3}$
SAE J661	68-105	480 – 1500	$5x10^{-4} – 5x10^{-3}$

brake pads specimen, 400.33 N/mm^2, is still below the minimum value of tensile strength according to SAE.

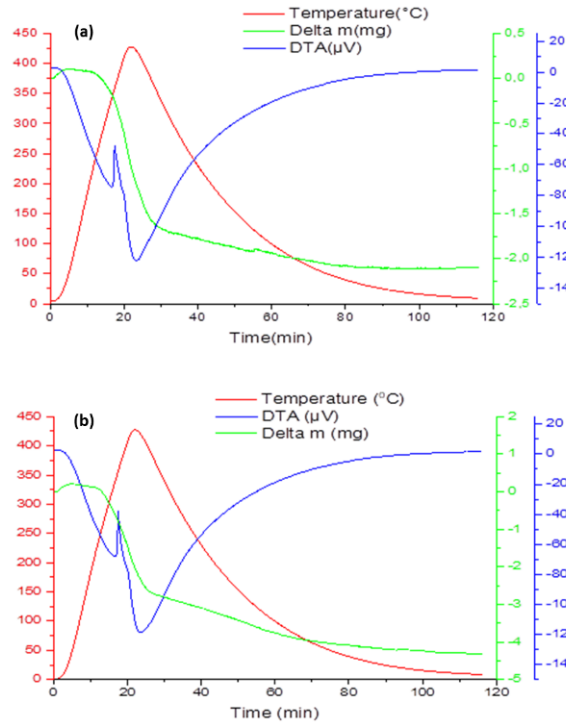

Figure 6. Graph of differential thermal analysis (DTA) of brake composite at 0°C – 450 °C for 120 minutes.

CONCLUSION

In conclusion, the composite brake pads containing carbon of mahogany peel revealed the best hardness of 69 HRB, while those containing coal fly ash indicated the best hardness of 78 HRB. We have found the best wear of composite brake lining with mahogany rind carbon correspond to $2.49x10^{-4}$ mm^2/kg, while those containing coal fly ash revealed the best wear of $10.1x10^{-4}$ mm^2/kg. The hardness and wear of these two types of brake composite materials meet the minimum requirements applied by SAE, JA661, and are close to the quality of Honda Genuine Parts and Asmoto Composite brake pads and exceed the quality of Indopart brand brake pads. Next, the water uptake on brake pad specimens with mahogany rind carbon confirmed that the addition of volume fraction has caused an increase in water absorption, whereas specimens containing coal fly ash showed that the increase of carbon volume fraction could cause the water absorption decrease. This recommends that a composite brake lining with coal fly ash material is more appropriate used in wet environments. Changes in enthalpies (delta m) of brake lining with mahogany rind carbon by 1.75 mg, while specimens containing coal fly ash material experienced enthalpy changes (delta m) by 2.50 mg.

ACKNOWLEDGEMENT

This research has received funding from the Ministry of Research, Technology and Higher Education, the Republic of Indonesia at Research Grant of University Research Flagship, Innovation Scheme, at Financial Year 2019 under contract No. SP DIPA-042.01.2.400899/2019.

REFERENCES

Adam, T., Hashim, U., Sutikno. 2012. Simulation of passive fluid driven micromixer for fast reaction assays in nano lab-on-chip domain. Procedia Engineering. 50: 416-425.

Ahlawat, V., Kajal, S., Parinam, A. 2020. Tribo-performance assessment of milled fly ash brake friction composites. Polymer Composites. 41(2): 707-718.

Ahlawat, V., Kajal, S., Parinam, A. 2019. Exploring the suitability of milled fly ash

for brake friction composites: characterization and tribo-performance. Material Research Express. 6(4): 045311

Ahmadijokani, F., Alaei, Y., Shojaei, A., Arjmand, M., Yan., N. 2019. Frictional behavior of resin-based brake composites: Effect of carbon fibre reinforcement. Wear. 420–421: 108–115.

Ahmadijokani, F., Shojaei, A., Dordanihaghighi, S., Jafarpour, E., Mohammadi, S., Arjmand, M. 2020. Effects of hybrid carbon-aramid fiber on performance of non-asbestos organic brake friction composites. Wear. 452–453: 203280.

Arvinte, A., Sesay, A.M., Virtanen, V. 2020. Designing carbon reinforced PMMA composites for integrated electrodes as electrochemical detectors in PMMA microchips. Journal of Electroanalytical Chemistry. 876: 114486.

Chen, Y., Shah, N., Huggins, F.E., Huffman, G.P. 2005. Transmission electron microscopy investigation of ultrafine coal fly ash particles. Environmental Science & Technology. 39(4): 1144–1151.

Cong, P., Wang, H., Wu, X., Zhou, G., Liu, X., Li., T. 2012. Braking performance of an organic brake pad based on a chemically modified phenolic resin binder. Journal of Macromolecular Science, Part A. 49: 518–527.

Dadkar, N., Tomar, B.S., Satapathy, B.K. 2009. Evaluation of fly ash-filled and aramid fibre reinforced hybrid polymer matrix composites (PMC) for friction braking applications. Material and Design. 30: 4369–4376.

Dang, A., Li, T., Wang, J., Zhao, T., Xia, Y., Chen, X., Li, H., Tang, C., Xiong, C. 2019. Preparation and mechanical properties of CCF reinforced RBSC braking composite from pre-liquid dispersion. Ceramics International. 45(5): 6528-6534.

Erol, M., Küçükbayrak, S., Ersoy-Meriçboyu, A. 2008. Comparison of the properties of glass, glass ceramic and ceramic materials produced from coal fly ash. Journal of Hazardous Material. 153: 418–425.

Hao, M., Luo, R., Hou, Z., Yang, W., Xiang, Q., Yang, C. 2014. Effect of fiber-types on the braking performances of carbon/carbon composites. Wear. 319: 145–149.

Ilic, M., Cheeseman, C., Sollars, C., Knight, J., 2003. Mineralogy and microstructure of sintered lignite coal fly ash. Fuel. 82: 331–336.

Jeganmohan, S., Sugozu, B., 2020. Usage of powder pinus brutia cone and colemanite combination in brake friction composites as friction modifier. Materials Today: Proceedings. 27(P3): 2072-2075.

Külaots, I., Hurt, R.H., Suuberg, E.M., 2004. Size distribution of unburned carbon in coal fly ash and its implications. Fuel. 83: 223–230.

Madnasri, S., Edi, S.S., Saputra, D.S. 2013. Crystal structures thermal properties of bamboo nanofiber reinforced-composite friction materials of glass and metal wastes. Advance Material Research. 789: 49-55.

Maleque, M.A., Atiqah. A. 2013. Development and Characterization of Coir Fibre Reinforced Composite Brake Friction Materials. Arabian Journal for Science and Engineering. 38: 3191–3199.

Prabhu, T.R. 2016. Effect of bimodal size particles reinforcement on the wear, friction and mechanical properties of brake composites. Tribology - Materials, Surfaces & Interfaces. 10(4): 163-171.

Pujari, S., Srikiran, S. 2019. Experimental investigations on wear properties of Palm kernel reinforced composites for brake pad applications. Defence Technology. 15: 295-299.

Shojaei, A., Fahimian, M., Derakhshandeh, B. 2007. Thermally conductive rubber-based composite friction materials for railroad brakes-thermal conduction characteristics. Composites Science and Technology. 67: 2665–2674.

Singaravelu, D.L., Vijay, R., Filip., P. 2019. Influence of various cashew friction dusts on the fade and recovery characteristics of non-asbestos copper-free brake friction composites. Wear. 426–427: 1129–1141.

Singh, T., Tiwari, A., Patnaik, A., Chauhan, R., Ali, S. 2017. Influence of wollastonite shape and amount on tribo-performance of nonasbestos organic brake friction composites. Wear. 386–387: 157–164.

Singh, T., Patnaik, A. 2015. Performance assessment of lapinus-aramid based brake pad hybrid phenolic composites in friction

braking. Archives of Civil and Mechanical Engineering. 15: 151-161.

Sugözü, B. 2018. Tribological properties of brake friction materials containing fly ash. Industrial Lubrication and Tribology. 70(5): 902-906.

Sutikno, M., Marwoto, P., Rustad, S. 2010. The Mechanical properties of carbonized coconut char powder-based friction materials. Carbon. 48: 3616-3620.

Sutikno, M., Edi, S.S., Saputra, D.S. 2013. Crystal structures and thermal properties of bamboo nanofiber reinforced-composite friction materials of glass and metal wastes. Advanced Materials Research. 789: 49-55.

Sutikno, Sukiswo, S.E., Dany, S.S. 2012. Sifat mekanik bahan gesek rem komposit diperkuat serat bambu. Jurnal Pendidikan Fisika Indonesia. 8: 83-89.

Wasilewski, P. 2017. Experimental study on the effect of formulation modification on the properties of organic composite railway brake shoe. Wear. 390–391: 283–294.

JBAT 11(1) (2022) 33 – 36

Jurnal Bahan Alam Terbarukan

Accredited SINTA 2 by Ministry of Research and Technology/National Research and Innovation Agency
SK No. 200/M/KPT/2020
http://journal.unnes.ac.id/nju/index.php/jbat

p-ISSN 2303 0623
e-ISSN 2407 2370

Effect of Ultrasonication Extraction Time on Determination of Flavonoid Levels in Ciplukan Plants

Ummul Habibah Hasyim✉, Fatma Sari, Ika Kurniaty, Annisya Ramadhani

DOI: https://doi.org/10.15294/jbat.v11i1.35254

Jurusan Teknik Kimia Fakultas Teknik Universitas Muhammadiyah Jakarta, Jl. Cempaka Putih Tengah 27 Cempaka Putih Jakarta Pusat 10510

Article Info

Article history:
Received
March 2022
Accepted
May 2022
Published
June 2022

Keywords:
Ciplukan;
Extraction;
Flavonoid;
Physalis angulate;
Ultrasonic

Abstract

Ciplukan contains bioactive substances in the form of flavonoids, saponins, alkaloids, polyphenols, vitamin C, stearic acid, palmitic acid. Bioactive substances from natural ingredients are known to function as immunomodulators that can increase the body's immune system, activate the body's natural defenses and restore immune system imbalances. Immunomodulators are important in studies related to the issue of the coronavirus disease 19 (Covid-19) pandemic. The purpose of this study was to determine the effect of the extraction time on the ultrasonic method on the flavonoid yield of ciplukan plants using methanol as a solvent. The method used is ultrasonication extraction with a variable extraction time. The analysis was carried out by qualitative analysis using a solution of qursetin to determine the concentration of flavonoids. The results of the study obtained the optimum flavonoid concentration at the extraction time of 15 minutes.

INTRODUCTION

Utilization of natural materials is currently a matter of much research to be developed into useful new materials. especially during the covid-19 pandemic, where most indonesian people believe that the content or efficacy of natural ingredients can be active substances that ward off the virus. In addition, the use of natural materials is also in accordance with the mandate of the state, which in 2022 will focus one of them on the green economy, namely maximizing natural materials that can improve the indonesian economy.

One of the plants that has the potential to be researched is ciplukan. This plant comes from America, but is now widely grown in tropical areas. Ciplukan can grow in areas with a height of 1 to 1550 meters above sea level. This plant consists of stems, shoots, roots, fruits and leaves. This plant is known by the Latin name physalis angulate L, and in Indonesian it is known as Ciplukan, each region has a different name for this plant.

Ciplukan contains bioactive substances in the form of flavonoids, saponins, alkaloids, polyphenols, vitamin C, stearic acid, palmitic acid. Bioactive substances from natural ingredients are known to function as immunomodulators that can increase the body's immune system, activate the body's natural defenses and restore immune system imbalances. Immunomodulators are important in studies related to the issue of the coronavirus disease 19 (Covid-19) pandemic.

Studies related to the content of ciplukan with process technology that still tends to be simple so that the optimization of the potential content of other ciplukan plants cannot be utilized optimally. With considerable development potential as a source of herbal medicinal raw materials, it is necessary to conduct a comprehensive study related to the optimization of ciplukan plant flavonoid

✉ Corresponding author:
E-mail: ummul.hh@umj.ac.id

extraction starting from the roots, stems, leaves to the fruit as immunomodulators.

It is mentioned in (Zheng, Wen, Yuan, & Gao, 2016) that distillation or liquid extract with solvent is the traditional method used in the extraction of flavonoids. Where the extraction method in the process of extracting flavonoids from plants often requires a long extraction time, the solvent is required in large quantities, and the efficiency is low. Especially if the type of flavonoid is (Ridwanuloh F. , 2019) thermally unstable and easily degraded during the extraction process. Ultrasonic assisted extraction (UAE) or so-called ultrasonic extraction is an extraction method with the help of ultrasonic waves. Where ultrasonic waves have a frequency of 70kHz which means they have a frequency above the frequency of human hearing. In extracting natural ingredients with content such as antioxidants, sonication extraction method can produce higher yields in a relatively short time. The process that occurs in the extraction of organic compounds in plants and grains using organic solvents is to break down the cell walls with ultrasonic vibrations so that the content in the extraction raw materials can come out easily (Ashley, Andrews, Cavazos, & Demange, 2001). In this literature study, it is known that UAE or sonication extraction is carried out in 2 methods, namely direct sonication and indirect sonication. The indirect sonication method is carried out with water heating media or is called an ultrasonic water bath. In this method, the extracted material or solution is not in direct contact with the ultrasonic wave sensor. (Sharma & Janmeda, 2014). In the previous research method, it is known that the maceration extraction method has not been able to show optimal results in the amount of extract yield. In the Application of Ultrasonic Waves to Increase Extraction Yield and Effectiveness of Antioxidants and Mangosteen Peel in 2017, it is known that ultrasonic extraction technology has been widely used to increase yields up to 30% and reduce extraction time so that it will be more effective (Aminah, Tomayahu, & Abidin, 2011).

Flavonoids are known as polar substances. As is known in the principle like dissolves like, that the effectiveness of the solubility of a compound depends on the type of solvent. Polar solvents and have been widely used in the extraction process are water, acetone, methanol, ethanol. For this reason, in the research carried out, methanol was chosen as a solvent which has shown the effectiveness of the solubility of flavonoid compounds. (Verdiana, Widarta, & Permana, 2018) (Kusmaningtyasa, Laily, & Putri, 2015)

Based on the literature review that has been carried out, this study aims to determine the effect of extraction time on the ultrasonic method on the flavonoid yield of ciplukan plants using methanol as a solvent.

MATERIALS AND METHODS

Materials

The materials used are all parts of the ciplukan plant; dried roots, stems, leaves and fruit. In addition, in the extraction process 90% methanol is used.

Equipments

In this study, ultrasonic waves assisted extraction using a water bath, rotary evaporator, white man filter paper, a blender used to chop ciplukan plant raw materials, and screening were used.

Preparation

The ciplukan plants that have been taken are then cleaned of dirt and soil attached to the roots. Then the dried ciplukan plant, cut into small pieces. After getting a smaller size, the ciplukan plant was mashed using a blender and sieved to get a uniform size.

Extraction Process

The extraction process was carried out by varying the ultrasonication extraction time starting from 5, 10, 15, 20, 25 and 30 minutes with a variable mass of 30 g of ciplukan sample. After getting the extraction process, then all the filtrate was filtered using a funnel and Whiteman filter paper. All the filtrate was combined and concentrated using a rotary evaporator until no more liquid dripped so that a concentrated extract of ciplukan was obtained.

Qualitative Analysis with Determination of Quarcetin Wavelength

The maximum wavelength of quarcetin was determined. Determination of the maximum wavelength of quercetin was carried out by running the quercetin solution at a wavelength of 380 - 500 nm. The results of the measurement of the maximum wavelength is at the point of 420 nm with

Table 1. Corelation Between Time of Extraction and Total Flavonoid Content

Time (minute)	Concentration Flavonoid	Extract Weight (g)	Total Flavonoid Content (%)
10	19.3125	0.93	20.7661
15	137.1250	1.83	74.9317
20	59.0875	2.24	26.3783
25	20.3500	1.6	12.7188
30	57.8750	2.12	27.2995

an absorbance of 0.1158. The maximum wavelength is used to measure the absorption of the ciplukan extract sample

Quarcetine Standard Curve

Weighed as much as 25 mg of standard quercetin and dissolved in 25 mL of methanol. The stock solution was pipetted as much as 1 mL and the volume was made up to 10 mL with methanol to obtain a concentration of 100 ppm. From a standard solution of 100 ppm quercetin, then several concentrations were made, namely 2 ppm, 4 ppm, 6 ppm, 8 ppm, and 10 ppm. From each concentration of the standard solution of quercetin, 1 mL was pipetted. Then 1 mL of 2% AlCl3 and 1 mL of 120 mM potassium acetate were added. Samples were incubated for one hour at room temperature. The absorbance was determined using the UV-Vis spectrophotometric method at a maximum wavelength of 420 nm.

Determination of total extract flavonoid content

Weighed 15 mg of extract, dissolved in 10 mL of methanol, in order to obtain a concentration of 1500 ppm. 1 mL of this solution was pipetted and then 1 mL of 2% AlCl3 solution and 1 mL of 120 mM potassium acetate were added. Samples were incubated for one hour at room temperature. The absorbance was determined using the UV-Vis spectrophotometric method at a maximum wavelength of 420 nm.

RESULTS AND DISCUSSION

In this study, all parts of the ciplukan plant were used. This is intended to obtain the optimum flavonoid concentration. Flavonoids are found in almost all parts of plants including fruits, roots, leaves, and outer bark of stems. Flavonoids are natural compounds that have the potential as antioxidant active substances that can counteract free radicals that play a role in the emergence of degenerative diseases through the mechanism of destroying the body's immune system, lipid and protein oxidation.

Quantitative analysis of total flavonoid compounds using UV-Vis spectrophotometry was carried out to determine how much total flavonoid content contained in the methanol extract of the ciplukan plant. The analysis of flavonoids was carried out using UV-Vis spectrophotometry because flavonoids contain a conjugated aromatic system so that they show strong absorption bands in the ultraviolet and visible spectrum regions.(Harborne, J.B 1987).

In this study, to determine the total flavonoid content in the sample, quarcetin was used as a standard solution with a concentration series of 2, 4, 6, 8, and 10 ppm. Concentration series is used because the method used in determining the concentration is a method that uses a standard curve equation, to make a standard curve, several concentration series are first made to obtain a linear equation that can be used to calculate the percent concentration. Quarcetin is used as a standard solution because quercetin is a flavonoid of the flavonol group which has a keto group at C-4 and has a hydroxyl group at the C-3 or C-5 atom which is neighboring of flavones and flavonols. (Azizah dan Faramayuda 2014, h. 48).

The maximum wavelength absorption measurement was carried out from a wavelength of 380 to 500 nm. The results of running show that the maximum wavelength of quarcetin standard is at a wavelength of 420 nm. The maximum wavelength was used to measure the uptake of the ciplukan plant extract sample.

From these measurements, it can be concluded that the higher the concentration used, the higher the absorbance obtained. The standard yield of quercetin obtained was plotted between its concentration and absorbance, so that a linear

regression equation was obtained, namely y = 0.0888x - 0.0788 with an R2 value of 0.9814. The quercetin calibration curve equation can be used as a comparison to determine the concentration of total flavonoid compounds in the sample extract.

Table 2. The maximum wavelength

Concentration (ppm)	Absrobance
2	0.1058
4	0.1710
6	0.2992
8	0.3419
10	0.4645

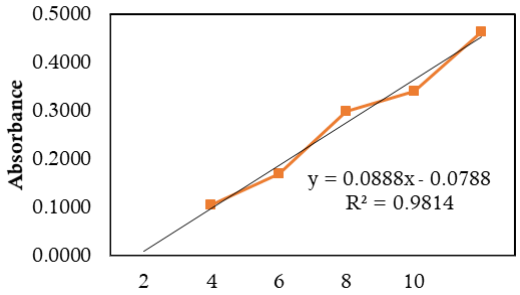

Figure 1. Quarcetine standard curve.

It is stated in that research related to the ciplukan extraction process needs to be developed with more appropriate methods. This is done to obtain a higher content of flavonoid active substances that can be used as immunomodulators. Therefore, based on the results obtained above, it shows that with the ultrasonic extraction method using methanol as a solvent, a fairly good concentration has been obtained. (Kusumaningtyasa, Laily, & Limandha, 2015).

CONCLUSION

Based on the results of research that has carried out, it can be concluded that the levels of flavonoid The total extract of the ciplukan plant extract was at the extraction time of 15 minutes. Where the resulting concentration of total flavonoid levels is 74.9317% extract.

ACKNOWLEDGEMENT

We would like to thank the Institute for Lembaga Penelitian dan Pengabdian Masyarakat (LPPM), University of Muhammadiyah Jakarta, which has provided funding assistance in this research.

REFERENCES

Aminah, A., Tomayahu, N., Abidin, Z. 2011. Penetapan Kadar Flavonoid Total Ekstrak Etanol Kulit. Jurnal Fitofarmaka Indonesia. 4(2): 226-230.

Ashley, K., Andrews, R., Cavazos, L., Demange, M. 2001. Ultrasonic extraction as a sample preparation technique for elemental analysis by atomic spectrometry. Journal of Analytical At Spectrom. 16(10): 1147-1153.

Kusumaningtyasa, R. W., Laily, N., Limandha, P. 2015. Potential of Ciplukan (Physalis angulata L.) as Source of Functional Ingredient. Procedia Chemistry. 14: 367-372.

Ridwanuloh, F. 2019. Isolasi Dan Identifikasi Senyawa Flavonoid Dari Batang Ciplukan (Physalis Angulata L.). Jurnal Sains dan Ilmu Farmasi. 4(1): 288-296.

Sharma, V., Janmeda, P. 2014. Extraction, isolation and identification of flavonoid from Euphorbia neriifolia leaves. Arabian Journal of Chemistry. 10(4): 509-5014.

Verdiana, M., Widarta, I. W., Permana, I. D. 2018. Pengaruh Jenis Pelarut Pada Ekstraksi Menggunakan Gelombang Ultrasonik Terhadap Aktivitas Antioksidan Ekstrak Kulit Buah Lemon (Citrus Limon) (Linn.) Burm F.). Jurnal Ilmu dan Teknologi Pangan. 7(4): 213-222.

Zheng, L. L., Wen, G., Yuan, M. Y., Gao, F. 2016. Ultrasound-assisted extraction of total flavonoids from corn silk and their antioxidant activity. Journal of Chemistry. 2015: 1-5.

JBAT 11(1) (2022) 37 – 49

Jurnal Bahan Alam Terbarukan

Accredited SINTA 2 by Ministry of Research and Technology/National Research and Innovation Agency
SK No. 200/M/KPT/2020
http://journal.unnes.ac.id/nju/index.php/jbat

p-ISSN 2303 0623
e-ISSN 2407 2370

Bio-Oil Production Using Waste Biomass via Pyrolysis Process: Mini Review

Nuraini[1], Noridah binti Osman[2], Erna Astuti[1,✉]

DOI: https://doi.org/10.15294/jbat.v11i1.37171

[1] Department of Chemical Engineering, Universitas Ahmad Dahlan, Campus 4 UAD Jl. Jend. Ahmad Yani, Tamanan Bantul, 55191, Indonesia
[2] Department of Chemical Engineering, Universiti Teknologi Petronas, Malaysia

Article Info

Article history:
Received
May 2022
Accepted
June 2022
Published
June 2022

Keywords:
Biomass;
Bio-oil;
Modifier;
Pyrolysis

Abstract

Pyrolysis process using abundantly available biomass waste fabric is a promising, renewable, and sustainable energy supply for bio-oil production. In this study, the pyrolysis of waste biomass determines the highest yield of diverse parameters of material type, temperature, reactor, method, and analysis used. From the differences in the parameters stated above, there is an opportunity to select the proper parameters to get the desired nice and quantity of bio-oil and the very best bio-oil yield. The maximum yield of each bio-oil product for pyrolysis primarily based on the above parameters was 68.9%; 56.9%; 44.4%; 44.16%; 41.05%; 39.99%. The bio-oil made out of pyrolysis was changed into analyzed using GC-MS, ft-IR, NMR, TGA, SEM, Thermogravimetric analysis, HHV, FESEM evaluation methods and the substances used had been plastic, seaweeds, oat straw, rice straw , water hyacinth, timber sawdust, sawdust, microalgae.

INTRODUCTION

The swiftly growing demand for energy and the increasing use of biomass as a renewable energy supply is increasingly considered to be the main desire to update commercial fossil fuels and the growing environmental and sustainability challenges (Khan et al., 2009). Biomass waste increases each year and ample biomass reserves can be renewed. The software of biomass fuels for heat and energy generation can affect the reduction of greenhouse fuel (GHG) emissions (UNFCCC, 2015).

Biomass is a potential material as a raw material for renewable energy and can be converted into chemical compounds that have higher values (Antal, 1983; Bridgewater & Grassi, 1991; Chum and Overend, 2001;). Biomass is a renewable and hygienic supply that may be shaped as an outstanding pyrolysis product because this material is very volatile and smell coffee (Deng et al., 2017). Rice husk is one of the main types of biomass, Rice husk production in China is more than forty million per year (Pode, 2016). The amount of rice husk is so large that it need instant treatment, so as not to harm the environment (Khan et al., 2009). Therefore, rice husk pyrolysis may be a powerful technique for putting off such massive-scale effluents, growing power usage, and product best of pyrolysis. Studies have attempted to study the technique of rice husk and sludge co-pyrolysis. Lin et al. (2018) discovered that those materials accelerated product oil best and accelerated the formation of H_2, CO, and C1eC2 invites.

Sources of biomass include agricultural and forestry residues, wood sawdust, crops, organic waste, municipal and business wastes (McKendry, 2002; Duanguppama et al., 2016). Sawdust is obtained from the process of cutting wood in sawmills. every hundred kg of wood in the sawmill produces about 12-25 kg of sawdust (Varma & Mondal, 2016). The raw materials for biomass in renewable biofuels come from timber waste, energy vegetation, forest residues, urban

✉ Corresponding author:
E-mail: erna.astuti@che.uad.ac.id

solid waste, animal waste, and agricultural residues (Azargohar et al., 2013; Agarwal, 2007). Pyrolysis is one of the biofuel technologies that address biomass uncooked substances consisting of municipal solid waste, agricultural residues, energy crops, and wooded area residues that are very appealing options to grow the possibilities for using less suited biomass. The advantage of biomass over fossil fuels is that it contains low sulfur and nitrogen, does not cause pollution due to the presence of carbon dioxide when burning (Probstein & Hicks, 1982).

Diverse styles of biomass use different wastes from plastics. Biomass mix with polymer and known as co-pyrolysis to improve the properties of the pyrolytic oil produced from biomass (Gollakota et al., 2016). Park et al (2019) used polyethylene terephthalate, polypropylene and polyethylene. Muneer et al., (2019) prefer chose polystyrene and polyethylene terephthalate. The other researchers use different types of waste: occasional rank coal (Wu et al., 2017), polyvinyl chloride (€zsin & Pütün, 2018), sewage sludge (Wang et al., 2020) and tires (Idris et al., 2020). The usage of combined biomass and plastics in the co-pyrolysis lower the activation strength (Bura & Grupta, 2018) and increase value bioproducts (Uzoejinwa et al., 2018).

The pyrolysis process is a thermal decomposition process, which happens in the absence of oxygen, which converts lignocellulosic biomass into carbon-wealthy solids and liquids. the principal components of lignocellulosic biomass, namely cellulose, lignin, and hemicellulose, are all thermally degraded in the temperature range of 300-500 C. in addition, pyrolysis is one way to launch energy stored in biomass via transformation into different beneficial products (Magdziarz et al., 2020). Pyrolysis includes diverse and complicated chemical reactions that arise at once (Mishra and Mohanty, 2020), the temperature variety for the gradual pyrolysis system of biomass is 300-650 C (Basu, 2018). The preliminary products resulting from pyrolysis are condensed fuel and solid biochar. Pyrolysis is a new generation that produces products inside the form of bio-oil, biochar, syngas, and ash that may be used as renewable energy (Azargohar et al., 2013).

Some of the parameters that affect pyrolysis are the composition and output of the product, in particular, rely on the form of biomass and its particle size, pyrolysis temperature, reactor type, and heating rate (Lu et al., 2009). Many types of reactors that use to biomass/waste pyrolysis are batch, semi batch or continue (Salehi et al., 2009; Arami-Niya et al., 2011; Abnisa et al., 2013; Azargohar et al., 2013). It is generally known that continues reactor produce better liquid output than the use of batch or semi-batch reactors. Pyrolysis of biomass closer to attaining excessive power performance and adjusting the necessities to shape the favored product kind contemplating enjoy and understanding of the effect of pyrolysis parameters on system performance, which include response rate, product selectivity & yield, product properties, and power performance (Lu et al., 2009).

The production of renewable energy from biomass and waste has implications for research on organic, biochemical, and thermochemical routes (Demirbas, 2009; Maity, 2015). Recent evaluations consistent with organic routes consist of anaerobic digestion (Hagos et al., 2017), saccharification, and fermentation (Pothiraj et.al., 2015), while biochemical routes consist of biodiesel manufacturing (Gumba et al., 2016; Saxena et al., 2009). Recent evaluations of thermochemical routes consist of catalytic cracking (Mante et al., 2011; Huber et al., 2006), thermal pyrolysis (Roy & Dias, 2017; Jones et al., 2009; Butler et al., 2011), catalytic pyrolysis (Kabir & Hamid, 2017; Yildiz et al., 2016; Venderbosch, 2015; Bank & Bridgwater, 2016), hydro-pyrolysis (Balagurumurthy & Bhaskar, 2014; Linck et al, 2014), gasification (Farzad et al., 2016; Sansaniwal et al., 2017) and hydrothermal liquefaction (Guo et al., 2015; Arturi et al., 2016).

The purpose of this study is to study the bio-oil production using pyrolysis with waste biomass as raw material. The focuses of studies are the material of pyrolysis, the parameters that influencing pyrolysis, the products of pyrolysis, properties of bio-oil as main products of pyrolysis and benefits of bio-oil.

METHODS

This research was designed in a literature survey by collecting, identifying, and comparing related research journals. The object of research is the pyrolysis of waste biomass. The research subject is the material of pyrolysis, the parameters that influencing pyrolysis, the products of pyrolysis, properties of bio-oil as main products of pyrolysis and benefits of bio-oil. Searching of journals were

done based on related keywords, namely biomass, bio-oil, modifier and pyrolysis. Selection or retrieval of source journals is based on the following conditions: the journal year ranges from 2005-2021, in the form of international journals. The source journal contains data on pyrolysis as the research object.

RESULTS AND DISCUSSION

The various of thermochemical processes, which is one of the best processes for converting biomass is pyrolysis because of its speed and simplicity (Samburova et al., 2016). In addition, pyrolysis produces versatile products, one of which is bio-oil which can be used as an alternative fuel for daily life (Lee et al., 2008; Park et al., 2010; Eom et al., 2013). The products produced from this pyrolysis process are liquid products such as bio-oil, gaseous products such as syngas, and carbon-rich solid residues such as bio-char (Bridgwater, 2012). There are several classifications of pyrolysis based on differences in operating conditions, namely, fast pyrolysis, slow pyrolysis, catalytic pyrolysis, hydrolytic pyrolysis, microwave-assisted, and flash pyrolysis.

Table 1. The effect of type of material and pyrolysis temperature on the products yield.

Material	Temperature	Bio-Oil	Bio-Char
Oat Straw	600°C	56.9%	-
Sawdust	500°C	41.05%	27.59%
Microalgae	185-570°C	39.99%	-
Rice straw	400°C	44.4%	-
Water hyacinth			
Wood Sawdust	500°C	44.16%	-
Plastic Seaweed	500°C	68.9%	-

The material and yield of Pyrolysis

Waste biomass using a wheat straw is high potential raw material to produce renewable energy in Poland. The experimental results obtained, that increase temperature causes the increase in gas and liquid yields. At 600◦C, the tar content was 56.9% and accumulated gases were 19.0%. The opposite condition occurs in charcoal production, the higher temperature produce less charcoal. At 300 °C, the yield of charcoal is 48.0%, decrease become 24.0% at temperature of 600 °C (Mlonka-Medrala et al., 2021).

Waste sawdust were used in in batch and continuous process (Soni, 2020). The batch pyrolysis produce the bio-oil yield of 34.9 wt% of and the biochar yield of 38.6% wt. On the other hand, the bio-oil yield of 41.05 wt% bio-oil and the biochar yield of 27.59 wt% was gotten from continuous pyrolysis. The continuous process has the potential to be used to produce to the industrial-scale production of bio-oil and bio-char. Varma et al. (2019) used a semi-batch reactor. The sawdust size used was 0.6<dp<1 mm. The maximum yield of bio oil obtained was 44.16 wt% with a flow rate of 100 cm^3/minute and temperature of 500 °C. The increasing temperature will decrease bio-oil yield, increased gas product yields and reduced bio-char yields with increasing temperature. The flow rate rise will increases the yield of bio oil and decreases the yield of biochar.

Co-pyrolysis of rice straw and water hyacinth in a 5:5 ratio, at an ideal temperature of 400 °C gives a yield of bio-oil higher than 44.4% by weight. The pyrolysis liquid produced from that mixed contains more aliphatic compounds and aromatic protons than the liquid obtained from each ingredient individually. This has been an additional FF determined through Gand C-MS analysis. Further studies are needed to get the reaction conditions to improve the applicability and feasibility of co-pyrolysis (Xu-Jin et al. 2019). Plastic waste and naturally-grown seaweed can be convert into crude vegetable oil using microwave vacuum pyrolysis. The ratio of ttwo compounds is 25:75 and the temperature is 500°C to get yield of bio-oil up to 68.9 wt% (Abomohra et al., 2021).

Parameters Influencing Biomass Pyrolysis

From various types of biomass, it's known that biomass affects the pyrolysis process and product. In addition, the mineral content and composition of the biomass also can be a reason that greatly affects the distribution and properties of the product because of its catalytic effect during the pyrolysis of biomass (Fahmi et al., 2008; Fahmi et al., 2007). The use of straw as raw material for pyrolysis is beneficial in obtaining bio-oil yields and reducing the cost of producing charcoal and gas (Guo et al., 2010).

From the varied types of materials used, it can be seen that wheat straw biomass produces

Table 2. Material and Method

References	Raw Material	Analysis	T (^{0}C)	Results
Xu-Jin et al., 2019	Rice straw and water hyacinth	TGA, GC-MS, FT-IR, NMR	400 ^{0}C	Bio-Oil : 44,4%
Varma et al., 2019	Wood sawdust	TA, FT-IR, GC-MS, NMR, FESEM	500 ^{0}C	Bio-Oil : 44,16%
Soni et al., 2020	Sawdust	TGA, GC-MS, FT-IR, NMR, SEM	500 ^{0}C	Bio-Oil : 41,05% Bio-Char : 27,59%
Gong et al., 2020	Microalgae	TGA, FTIR	570 ^{0}C	Bio-Oil : 39,99%
Mlonka-Medrala et al., 2021	Oat straw	TA, FTIR, micro-GC	600 ^{0}C	Bio-Oil : 56,9% Gas : 19%
Abomohra et al., 2021	Plastic Seaweeds	Analyzer, GC-MS, HHV	500 ^{0}C	Bio-Oil : 68,9%

Table 3. The reactor type and heating rate

References	Reactor type	Particle Size	Heating rate
Xu Jin et al., 2019	Fixed bed	-	20 ^{0}C/min
Varma et al., 2019	Semi batch	< 0.25 to > 1.7 mm	10 ^{0}C
Soni et al., 2020	Fixed bed	< 2 mm	-
Gong et al., 2020	Tube furnace	-	10 ^{0}C
Mlonka-Medrala et al., 2021	Semi-batch vertical	< 1 mm	50 ml/s
Abomohra et al., 2021	Fixed bed	< 3 mm	20 ^{0}C/min

the highest bio-oil products by 56.9% and gas by 19% with a temperature of 600 °C. Additionally, the highest biomass product was produced from a mixture of plastic and seaweed materials of 68.9% with a temperature of 500 °C.

The temperature in the pyrolysis process greatly affects the distribution and properties of the resulting a product (Horne & Williams, 1996; Westerhof et al., 2010) When the pyrolysis temperature exceeds 700°C, the amount carbon in the bio-oil increase in the form of polycyclic aromatic hydrocarbons, like pyrene and phenanthrene. This is due to decarboxylation and dehydration reactions (Akhtar & Amin, 2012). While the yield of bio-oil which reaches the highest concentration is at a temperature between 400°C and 500°C, which then the yield of the bio-oil will decrease after continued heating. When the temperature is above 600°C, the product in the sort of the bio-oil and charcoal becomes gas because of the dominant secondary cracking reaction (Li et al., 2007).

Particle size during the pyrolysis process greatly affects the ultimate result, therefore milling biomass into smaller particles is common way to prepare biomass before input to the reactor and increase pyrolysis performance, because the gradient of temperature across the particles will affect the mechanism of the pyrolysis of the biomass produced. To extend the resulting bio-oil product, The particle size must be smaller to get higher yield. Bigger diameter will increase the yield of charcoal and gas also because the density of charcoal and reduce the yield of bio-oil.

The heating rate wont to support the rapid fragmentation of the biomass produces more gas and produces less charcoal. Bio-oil production is increased at a quick heating rate because of reduced heat and mass transfer restrictions, and short time available for secondary reactions. The typical heating rate used during pyrolysis is 10 °C/min and 20°C/min. Many methods are used to analyze the pyrolysis products i.e Thermogravimetric analysis (TGA), gas chromatography and mass spectroscopy (GCMS), scanning electron microscope (SEM, thermal analysis (TA) and Fourier-transform infrared spectroscopy (FTIR). The use of different materials causes the yield obtained are also different.

Products of The Co-Pyrolysis Process

The liquid product of pyrolysis is bio-oil, dark brown natural liquid and can emerge as fuel for an extensive form of packages and emerge as a popular cloth for generating hydrocarbons that may be comfortably incorporated into current oil refineries or destiny biorefineries (Aysu & Sanna, 2015). These traits can motive destructive

Table 4. The raw material and their parameters

Raw Material	Analysis	Parameter
Rice straw Water hyacinth	TGA, GC–MS, FT-IR, NMR	• TGA : Weight (mg), Temperature (°C), heat rate (°C/menit). • GC-MS : Ratio, Temperature • FT-IR : Temperature • NMR : Chemical Shift (ppm)
Wood sawdust	TA, FT-IR, GC–MS, NMR, FESEM	• TA : Temperature (°C), heat rate (°C/menit). • FT-IR : Temperature • GC-MS : Ratio, Temperature • NMR : Chemical Shift (ppm) • FESEM : -
Sawdust	TGA, GC–MS, FT-IR, NMR, SEM	• TGA : Temperature (°C), Initial Weight Loss, Fluid Level • GC–MS : Ratio, Temperature, Retention Time • FT-IR : Wavenumber/cm, Transmitance (%) • NMR : Chemical Shift (ppm) • SEM :-
Microalgae	TGA, FTIR	• TGA : Temperature (°C), heat rate (°C/menit). • FTIR : Mass Recovery (%), Temperature (°C)
Oat straw	TA, FTIR, micro-GC	• TA : Temperature (°C), heat rate (°C/menit). • FTIR : Mass Recovery (%), Temperature (°C) • micro-GC : Ratio, Temperature, Retention Time
Plastic Seaweeds	TGA, Elemental Analyzer, GC–MS, HHV	• TGA : Temperature (°C), Mass loss rate (%/°C) • Elemental Analyzer : Temperature (°C), heat rate (°C/menit). • GC–MS : Temperature • HHV : Ratio

consequences on gasoline traits, together with low calorific value, decreased combustion efficiency, corrosion, and instability (Abnisa & Wan Daud, 2015). Furthermore, the highest yield of the bio-oil can be achieved with reformulate new methods or using putting off the oxygen (Hassan et al, 2016).

Wood-primarily based biomass, the use of a better lignin content material may also have a particularly better charcoal output. The impact of lignocellulosic compounds with inside the manufacturing of unstable substances has been studied appreciably through many researchers (Asadullah et al., 2008; Qu et al., 2011). The quantity of liquid product primarily based totally at the co-pyrolysis system may be predicted (low or excessive) while the biomass composition and the combination co-feed composition were stimulated typically the use of the proximate characterization evaluation method, which identifies 4 number-one biomass compositions: unstable be counted, constant carbon, moisture content material. , and ash content material. Volatile be counted and ash content material is the number one element which has an effect at the manufacturing of liquid output at some stage in pyrolysis. Many researchers said that the accelerated unstable era desired the

manufacturing of massive quantities of pyrolysis oil and led to excessive reactivity, however excessive ash content material (alkali metals) contributed to the lower in oil output, (Fei et al., 2012; Fahmi et al., 2008). The effects of the proximate evaluation of lignocellulosic biomass defined that the composition consists of cellulose, hemicellulose, and lignin as the number one component. Cellulose and hemicellulose play a crucial function in making unstable substances at some stage in pyrolysis however cellulose extra unstable than hemicellulose (Asadullah et al., 2008), main to a boom in oil output.

Production of bio-oil is the number one made from interest (Czernik et al., 1994), Bio-oil has been significantly examined as a candidate for combustion gasoline for the manufacturing of energy and warmth in boilers, furnaces, and combustion chambers (Freel et al., 1996; Gust, 1997), fuel line turbines (Crayford et al., 2010; Strenziok et al., 2001), and diesel engines (Chiaramonti et al., 2003), and. Bio-oil changed into effectively introduced to the diesel take a look at engine the usage of restricted working time, while long-time period operation changed into now no longer feasible because of negative bio-oil quality, eg negative volatility, excessive viscosity, excessive corrosiveness, and coke (Jembatan air, 1999).

Properties of Bio-Oil

The physical properties of bio-oil that need to be considered are solid content, pH, viscosity, and density (Soni & Karmee, 2020).

Table 5. The measurement for physical properties of bio-oil.

Parameter	measurement
Solid content	ASTM D7579-09
pH	pH meter
viscosity	ASTM D 445
density	density analyzer

Bio-oil contains more than 400 components such as aldehydes, ketones, alcohols, phenols and oligomers (Joshi & Lawal, 2012) and usually contains wood biomass materials such as 30% of phenolics, 20% of aldehydes and ketones, 15% of alcohol and 30% of water. The other properties of bio-oil are high oxygen content, bio-oil and water emulsion, low energy density, low pH and the presence of trapped char (Perkins et al., 2018).

Crude bio-oil is generally contained 20-30 %wt. of water from total product (Lede et al., 2006). Bio-oil can also be relied on to be a 2-phase microemulsion using pyrolytic lignin macromolecules dispersed in a continuous liquid phase. Hydrochloric acids, aldehydes, and oligomers cause water and oxygen content in crude bio-oil higher, which makes up the low energy density (Perkins et al., 2018).

Benefits of Bio-Oil

Bio-oil can be used as diesel fuel or used as raw material in the petrochemical industry (Varma et al., 2019), power generation, transportation, and chemical production (Anil et al., 2019). The bio-oil containing chemicals such as phenol, furfural, and cresol can be used as a standard material in various applications. Phenol and its derivatives can be used to make phenolic resins, bisphenol-A, and caprolactam, intermediate products to produce nylon adhesives, synthetic fibers, and plywood (Lazzari et al., 2016). Bio-oil can be used as a binder for the manufacture of briquettes and pallets based on combustible organic waste. In general, bio-oil can now be used as fuel for combustion, power generation, transportation, and chemical production (Anil et al., 2019).

CONCLUSION

Biomass waste is a promising energy source and has high potential as a liquid, solid, or gas energy source. Then pyrolysis is a promising technology to convert various lignocellulosic biomass into renewable energy. The pyrolysis products and their properties vary widely based on the composition and structure of the feedstock, and the process temperature, heating rate, and residence time. The advantages of this pyrolysis process are that it can reduce biomass waste in the environment into a fuel product or energy source, then the drawbacks of the pyrolysis process are that it cannot use a high oxygen content, has a low ph due to the presence of carboxylic acids, and if the temperature is too high, high, the production of bio-oil obtained will decrease and produce people will increase. Accelerated instability requires the manufacture of large quantities of pyrolysis oil and causes excessive reactivity, but excessive ash content (alkali metals) contributes to lower oil production.

Table 5. Raw material, parameter and the products

Author	Raw Material	Parameter Involved	Information Extracted	C
Mlonka-Medrala et al., 2021	oat straw	• Particle Size : <1 mm • residence time : 1-38 s • heating rate 50 ml/s • Reactor : semi-batch vertical • pressure • heating time on the yield of pyrolysis products • Temperature : 300°C, 400°C, 500°C, 600°C	• The material was collected from the Polish market • Increase temperature will increase the quality of the pyrolysis gas. The highest concentrations of the most valuable compounds such as methane and hydrogen were obtained at 600◦C. • The elements that detected in the raw fuel and chars are carbon (43.97 wt.%), hydrogen (6.16 wt.%), a little nitrogen and sulfur (0.11 wt.%) • The identification of the chemical bonds in the raw biomass and chars, and analysis of the changes in functional groups was done by FTIR and GCMS	57%
Soni et al., 2020	sawdust	• Effect of temperature variations 400-600°C • Particle Size : <2 mm • Reactor : fixed bed • heating rate • flow rate is constant • the split ratio was 20:1 • types of batch and continuous reactors on the yield of bio-oil, bio-char and pyrogas	• Raw material is from India • higher lower heating value (LHV, over 21MJ/kg, much higher than that of Ba) • elemental composition shows significant difference. Ba contains much higher oxygen content (43.18 wt.%) • The optimum temperature for sawdust pyrolysis was found at 500 °C using a batch reactor; produce bio-oil (34.9 wt%), bio-char (38.6 wt%) and pyro-gas (26.5 wt%) • Use of a vertical moving bed type continuous reactor with temperature of 500 °C increase yields	41%

Author	Raw Material	Parameter Involved	Information Extracted	C
			of products to bio-oil (41.05 wt%), bio-char (27.59 wt%) and pyro-gas (31.36 wt%)	
Gong et al., 2020	Microalgae	• Effect of temperature at 400-600°C • heating rate: 10°C /min • flow rate: 100 mL/min • Reactor : Tube furnace • The blending ratio of catalysts was 5 wt % • catalyst on bio-oil yield	• Oil components were get at 600 °C . • The content of gasoline components in pyrolysis oil rise with addition of KCl, MgO and Al_2HAI_3 • The addition of catalysts can effectively enhance the amount of CO and CHs and diminish CO_2 in the same time • elements (Na, K, Ca, Mg, Fe, Al) • HHV-High heating value : 8.98 MJ/Kg	-
Xu Jin et al., 2019	• Rice straw • Water hyacinth	• Temperature: 300 °C, 350°C, 400°C, 450°C • Reactor : fixed bed • stream rate for the segment: 1 mL/min • the split ratio: 20:1 • heating rate of 20°C/min and residence time	The yield of bio-oil increased by 24.7 wt% for WH and 28.2 wt% RH at temperature of 300 °C to 400 °C. At temperature above 400 °C, bio-oil was decreased • Co-pyrolysis of rice straw and water hyacinth in a 5:5 ratio, at temperature of 400 °C.is a valid technique for bio-oil preparation which gives higher yields than 44.4%	44,4%
Varma et al., 2019	• wood sawdust	• Temperature : 350-650°C • heating rate : 10 °C/min • flow rate : 200 cm3/min • particle size : <0.25 to >1.7 mm • Reactor : semi batch	• The gaseous products with composition (mol): 46.6% CO, 34.8% CO_2, 6.7% H_2, and 11.9% CH_4.were achieved at pyrolysis temperature of 500°C. • alkenes, alkanes, aromatics and many other chemical compounds were found with analyzing by FTIR	-
Abomohra et al., 2021	• Plastic • seaweeds	• Temperature : 400-600°C	• . HHV of bio-oil quality is influenced by the elemental composition	-

Author	Raw Material	Parameter Involved	Information Extracted	C
		• heating rate : 20 °C/min • particle size : < 3 mm • Reactor : fixed bed	• HHV of the bio-oil from 75% LDPE blend ratio is 2.3%, 10.0% higher than the maximum values of diesel and petroleum oil and 2.1% higher than the maximum HHV obtained from co-pyrolysis of HDPE with seaweeds	

ACKNOWLEDGEMENTS

The authors convey thank to Directorate General of Higher Education, Research and Technology which provided funding for the preparation of this article through The International Credit Transfer Program 2021.

REFERENCES

€zsin, G., Pütün, A. E. 2018. A comparative study on co-pyrolysis of lignocellulosic biomass with polyethylene terephthalate, polystyrene, and polyvinyl chloride: Synergistic effects and product characteristics. 205(December): 1127-1138.

Abnisa, F., Arami-Niya, A., Daud, W. W., Sahu, J. N., Noor, I. M. 2013. Utilization of oil palm tree residues to produce bio-oil and bio-char via pyrolysis. Energy Conversion and Management. 76(December): 1073-1082

Abnisa, F., Wan Daud, W. M. A. 2015. Optimization of fuel recovery through the stepwise co-pyrolysis of palm shell and scrap tire. Energy Conversion and Management . 99: 334- 345.

Abomohra, A. E. F., Sheikh, H. A. M., Naggar, A. H. E. N., Wang, Q. 2021. Microwave vacuum co-pyrolysis of waste plastic and seaweeds for enhanced crude bio-oil recovery: Experimental and feasibility study towards industrialization. Renewable and Sustainable Energy Reviews. 149: 1-13.

Agarwal, A. K. 2007. Biofuels (alcohols and biodiesel) applications as fuels for internal combustion engines. Progress in Energy and Combustion Science. 33: 233-271.

Akhtar, J., Amin, N. S. 2012. A review on operating parameters for optimum liquid oil yield in biomass pyrolysis. Renewable Sustainable Energy Review. 16: 5101–5109.

Anil, K. V., Lokendra, S. T., Ravi, S., Prasenjit, M. 2019. Pyrolysis of wood sawdust: Effects of process parameters on products yield and characterization of products. Uttarakhand, India. 89: 224-235

Antal, M. J. 1983. Biomass pyrolysis: a review of the literature part-1—carbohydrate pyrolysis. Advance Solar Energy. 1: 61–109.

Arami-Niya, A., Abnisa, F., Sahfeeyan, M. S., Daud, W. W., Sahu, J. N. 2011. Optimization of synthesis and characterization of palm shell-based bio-char as a by-product of bio-oil production process. BioResources. 7 (1): 246–264.

Arturi, K. R., Toft, K. R., Nielsen, R. P., Rosendahl, L.A., Søgaard, E. G. 2016. Characterization of liquid products from hydrothermal liquefaction (HTL) of biomass via solid-phase microextraction (SPME). Bioenergi Biomassa. 88:116-125.

Asadullah, M, Rahman A. M., Ali, M. M., Motin, A. M., Sultan, B. M., Alam, M. R. 2008. Jute stick pyrolysis for bio-oil production in fluidized bed reactor. Bioresource Technology. 99:44–50.

Aysu, T., Sanna, A. 2015. Nannochloropsis algae pyrolysis with ceria-based catalysts for production of high-quality bio-oils. Teknologi Sumber Daya Hayati. 194: 108-116.

Azargohar, R., Jacobson, K. L., Powell, E. E., Dalai, A. K. 2013. Evaluation of properties of fast pyrolysis products obtained, from Canadian waste biomass. Journal of Analytical and Applied Pyrolysis. 104(November): 330-340.

Balagurumurthy, B., Bhaskar, T. 2014. Hydropyrolysis of lignocellulosic biomass: state of the art review. Biomass Conversion and Biorefinery. 4:67-75.

Bank, S. W., Bridgwater, A. V. 2016. Catalytic fast pyrolysis for improved liquid quality. Handbook of Biofuels Production (Second Edition); pp. 391-429.

Basu, P. 2018. Biomass gasification. Pyrolysis and Torrefaction. Elsevier Inc. Academic Press.

Bridgewater, A., Grassi, G. 1991. Biomass Pyrolysis Liquids Upgrading and Utilisation. Elsevier Applied Science, England.

Burra, K. G., Gupta, A. K. 2018. Kinetics of synergistic effects in co-pyrolysis of biomass with plastic wastes. Applied Energy. 220(June): 408-418

Butler, E., Devlin, G., Meier, D., McDonnell, K. 2011. A review of recent laboratory research and commercial developments in fast pyrolysis and upgrading. Renewable Sustainable Energy Review. 15:4171-4186.

Chiaramonti, D., Bonini, A., Fratini, E., Tondi, G., Gartner, K., Bridgwater, A. V. 2003. Development of emulsions from biomass pyrolysis liquid and diesel and their use in engines—Part 2: tests in diesel engines. Bioenergi Biomassa. 25:101–111.

Chum, H. L., Overend, R. P. 2001. Bioamss and renewable fuels. Fuel Processing Technology. 71: 187–195.

Crayford, A. P., Bowen, P. J., Kay, P. J., Laget, H. 2010. Comparison of Gas-Oil and Bio-Oil Spray Performance for Use in a Gas Turbine.In: Prosiding ASME Turbo Expo. 1: 659–667.

Czernik, S., Johnson, D. K., Black, S. 1994. Stability of wood fast pyrolysis oil. Bioenergi Biomassa. 7:187–192.

Demirbas, M. F. 2009. Biorefineries for biofuel upgrading: A critical review. Applied Energy. 86: S151-S161.

Deng, S., Tan, H., Wang, X., Yang, F., Cao, R., Wang, Z., Ruan, R.. 2017. Investigation on the fast co-pyrolysis of sewage sludge with biomass and the combustion reactivity of residual char, arang. Bioresource Technology. 239: 302-310

Duanguppama, K., Suwapaet, N., Pattiya, A., 2016. Rapid pyrolysis of contaminated sawdust in a circulating fluidized bed reactor. Journal of Analytical and Applied Pyrolysis. 118(March): 63-74

Eom, M., Lee, S., Yoo, K., Park, Y.-K., Lee, J., Kim, J. 2013. Production of bio oil by using larch sawdust in a bubbling fluidized bed reactor. Energy Sources Part A. 35 (13): 1225–1232.

Fahmi, R., Bridgwater, A. V., Darvell, L. I., Jones, J. M., Yates, N., Thain, S. 2007. The effect of alkali metals on combustion and pyrolysis of Lolium and Festuca grasses, switchgrass and willow. Fuel. 86: 1560–1569.

Fahmi, R., Bridgwater, A. V., Donnison, I., Yates N., Jones, J. M. 2008. The effect of lignin and inorganic species in biomass on pyrolysis oil yields, quality and stability. Fuel. 87: 1230–1240.

Farzad, S., Mandegari, M. A., Gorgens, J. F. 2016. A critical review on biomass gasification, co-gasification, and their environmental assessments. Biofuel Resource Journal. 3: 483-495.

Fei, J., Zhang, J., Wang, F., Wang, J. 2012. Synergistic effects on co-pyrolysis of lignite and high-sulfur swelling coal. Journal of Analytical Applied Pyrolysis. 95: 61–67.

Freel, B. A., Graham, R. G., Huffman, D. R. 1996. Commercial aspects of rapid thermal processing (RTM). In: Bridgwater AV, Hogan E, editor. Production and utilization of bio-oil. Newbury, Inggris: CPL Press. pp. 86–95.

Gollakota, A. R. K., Reddy, M., Subramanyam, M. D., Kishore, N. 2016. Review Teknik Upgrade Minyak Pirolisis, Renew. Mempertahankan. Energi Review. 58 (2016): 1543-1568.

Gong, Z., Fang, P., Wang, Z., Li, Q., Li, X., Meng, F., Zhang H., Liu, L. 2020. Catalytic pyrolysis of chemical extraction residue from microalgae biomass. Renewable Energy. 148: 712-719.

Gumba, R. E., Saallah, S., Misson, M., Ongkudon, C. M., Anton, A. 2016. Green biodiesel

production: a review on feedstock, catalyst, monolithic reactor, and supercritical fluid technology. Biofuel Reseaerch Journal. 3(3):431-447.

Guo, X., Wang, S., Wang, K., Liu, Q., Luo, Z. 2010. Influence of extractives on mechanism of biomass pyrolysis. Journal of Fuel Chemistry and Technology. 38: 42–46.

Guo, Y., Yeh, T., Song, W., Xu, D., Wang, S. A. 2015. review of bio-oil production from hydrothermal liquefaction of algae. Renew Sustainable Energy Review. 48: 776-790.

Gust, S. 1997. Combustion Experiences of Flash Pyrolysis Fuel in Intermediate Size Boilers In: Bridgwater AV, Boocock DGB, editor. Developments in thermochemical biomass conversion. London: Blackie Academic & Profesional. pp. 481–488.

Hagos, K., Zong, J., Li, D., Liu, C., Lu, X. 2016. Anaerobic co-digestion process for biogas production. Renewable and Sustainable Energy Reviews. 76: 148514-96.

Hassan, H., Lim, J. K., Hameed, B. H. 2016. Recent progress on co-pyrolysis conversion into high-quality bio-oil. Bioresource Technology. 221: 645-655.

Horne, P. A., Williams, P. T. 1996. Influence of temperature on the products from the flash pyrolysis of biomass. Fuel. 75: 1051–1059.

Huber, G., Iborra, S., Corma, A. 2006. Synthesis of Transportation Fuels from Biomass: Chemistry, Catalysts, and Engineering. Chemal Reviews. 106: 4044-4098.

Idris, R., Chong, C. T., Asik, J. A., Ani, F. N. 2020. Optimization studies of microwave-induced co-pyrolysis of empty fruit bunches/waste truck tire using response surface methodology. Journal of Cleaner Production. 244(2): 118649

Jembatan-air, A. V. 1999. Principles and practice of biomass fast pyrolysis processes for liquids. Joournal of Analytical Applied Pyrolysis. 51: 3–22.

Jones, S. B., Holladay, J. E., Valkenburg, C., Stevens, D. J., Walton, C. W., Kinchin, C.. 2009. Production of Gasoline and Diesel from Biomass Via Fast Pyrolysis, Hydrotreating and Hydrocracking: A Design Case. Pacific Northwest National Lab.

Joshi, N., Lawal, A. 2012. Hydrodeoxygenation of pyrolysis oil in a microreactor. Chemical Engineering Science . 74:1–8.

Kabir, G., Hamid, B. H.2017. Recent progress on catalytic pyrolysis of lignocellulosic biomass to high-grade bio-oil and bio-chemicals. Renewable and Sustainable Energy Review. 70: 945-967.

Khan, A. A., de Jong, W., Jansens, P. J., Spliethoff, H. 2009. Biomass combustion in flui- dized bed boilers: potential problems and remedies. Fuel Process Technology. 90: 21–50.

Lazzari, E., Schena, T., Primaz, C. T., da Silva Maciel, G. P., Machado, M. E., Cardoso, C. A. L., Jacques, R. A., Caramão, E. B. 2016. Production and chromatographic characterization of bio-oil from the pyrolysis of mango seed waste. Industrial Crops and Products. 83: 529–536.

Lede, J., Broust, F., Ndiaye, F.-T., Ferrer Monique. 2007. Properties of bio-oils produced by biomass fast pyrolysis in a cyclone reactor. Fuel. 86: 1800–1810.

Lee, S. –H., Eom, M. S., Yoo, K.-S., Kim, N.-C., Jeon, J.-K., Park, Y.-K. 2008. The yields and composition of bio-oil produced from Quercus Acutissima in a bubbling fluidized bed pyrolyzer. Journal of Analytical Applied Pyrolysis. 83(1): 110–114.

Li, J., Yan, R., Xiao, B., Wang, X. L., Yang, H. P. 2007. Influence of temperature on the formation of oil from pyrolyzing palm oil wastes in a fixed bed reactor. Energy Fuels. 21: 2398–407.

Lin, B., Huang, Q., Chi, Y. 2018. Co-Pyrolysis Characteristics and Kinetic Analysis of Oil Sludge with Different Additives Journal of Thermal Science. 30: 1452–1467.

Linck, M., Felix, L., Marker, T., Roberts, M. 2014. Integrated biomass hydropyrolysis and hydrotreating: a brief review. WIREs Energy and Environment. 3: 5755-81.

Lu, Q., Li, W. Z., Zhu, X. F. 2009. Overview of fuel properties of fast pyrolysis of oil biomass. Energy Conversion and Management. 50(5): 1376-1383

Magdziarz, A., Wilk, M., Wadrzyk, M. 2020. Pyrolysis of hydrochar derived from biomass – Experimental investigation. Fuel. 267: 117246.

Maity, S. K. 2015. Opportunities, recent trends and challenges of integrated biorefinery: Part II. Renewable and Sustainable Energy Reviews Review. 43: 1446-1466.

Mante, O. D., Agblevor, F. A., McClung, R. 2011. Fluid catalytic cracking of biomass pyrolysis vapors. Biomass Conversion and Biorefinery. 1: 189-201.

McKendry, P. 2002. Energy production from biomass (Part 1): Overview of biomass, Bioresource Technology . 83(1): 37-46.

Mishra, R. K., Mohanty, K. 2020. Kinetic analysis and pyrolysis behaviour of waste biomass towards its bioenergy potential. Bioresource Technology. 311: 123480.

Mlonka-Mędrala, A., Evangelopoulos, P., Sieradzka, M., Zajemska, M., Magdziarz., A. 2021. Pyrolysis of agricultural waste biomass towards production of gas fuel and high-quality char:Experimental and numerical investigations. Fuel. 296: 120611.

Muneer, B., Zeeshan, M., Qaisar, S., Razzaq, M., Iftikhar, H. 2019. Influence of in-situ and ex-situ HZSM-5 catalyst on co-pyrolysis of corn stalk and polystyrene with a focus on liquid yield and quality. July 2019. Journal of Cleaner Production. 237(3): 117762.

Park, D. K., Kim, S. D., Lee, S. H., Lee, J. G. 2010. Co-pyrolysis characteristics of sawdust and coal blend in TGA and a fixed bed reactor. Bioresource Technology. 101(15): 6151–6156.

Park, Y.-K., Jung, J., Ryu, S., Lee, HW, Siddiqui, MZ, Jae, J., Watanabe, A., Kim, Y.-M., 2019. Catalytic Pyrolysis of Waste Polyethylene Terephthalate over Waste Concrete. Applied Chemistry for Engineering. 30(6): 707-711.

Perkins, G.,Bhaskar, T., Konarova, M. 2018. Process development status of fast pyrolysis technologies for the manufacture of renewable transport fuels from biomass. 90: 292-315.

Pode, R. 2016. Potential applications of rice husk ash waste from rice husk biomass power plant, Renewable and Sustainable Energy Reviews. 53: 1468-1485.

Pothiraj, C., Arun, A., Eyini, M. 2015. Simultaneous saccharification and fermentation of cassava waste for ethanol production. Biofuel Research Journal 2(1): 196-202.

Probstein, R. F., Hicks, R. E. 1982. Synthetic Fuels. McGraw-Hill Book Company, New York.

Qu, T., Guo, W., Shen, L., Xiao, J., Zhao, K. 2011. Experimental Study of Biomass Pyrolysis Based on Three Major Components: Hemicellulose, Cellulose, and Lignin. Industrial & Engineering Chemistry Research.50: 10424–10433.

Roy, P., Dias, G. 2017. Prospects for pyrolysis technologies in the bioenergy sector: A review. Renewable and Sustainable Energy Review. 77: 59-69.

Salehi, E., Abedi, J., Harding, T. 2009. Bio-oil from Sawdust: Pyrolysis of Sawdust in a Fixed-Bed System. Energy Fuel. 23(7): 3767–3772.

Samburova, V., Connolly, J., Gyawali, M., Yatavelli, R. L., Watts, A. C., Chakrabarty, R. K. 2016. Polycyclic aromatic hydrocarbons in biomass-burning emissions and their contribution to light absorption and aerosol toxicity. Science of the Total Environment. 568: 391–401.

Sansaniwal, S. K., Rosen, M. A., Tyagi, S. K. 2017. Global challenges in the sustainable development of biomass gasification: An overview. Renewable and Sustainable Energy Review. 80: 23-43.

Saxena, R. C., Adhikari, D. K., Goyal, H. B. 2009. Biomass-based energy fuel through biochemical routes: A review. Renewable and Sustainable Energy Reviews. 13:167-178.

Soni, B., Karmee, S. K. 2020. Towards a continuous pilot scale pyrolysis based biorefinery for production of biooil and biochar from sawdust. Gujarat, India. pp. 1-11.

Strenziok, R., Hansen, U., Künster, H. 2001. Combustion of Bio-Oil in a Gas Turbine. In: Bridgwater AV, editor. Advances in thermochemical biomass conversion. Wiley Online Library. pp. 1452–1458.

UNFCC. 2015. Proposal by the President. Paris Climate Change Conference – November 2015, COP 21. Paris, France.

Uzoejinwa, B., He, X, Wang, S., Abomohra, A. E. F., Hu, Y, Wang, Q. 2018. Co-pyrolysis of biomass and waste plastics as a thermochemical conversion technology for

high-grade biofuel production: Recent progress and future directions elsewhere worldwide. 163: 468-492.

Varma, A. K., Mondal, P. 2016. Physicochemical characterization and pyrolysis kinetics of wood sawdust . Energy Sources, Part A: Recovery, Utilization, and Environmental Effects. 38(17): 2536-2544.

Venderbosch, R. H. 2015. A critical view on catalytic pyrolysis of biomass. ChemSusChem. 8(8): 1306-1316.

Wang, T., Chen, Y., Li, J., Xue, Y., Liu, J., Mei, M., Hou, H., Chen, S. 2020. Co-pyrolysis behavior of sewage sludge and rice husk by TG-MS and residue analysis. Journal of Cleaner Production. 250: 1048-1066.

Westerhof, R. J. M., Brilman, D. W. F., van Swaaij, W. P. M., Kersten, S. R.A. 2010. Effect of temperature in fluidized bed fast pyrolysis of biomass: oil quality assessment in test units. Industrial & Engineering Chemistry Research. 49: 1160–1168.

Wu, Z., Yang, W., Tian, X., Yang, B., 2017. Synergistic effects from co-pyrolysis of low-rank coal and model components of microalgae biomass. Energy Conversion and Management. 135: 212-225

Xu-Jin, N., Chen-yang, Z., Deng-yin, G., Yan-hui, H., Qi-min, X., Yu-hong. 2019. Co-pyrolysis of rice straw and water hyacinth: Characterization of products, yields and biomass interaction effect. Biomass and Bioenergy. 127: 105281

Yildiz, G., Ronsse, F., Duren, R. van, Prins, W. 2016. Challenges in the design and operation of processes for catalytic fast pyrolysis of woody biomass. Renewable and Sustainable Energy Reviews. 57: 1596-1610.

JBAT 11(1) (2022) 50 – 57

Jurnal Bahan Alam Terbarukan

Accredited SINTA 2 by Ministry of Research and Technology/National Research and Innovation Agency
SK No. 200/M/KPT/2020
http://journal.unnes.ac.id/nju/index.php/jbat

p-ISSN 2303 0623
e-ISSN 2407 2370

Study of Sonocatalytic Activity ZnO-WO_3 Composite on Degradation Phenol in Aqueous Solution

Noor Hindryawati[1,2,✉], Gaanty Pragas Maniam[3], Irvan Resi Pratama[1], Rahmat Gunawan[1]. Soerja Koesnarpadi[1]

DOI: https://doi.org/10.15294/jbat.v11i1.37475

[1] Faculty of Mathematics and Natural Sciences, Mulawarman University, Samarinda, East Kalimantan, Indonesia
[2] Inorganic Laboratory, Chemistry Department, Faculty of Mathematics and Natural Sciences, Mulawarman University, Samarinda, East Kalimantan, Indonesia
[3] Faculty of Industrial Sciences and Technology, Universiti Malaysia Pahang, Lebuhraya Tun Razak, 26300 Gambang, Kuantan, Pahang, Malaysia

Article Info

Article history:
Received
April 2022
Accepted
June 2022
Published
June 2022

Keywords:
WO_3;
ZnO;
Phenol;
Sonocatalysis

Abstract

Sonocatalysis was used to study phenol degradation using a ZnO/WO_3 composite. The degradation was assisted by ultrasonic waves at 40 KHz and conducted using the sonocatalysis technique. The degradation percentage was calculated using data from the UV-Vis spectrophotometer. The composite characterization results showed that the samples containing WO_3, ZnO and also contained a new structure $ZnWO_4$. The morphological length and width of the composites were revealed by SEM examination. Furthermore, heterogeneous particle sizes were discovered. The surface area of composite was bigger than before combined. The optimum condition in degradation of phenol by ZnO-WO_3 composite are 0,4 g of catalyst at 30 ppm of phenol, 7 min reaction time with the greatest phenol degradation at 92,5%. The catalyst can be reused 5 times to degrade phenol at 85%. The composite catalyst and assisted with ultrasonic as the sonocatalytic technique are one of the most environmentally and cost effective.

INTRODUCTION

The expansion of the industrial sector results in an increase in polluting chemicals in the environment (Chung & Chen, 2009). Herbicides, fungicides, coal gasification, paper mills, coke factories, resin polymer manufacturing, oil refining, paint industries, textile, food processing industry, and biotechnology all produce phenol, a hazardous hydroxyl benzene compound (Borji et al., 2014). Phenol can induce skin burns, central nervous system paralysis, and a significant drop in body temperature, as well as damage to internal systems such as the kidneys, liver, spleen, lungs, and heart (Rappoport, 2003). At quantities of 5-25 mg/L, phenol toxicity can harm aquatic microorganisms and kill fish. The content of phenol in drinking water should not exceed 1 g/L, and in waterways should not exceed 1 mg/L, according to World Health Organization rules (Yunus et al., 2017). Therefore, it is necessary to develop an effective and efficient organic waste treatment method.

Organic contaminants in liquid waste have been degraded using a variety of methods. In particular, there are three different types of traditional ways for dealing with liquid waste. Physical, chemical, and biological techniques are the three types. Adsorption, filtration, and reverse osmosis are physical techniques. Ion exchange and extraction are chemical techniques, whereas aerobic and anaerobic processes are biological ones (Mozia et al., 2005). These three techniques, however, each have their own set of drawbacks. These three approaches generate waste and are not

✉ Corresponding author:
E-mail: hindryawati@gmail.com

cost-effective (Kumar et al., 2012). Several studies have investigated that *Advanced Oxidation Processes* (AOPs) having the potential to oxidize organic pollutants without producing *secondary waste* (Azbar et al., 2004).

The sonocatalytic technique is one of the most environmentally benign AOPs, because it generates CO_2 and H_2O. Typically, this technique uses ultrasonic vibrations and a catalyst to breakdown organic compounds in aqueous medium. The cavitation effect bubbles produced by the liquid under ultrasonic radiation are the basis for this technique. It has the ability to collect sound energy and collapse to release energy in a very short amount of time, while also having a high temperature and pressure (Li et al., 2018).

TiO_2, ZnO, CdS, Fe_2O_3, and WO_3 are some of the most often used catalysts. Tungsten trioxide (WO_3) is a semiconductor material that can accelerate the degradation process under visible radiation. Tungsten (VI) oxide, also known as tungsten trioxide or tungstate anhydride, is a chemical compound containing oxygen and tungsten. Tungsten trioxide (WO_3) has a very good ability under visible light irradiation with better absorption ability than other semiconductors because WO_3 has a band gap of about 2.7 – 2.8 eV which makes it more sensitive to visible light (Sajjad et al., 2018). Meanwhile, zinc oxide (ZnO) is known as an ideal and suitable catalyst because it is stable, inexpensive and environmentally friendly (Hunge et al., 2018). The combination of these two components has a beneficial role in increasing the charge separation and ZnO response in ultrasonic radiation so that high catalyst efficiency can be obtained in the separation of organic particles (Meng et al., 2014). Thus, the goal of this study is to create a ZnO-WO_3 composite material with increased sonocatalytic activity against phenol degradation.

MATERIALS AND METHODS

Materials

The materials used in this research are ZnO, WO_3, $K_3Fe(CN)_6$, NH_4OH, phosphate buffer, 4-*Aminoantipyrine*, Ethanol, Phenol (All chemicals were purchased from Sigma-Aldrich), distillate water, Whatman paper.

ZnO-WO_3 Preparation and Characterizations

10 mL of ethanol is added to a solid mixture of 5g ZnO and 14,2g WO_3. This combination was allowed to sit for 3 hours till it turned into powder. It was then dried for 24 hours at 100°C in an oven. Crushed in a mortar and then filtered through a 150-mesh filter and furnaced in 800°C for 8 hours. After that, this sample was characterized. The structure of material characterizes using X-ray diffraction (Rigaku) with Cu Kα X-ray as a source. The morphology of catalyst was observed by JEOL JSM-6700F SEM and surface analysis of the catalyst was examined by using Micromeritics ASAP 2000.

Maximum Wavelength Determination

50 mL of Phenol solution was added with 2.5 mL of 0.5N NH_4OH then added phosphate buffer solution, 1 mL of 8% aminoantipyrine and 1 mL of $K_3Fe(CN)_6$. It was then analyzed by using a UV-Vis spectrophotometer in a range 200-800 nm wavelength in order to obtain the maximum Phenol wavelength.

Standard Curve of Phenol

1000 ppm phenol solution was diluted to 100 ppm. Then the 100 ppm Phenol solution was diluted with various concentrations of 2, 4, 6, 8 and 10 ppm. The solution is then measured its absorbance using a UV-Vis Spectrophotometer at the optimum wavelength (664 nm) that has been obtained.

Phenol Degradation By Sonocatalytic Test Using ZnO-WO_3 Catalyst

Variation Weight of ZnO-WO_3 Catalyst

ZnO-WO_3 as much as 0.1, 0.2, 0.3, 0.4 and 0.5g were put into 50 mL of 30 ppm Phenol.They were then placed into the sample container and exposed to ultrasonic wave. After that, they were filtered and taken as much as 1 mL. The absorbance was measured using a UV-Vis Spectrophotometer at the maximum wavelength (664 nm). The percentage of degradation is calculated.

Effect Reaction Duration

A total of 0.4 grams of ZnO-WO_3 was put into 50 mL of 30 ppm Phenol. It was placed into the sample container before being placed in a sonicator

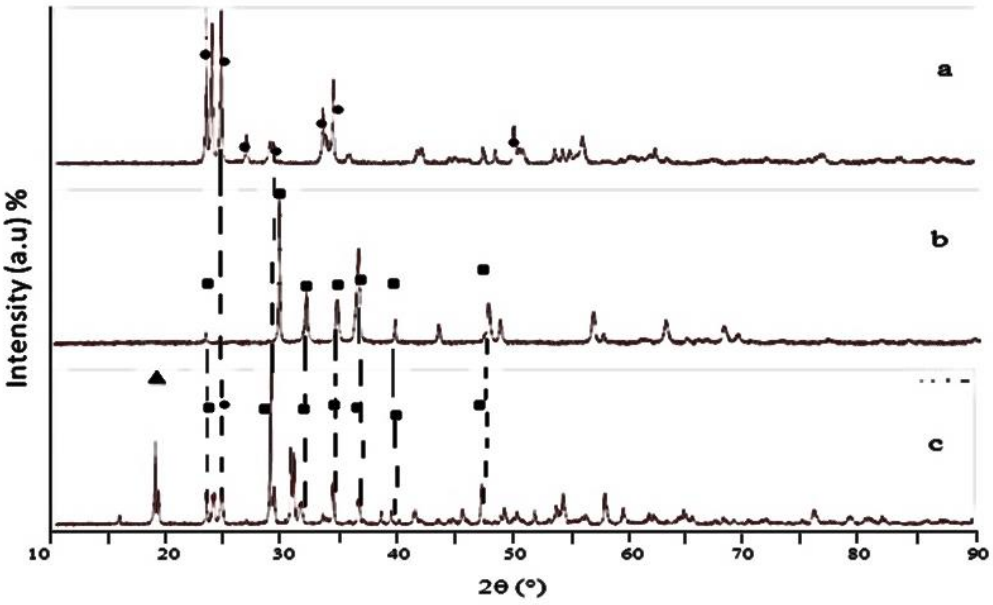

Figure 1. The XRD Result of (a)WO_3 (●), (b) ZnO (■) and (c) ZnO-WO_3 (▲)

(ultrasonic waves at 40kHz) for 3, 5, 7, 9, 13 minutes time variations. After that, it was centrifuged to separate and the filtrate was taken as much as 1mL. The absorbance was measured using a UV-Vis Spectrophotometer. The percentage of degradation is calculated.

Effect of Phenol Concentration

A total of 0.4 grams of ZnO-WO_3 were put into 50mL was added to various concentrations of 10, 20, 30, 40 and 50 ppm phenol solution. It was placed into the sonicator in the optimum contact time that has been decided. It was then separated and taken as much as 1 mL of the filtrate. The absorbance was measured using a UV-Vis Spectrophotometer and the degradation percentage was calculated.

The Effectiveness Test of ZnO-WO_3 Catalyst Reusability and Material Type in Phenol Degradation

The ZnO-WO_3 composite was tested for reusability by separating ZnO-WO_3 from phenol and washing it with distilled water several times. It was then dried for 1 hour at 120°C in the oven before being calcined for 2 hours at 800°C. Furthermore, ZnO-WO_3 was reused for phenol degradation.

Variations in material types were carried out to determine the performance of the material by comparing ZnO, WO_3 and ZnO-WO_3 using the optimum conditions obtained previously against.

Data Analysis

The data was obtained by measuring absorbance in a UV-Vis Spectrophotometer based on ZnO-WO_3 changes in contact time, concentration, and weight in degrading Phenol in order to compute the degradation percentage by the formula below where are the c_0 is initial concentration and c_e is final concentration:

$$\% \text{ Degradation} = \frac{CO - Ce}{CO} \; x \; 100\% \qquad (1)$$

RESULTS AND DISCUSSION

Catalyst Characteristics

XRD was used to determine if the structure of ZnO and WO_3 was changing or whether a new ZnO-WO_3 composited diffraction peak had appeared. In figure 1 (a), the diffraction pattern at 2θ = 29.42°, 34.41°, 35.95°, 36.22°, 39.43°, 47.18°, 48.52°, and 57.42° was indicating that the material is WO_3 refer to JCPDS No. 43-1035, where the WO_3 has a monoclinic structure. Furthermore, based on the research of Shakya et al. (2017) there are some similarities in the diffraction pattern which indicates the material is WO_3. The diffraction pattern peak at 2θ= 23.60°, 26.60°, 28.92°, 33.58°, 34.15°, 50.32°, and 55.88° is shown in figure 1 (b), which is based on the standard data JCPDS No. 36-1451 the compound was ZnO with the hexagonal structure. This data was similar with Yu et al. (2011) there are some similarities in diffraction patterns which indicate the material is

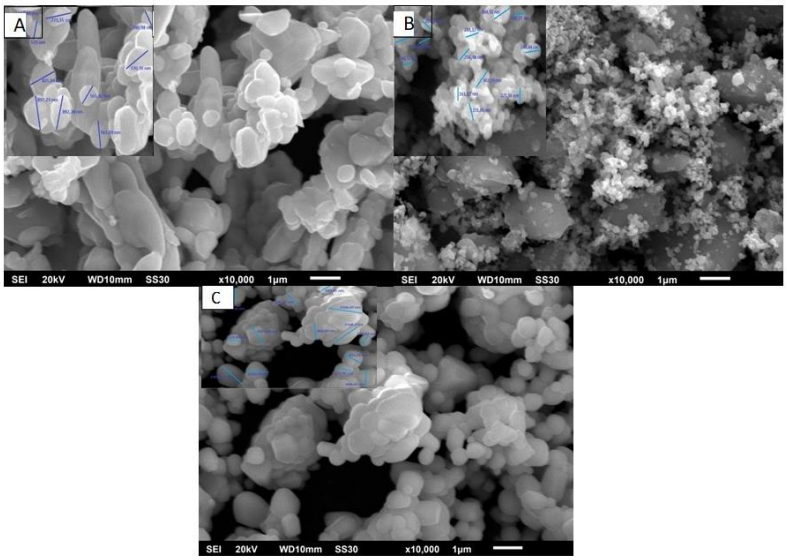

Figure 2. SEM image of (a) WO_3, (b) ZnO, and (c)ZnO-WO_3

ZnO. Figure 1(c) is after WO_3 and ZnO were composited, the XRD data was shows a new compound diffraction pattern $ZnWO_4$ at 2θ =18,62. This new ZnO-WO_3 diffraction peak is compared to the standard data JCPDS No. 73-544 explaining ZnO-WO_3 having monoclinic structure. The ZnO-WO_3 composite synthesized by solid method shows a constant ZnO and WO_3 diffraction peak, however it has a lower intensity than before it was composited. The diffraction of WO_3 at 2θ = 23.12°, 24.37°, 28.92°, 33.26°, 34.16°, 50.69°, 55.88°. The ZnO diffraction at 2θ = 23.82°, 29.42°, 31.74°,34.41°, 36.22°, 39.43°,48.52°, 57.42°.

In addition, SEM examination was performed to determine the ZnO, WO_3, and ZnO-WO_3 morphological forms. SEM data result by 10,000 times magnification at Figure 2 shows that Figure 2 (a) the form of WO_3 is like grains with an elongated and widened shape. Measurement by using ImageJ software shows the smallest particle is 390.98nm, the biggest is 897.23nm and the average size is 707.97nm. The Figure 2 (b) shows the morphology of ZnO which consisted of irregular and randomly distributed small particle. The smallest ZnO particle is 160.33nm, the biggest is 337.10nm, and the average size is 231.42. The smallest particle of ZnO-WO_3 is 577.43nm, the biggest is 1566.07nm, and the average size is 957.62nm. Based on those measurements, it is confirmed that the WO_3 particle is bigger than ZnO particle. Figure 2(c) shows the ZnO-WO_3 composite form, it can be observed that there are 2 kinds particle suspecting that WO_3 particle is bigger than ZnO particle. Both particles are tends to stick and joined to each other. This is also confirmed at the particle size which becoming bigger when both are composited.

The surface area of WO_3 and ZnO before and after being composited into WO_3-ZnO can be seen in Table 1.

Table 1. The result of ZnO, WO_3 and ZnO-WO_3 composited.

Sample	Surface Area (m^2/g)
WO_3	105.15
ZnO	112.52
ZnO-WO_3 composite	180.75

The data shows that the ZnO-WO_3 surface area becoming larger than pure WO_3. This occurs as a result of the inclusion of ZnO after both have been composited, as ZnO has a larger surface area than WO_3.

Phenol Sonocatalytic Test Using ZnO-WO_3

Effect of Catalyst Weight

Catalyst weight variation is conducted to know the optimum weight needed by ZnO-WO_3 in degrading phenol. Figure 3 depicts the relation of catalyst weight toward the degradation percentage.

Based on Figure 3, 0.1g catalyst resulted in 60% phenol degradation. A little quantity of catalyst is insufficient to degrade. Then, 0.2g catalyst got 80% and it got increased at 0.3% to 83% and tends to be similar at 0.4g as many 90.1%. Based on the data, it shows the optimum weight is

0.4 g of catalyst. The percentage of phenol degradation will rise as the amount of ZnO-WO_3 increases. The surface area of the sonocatalysis process expands, increasing the supply of OH radical. The phenol degradation process becomes more effective as the radical quantity increases, and the phenol degradation percentage rises. Furthermore, it slightly decreases at 0,5g catalyst to 84.64 %. The percentage of degradation experienced a slight decrease due to the addition of excess catalyst mass causing turbidity in the solution so that the ultrasonic waves entering the solution were blocked and the electron excitation on the catalyst surface would decrease (Arfi et al., 2017).

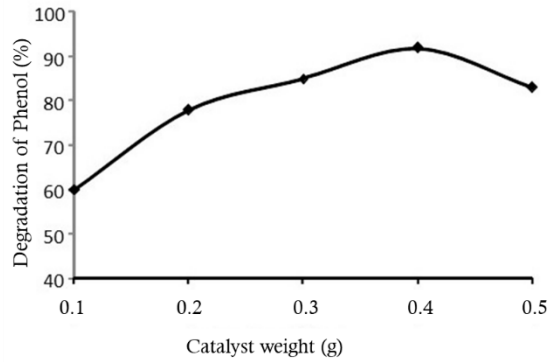

Figure 3. Effect of Catalyst weight.

Effect of reaction duration on Phenol Degradation

Reaction duration was used in this study to determine the optimal contact time required by ZnO-WO_3 to degrade phenol. The contact time was varied 3-13 min, Figure 4 shows the effect of contact time on the percentage of phenol degradation.

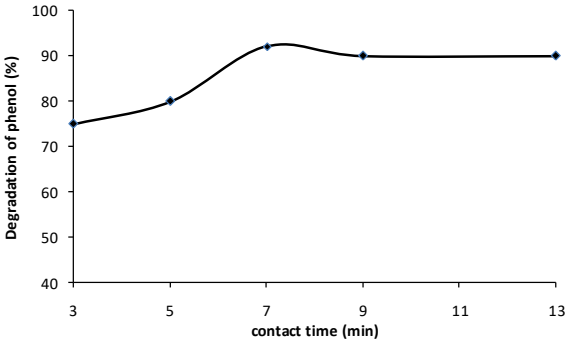

Figure 4. Effect reaction duration.

The percentage of phenol degradation tends to rise from the third minute to the seven-minute reaction duration, as seen in the Figure 4. The percent degradation was 78.2% after three minutes, and it continued to rise until the seventh minute, when it reached 92.5%. According to Zhou et al. (2015) free electrons (e^-) and holes (h^+) are produced sonocatalytically by WO_3 and ZnO catalysts. Following that, electrons in the valence band will be excited into the conduction band. The sonoluminescence mechanism has been used to explain this. Light enters through the recombination of free radicals produced by cavitation bubbles in sonoluminescence. The formation of OH radicals, which can degrade phenol, follows. The more time it takes for ZnO/ WO_3 to develop, the more OH radicals it produces. It improves the catalyst's capacity to degrade phenol. The greater the number of OH radicals generated; the more phenol is degraded.

However, the trend did not rise between the 9 and 13 minutes. According to Sheydaei et al. (2019) may be related to the formation of cavities in the solution through the cavitation phenomenon. With increasing time, the continuous mechanical shock of the cavitation bubbles can cause damage to the particle morphology and reduce its catalytic efficiency. In addition, according to Arfi et al. (2017), the contact time being too long in the reaction system causing the adsorption of phenol in surface of catalyst causing agglomeration so that the number of active sites of the catalyst was also reduced in degrading phenol. As a result, the optimal time for degrading 30 ppm phenol is 7 minutes, with a 92.5% degradation rate.

Effect of Phenol Concentration

A concentration of 30 ppm phenol resulted in 91% decomposition, according to the graph above. At a concentration of 40-50 ppm, the percentage tends to drop to 88-78%. The adsorption rate and the degradation rate will be directly proportional as the phenol content decreases. However, at higher concentrations (40-50 ppm), phenol saturation causes the rate of phenol adsorption on the catalyst surface to be not directly proportional to the rate of degradation. According to Moradi et al. (2018), a catalyst's surface being occupied by a greater concentration of pollutants, which prevents the catalyst's surface from having enough active sites, thereby inhibiting the degradation process. Furthermore, that when phenol solution concentration rises, UV photons have a harder time entering the solution and their route lengths shorten. The catalyst's surface is not

photoexcited by the decreased photon absorption, which also slows down photodegradation.

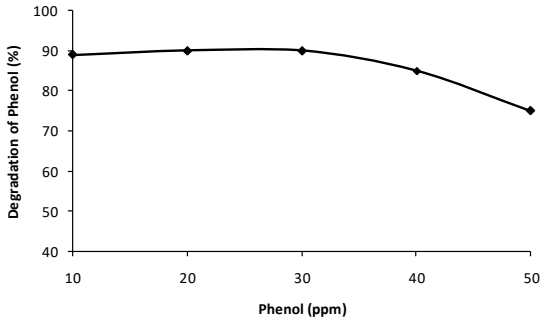

Figure 5. Effect of phenol concentrates.

Reusability of Catalyst

The reuse of ZnO-WO_3 was conducted to see how efficient it was in degrading phenol through a sonocatalytic process. The procedure is carried out by washing the ZnO-WO_3 that was utilized in the preceding sonocatalytic test with distilled water until any remaining phenol dissolves. To eliminate the phenol that was still adhered to the catalyst's surface, the ZnO-WO_3 residue was heated and recalcined. The technique was then repeated under the same ideal conditions as the prior sonocatalytic test.

The percentage of degradation decreases from 92% in the first cycle to 88% in the hird repetition, and endure at 85% in five cycles as shown in Figure 6.

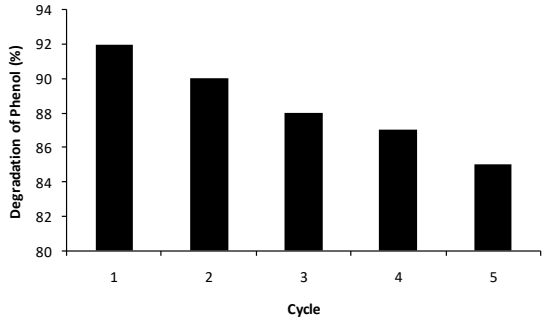

Figure 6. The reusability of Catalyst.

Based on the data gathered, it may be inferred that reusability has decreased by up to five times. It is stated that ZnO-WO_3 has sonocatalytic reusability efficiency in degrading phenol. One of the possible reasons for the decrease in activity, could be due to surface leaching during the catalytic reaction which is associated with loss of active sites. This occurs when the ZnO-WO_3 catalyst gets leached after prolonged usage, resulting in less radical production OH and its capacity to act as a sonocatalyst are likewise decreasing (Lestari, et al., 2015). The successive heating treatment after each iteration can reduce the surface area of the catalyst resulting in partial aggregation of the catalyst. The intermediate compounds formed during the catalytic process can also be adsorbed on the surface, thereby reducing the overall efficiency of the catalyst. In addition, the loss of catalyst also occurs during the iterative process which results in reduced catalyst reactivity (Adhikari et al., 2015). From the data obtained, it can be concluded that with 3 reuses there is only a slight decrease so that it can be said that ZnO-WO_3 can be reused in sonocatalytically degrading phenol.

Material Type

In this research, various types of materials were conducted to determine the process of degradation phenol using ZnO, WO_3, ZnO-WO_3 (Figure 7). The optimum conditions in the sonocatalytic test were 0.4 grams of catalyst mass, 7 minutes of contact time, and 30 ppm phenol concentration. In figure 7, the usage of WO_3 degraded 80.69%. The ZnO degradation percentage was 51.06%.

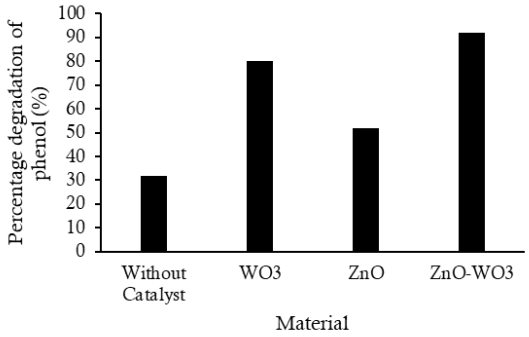

Figure 7. Effect of material on the phenol degradation.

The usage of ZnO-WO_3 degraded 85.93%. Due to charge transfer between the two, WO_3 composited with ZnO showed a greater percentage of phenol degradation, with h^+ in ZnO being transferred to WO_3 and e^- in WO_3 being transferred to ZnO (Zhang, 2010). As a result, sufficient time is available for phenol to be maximally on the surface of the WO_3-ZnO catalyst, resulting in greater sonocatalytic activity than WO and ZnO.

CONCLUSION

The synthesis of ZnO-WO3 composite has been successfully by solid state reaction. The composite showed the new diffraction peak (ZnWO4) with monoclinic structure. The morphology of composite from SEM showed the heterogeneous particle size, and the surface area was bigger than before combined. The results of the degradation test on phenol with a concentration of 30 ppm showed that the optimum condition of ZnO-WO3 was 92.5 %, then at 7 minutes reaction duration. ZnO-WO3 has been used until five cycles with percent degradation of phenol at 85%.

AKCNOWLEDGEMENT

The author would like to express the gratefulness to the Ministry of Education and Culture for the assistance and support in doing this Research. Faculty of Mathematic and Natural Sciences for their support

REFERENCES

Adhikari, S., Sarkar, D., Madras, G. 2015. Highly efficient WO_3-ZnO mixed oxides for photocatalysis. RSC Advances. 5(16): 11895–11904.

Arfi, F., Safni, S., Abdullah, Z. 2017. Degradasi Senyawa Paraquat Dalam Pestisida Gramoxone Secara Sonolisis dengan Penambahan ZnO. Lantanida Journal. 3(1): 71.

Azbar, N., Yonar, T., Kestioglu, K. 2004. Comparison of various advanced oxidation processes and chemical treatment methods for COD and color removal from a polyester and acetate fiber dyeing effluent. Chemosphere. 55(1): 35–43.

Borji, S. H., Nasseri, S., Mahvi, A. H., Nabizadeh, R., Javadi, A. H. 2014. Investigation of photocatalytic degradation of phenol by Fe(III)-doped TiO_2 and TiO_2 nanoparticles. Journal of Environmental Health Science and Engineering. 12: 101.

Chung, Y. C., Chen, C. Y. 2009. Degradation of azo dye reactive violet 5 by TiO_2 photocatalysis. Environmental Chemistry Letters. 7(4): 347–352.

Hunge, Y. M., Yadav, A. A., Mathe, V. L. 2018. Ultrasound assisted synthesis of WO_3-ZnO nanocomposites for brilliant blue dye degradation. Ultrasonics Sonochemistry. 45: 116–122.

Kumar, P. S., Paik, P., Raj, A. D., Mangalaraj, D., Nataraj, D., Gedanken, A., Ramakrishna, S. 2012. Biodegradability study and pH influence on growth and orientation of ZnO nanorods via aqueous solution process. Applied Surface Science. 258(18), 6765–6771.

Lestari, Y. D., Wardhani, S., Khunur, M. M. 2015. Degradasi Methylene Blue Menggunakan Fotokatalis TiO_2-N/Zeolit Dengan Sinar Matahari. Jurnal Ilmu Kimia. 1(1): 592–589.

Li, T., Song, L., Zhang, S. 2018. A novel WO_3 sonocatalyst for treatment of rhodamine B under ultrasonic irradiation. Environmental Science and Pollution Research. 25(8): 7937–7945.

Meng, Z. Da, Sarkar, S., Zhu, L., Ullah, K., Ye, S., Oh, W. C. 2014. Sonocatalytic degradation of rhodamine B in the presence of TIO2 nanoparticles by loading WO_3. Korean Journal of Materials Research. 24(1): 6–12.

Moradi, N., Amin, M. M., Fatehizadeh, A., Ghasemi, Z. (2018). Degradation of UV-filter Benzophenon-3 in aqueous solution using TiO_2 coated on quartz tubes. Journal of Environmental Health Science and Engineering. 16(2): 213–228.

Mozia, S., Tomaszewska, M., Morawski, A. W. 2005. A new photocatalytic membrane reactor (PMR) for removal of azo-dye Acid Red 18 from water. Applied Catalysis B: Environmental. *59*(1–2): 131–137.

Rappoport, Z. 2003. The chemistry of phenols. In PATAI'S Chemistry of Functional Groups. John Wiley & Sons.

Sajjad, A. K. L., Sajjad, S., Iqbal, A., Ryma, N. ul A. 2018. ZnO/WO_3 nanostructure as an efficient visible light catalyst. Ceramics International. 44(8): 9364–9371.

Shakya, V., Pandey, N. K., Misra, S. K., Roy, A. 2017. Electrical and optical properties of ZnO-WO_3 nanocomposite and its application as a solid-state humidity sensor. Bulletin of Materials Science. 40(2): 253–262.

Sheydaei, M., Fattahi, M., Ghalamchi, L., Vatanpour, V. 2019. Systematic comparison of sono-synthesized Ce-, La- and Ho-doped ZnO nanoparticles and using the optimum catalyst in a visible light assisted continuous sono-photocatalytic membrane reactor. Ultrasonics Sonochemistry. 56(April): 361–371.

Yu, C., Yang, K., Shu, Q., Yu, J. C., Cao, F., Li, X. 2011. Preparation of WO_3/ZnO composite photocatalyst and its photocatalytic performance. Cuihua Xuebao/Chinese Journal of Catalysis. 32(4): 555–565.

Yunus, N. N., Hamzah, F., So'Aib, M. S., Krishnan, J. 2017. Effect of Catalyst Loading on Photocatalytic Degradation of Phenol by Using N, S Co-doped TiO_2. IOP Conference Series: Materials Science and Engineering. 206(1):

Zhang, D. (2010). Synthesis and characterization of ZnO-doped cupric oxides and evaluation of their photocatalytic performance under visible light. Transition Metal Chemistry. 35(6): 689–694.

Zhou, M., Yang, H., Xian, T., Li, R. S., Zhang, H. M., Wang, X. X. 2015. Sonocatalytic degradation of RhB over $LuFeO_3$ particles under ultrasonic irradiation. Journal of Hazardous Materials. 289: 149–157.

JBAT 11(1) (2022) 1 – 7

Jurnal Bahan Alam Terbarukan

Accredited SINTA 2 by Ministry of Research and Technology/National Research and Innovation Agency
SK No. 200/M/KPT/2020
http://journal.unnes.ac.id/nju/index.php/jbat

p-ISSN 2303 0623
e-ISSN 2407 2370

Synthesis of Activated Carbon from Petung Bamboo Stems (*Dendrocalamus Asper*) Using Microwave-Assisted Pyrolysis (MAP) Process for Biogas Storage

Widi Astuti[1]✉, Triastuti Sulistyaningsih[2], Raihan Mukti Ramadhan[1], Vista Ayudya Octaviany[1]

DOI: https://doi.org/10.15294/jbat.v11i1.36939

[1]Department of Chemical Engineering, Faculty of Engineering, Universitas Negeri Semarang, Gd. E1 lt.2, Sekaran, Gunungpati, Semarang 50229, Indonesia
[2]Department of Chemistry, Faculty of Engineering, Universitas Negeri Semarang, Gd. D6 lt.2, Sekaran, Gunungpati, Semarang 50229, Indonesia

Article Info

Article history:
Received
May 2022
Accepted
June 2022
Published
June 2022

Keywords:
Adsorption;
KOH;
Pyrolysis;
Microwave heating;
Hybrid heating

Abstract

Biogas has emerged as a promising alternative to gasoline due to the depletion of fossil energy and environmental concerns. An investigation was conducted to study the technical feasibility of an adsorbed natural gas (ANG) storage system using petung bamboo-activated carbons. The activated carbons were prepared by microwave-assisted pyrolysis (MAP) and a hybrid heating system for comparison. Microwave-assisted pyrolysis is a promising alternative technology for biochar production because it has several advantages over conventional pyrolysis such as uniform heating temperature, lower energy consumption, and uniform pore size. The characteristics of the obtained activated carbons were evaluated by scanning electron microscope (SEM) and Fourier transform infrared spectroscopy. The results showed that the higher power led to the shorter pyrolysis time. However, at a certain point, the higher power causes the biomass is not degraded completely. In this case, a microwave oven with 2 magnetrons produces a better heating temperature profile than the use of 1 magnetron. The character of activated carbon prepared using 70% power output (1120 W) is better than activated carbon prepared using 60% power output (960 W). In this condition, the pore size is more uniform and the number of functional groups is less. This implies that the petung bamboo activated carbon is the ideal candidate for ANG storage.

INTRODUCTION

Biogas has emerged as a promising alternative to gasoline due to the depletion of fossil energy and environmental concerns (Li and Su, 2017). Compared to other fuels, biogas containing methane i.e., CH_4 (70-90%) has a clean, safe, and cheap combustion (Sieminsky, 2014) with great efficiency and caloric value, high flammability range, and high auto-ignition temperature (Pratama et al., 2014). However, biogas storage technology is still a serious problem. A storage system using compressed natural gas (CNG) vessel requires very high pressure (20-30 MPa) thus it needs a specially designed pressure vessel with high production and filling costs (Górniak et al., 2018). The adsorbed natural gas (ANG) storage technique is a promising alternative (Wu et al., 2021). Biogas is adsorbed by a suitable adsorbent (i.e., porous materials) thus higher biogas concentration can be achieved at lower pressure (3.5 MPa) and moderate temperatures (atmospheric conditions). The ANG performance is influenced by adsorbent characters, thermal management during the adsorption process, and vessel design (Khurana et al., 2019). Biogas adsorption on porous materials occurs through van der waals attraction between biogas (i.e., CH_4) molecules and pore walls, thus the use of suitable adsorbents should be considered to maximize the storage capacity (Zheng et al., 2018).

✉ Corresponding author:
E-mail: widi_astuti@mail.unnes.ac.id

In this case, activated carbon (AC) having a micropore structure and a limited number of functional groups is a promising adsorbent for biogas storage (Mestre et al., 2014) because the existence of functional groups can interfere physisorption process of CH_4 molecules (Kuang et al., 2020).

The most common methods used for AC production are pyrolysis and activation process (Rijali et al., 2015). There are two types of activation processes, namely physical and chemical activation (Zhang et al., 2014). In physical or thermal activation, carbon is modified using two gasifying agents carbon dioxide and water vapor, either singly or together. This agent extracts carbon atoms from the porous carbon structure according to the following reaction (Mistar et al., 2020).

$$C + CO_2 \rightarrow 2\ CO \quad (1)$$

$$C + H_2O \rightarrow CO + H_2 \quad (2)$$

Meanwhile, chemical activation is carried out by immersing biochar in chemicals as activating agents such as phosphoric acid (H_3PO_4), sulfuric acid (H_2SO_4), potassium hydroxide (KOH), sodium hydroxide (NaOH), and zinc chloride ($ZnCl_2$) (Riyanto et al., 2020). Synthesis of AC derived from mangrove propagule waste using H_3PO_4 as activating agent produced AC with a surface area of 267.45 m^2/g (Astuti et al., 2017). Ogungbenro et al., (2020) used palm plants as raw materials with H_2SO_4 activation to produce AC having a surface area of 577.34 m^2/g. Coconut shells AC produced through $ZnCl_2$ activation had a surface area of 15 m^2/g (Astuti et al., 2018). Activated carbon derived from ratan plant stalks using NaOH activation had a surface area of 1135 m^2/ g (Islam et al., 2017), while the use of KOH as an activating agent can produce microporous activated carbon with a high surface area, up to 2000 $m^{2/}$g (Elmouwahidi et al., 2012; Astuti et al., 2019). Generally, AC produced by chemical activation has advantages including higher yield, larger specific surface area, and better development of porous structure (Mistar et al., 2020). Chemical activation can be carried out in one or two steps. In one step, the activator is mixed with raw materials, while in two steps the activator is mixed with pyrolysis charcoal. In this sense, the microstructure and adsorption characteristics of AC depend on the chemical composition of the raw material, production route (i.e., one or two steps), and conditions of the pyrolysis and activation process. Therefore, optimization of process conditions is required to synthesize AC for energy and environmental applications.

Several attempts have been made to utilize agricultural residues, forest wastes, and other inexpensive renewable materials as precursors in AC preparation such as rice straw (Chang et al., 2014), tabah bamboo (Negara et al., 2017), tamblang bamboo (Negara et al., 2017), randu wood (Chafidz et al., 2018), coconut shell (Astuti et al., 2018), pineapple leaf (Astuti et al., 2019), petung bamboo (Qanytah et al., 2020), yellow bamboo (Mistar et al., 2020), and corn cobs (Medhat et al., 2021). Petung bamboo stem waste contains 45.02% cellulose, 10.81% hemicellulose, and 28.35% lignin with a low inorganic content (Larasati et al., 2019) which can be used as raw materials in the AC preparation (Krismayanti et al., 2018).

Utilization of petung bamboo stem waste as raw material in the AC preparation has been carried out by Qanytah et al., (2020). The AC obtained has a pore diameter of 1.18 nm which belongs to the micropore type. Another study that also used petung bamboo as a precursor in the AC preparation showed a surface area of 1954.95 $m^{2/}$g (Wirawan et al., 2018). Both studies used conventional heating, i.e., furnace. In conventional heating, energy is transferred from a heat source located outside the material bed to the interior through convection, conduction, and radiation mechanism. It produces a thermal gradient in the material from the hottest surface to the interior until steady conditions are reached. To solve the thermal gradient problem, a slower heating rate is used. It results in a longer heating time and increased energy consumption. The existence of a temperature gradient causes the pores of the activated carbon to be non-uniform (Ahmed, 2016). Nowadays, microwave heating is a viable alternative to conventional heating. Unlike conventional heating, microwave heating is internal and volumetric in that there is no temperature gradient in the material bed, resulting in biochar with a more uniform pore size (Ao et al., 2018). This research used a microwave oven with 2 magnetrons to produce a more even heat distribution. In this sense, the effect of power on the temperature profile as well as the yield and character of petung bamboo stems AC are discussed further.

MATERIALS AND METHODS

Materials

The petung bamboo used as a precursor in this study was obtained from Magelang, Indonesia. Potassium hydroxide (KOH) and hydrochloric acid (HCl) were acquired from Merck (Germany).

Preparation of Petung Bamboo Powder

The petung bamboo powder was dried in sunlight for one day, then sieved using a 10-18 mesh sieve and heated using an oven (Memmert type UN55, Germany) at a temperature of 105°C until the dried sample weight was constant.

Preparation of Activated Carbon

Microwave-assisted pyrolysis of bamboo powder was carried out by loading 50 g of dry sample into an alumina reactor installed in a microwave oven (Electrolux type EMM 2308 with modification of 2 magnetrons). Pyrolysis was carried out under a stream of N_2 with a flow rate of 100 cm^3/min at 60% (960W) and 70% (1120W) power output while the final temperature was set at 500°C. After cooling to ambient temperature, the obtained biochar was weighed. The yield of biochar was calculated using Eq. (3).

$$\textit{yield of biochar (\%):} \quad \frac{weight\ of\ biochar}{weight\ of\ bamboo\ powder} x\ 100\% \qquad (3)$$

The biochar was further mixed with KOH and 10 mL of distilled water, and stirred for 120 minutes. The weight ratio of KOH: biochar was 3:1. Biochar was then dried using an oven at 105°C for 24 hours before activation process. In the activation process, the impregnated biochar was placed in an alumina reactor installed in the microwave oven (Electrolux type EMM 2308 with modification of 2 magnetrons). The activation process was conducted at a power output of 70% (1120W) under a nitrogen flow rate of 100 cm^3/min until the temperature reach 500°C (Astuti et al., 2019). The activated carbon was washed using 0.1 M HCl and distilled water until the pH reached 6.5-7. In the last stage, the activated carbon was dried using an oven at 110°C for 24 hours (Mistar et al., 2020).

Characterization of Adsorbent

The surface morphology of the biochar and activated carbon were analyzed using Scanning Electron Microscope with Energy Dispersive X-ray (SEM-EDX) (JSM-6360). The surface functional groups of the biochar and activated carbon were analyzed using Fourier Transform Infrared (FTIR) Spectroscopy (Perkin Elmer Spectrum IR 10.6.1) recorded between 450 and 4000 cm^{-1}.

RESULTS AND DISCUSSION

Effect of Microwave Power on The Pyrolysis Temperature Profile

The use of microwaves in the pyrolysis process can improve the properties and character of biochar. In this sense, microwave power is an important factor because it can affect the heating rate. Higher power can increase the interaction between the material and the microwave field leading to rotation, collision, torsion, and friction of the molecules in the material thereby increasing the potential to convert absorbed microwaves into thermal energy. On the other hand, if the microwave power is too low, the interaction between the material and the microwave is too weak and causes molecular cleavage (Y. Zhang et al., 2022). The temperature profile at various microwave power is presented in Figure 1. Based on Figure 1, it can be seen that the temperature profile for each microwave is different. At a power output of 50% (800 W), the temperature increase was very slow and can only reach the final temperature of 242°C, far from the desired pyrolysis temperature (500°C). It takes 34 minutes to reach temperature of 240°C, after 34 minutes temperature dropped slightly and then constant at 235°C. Meanwhile, at 80% power output (1280 W) the temperature rise too fast in which the temperature of 500°C was reached in just 2 minutes. The higher the microwave power used, the greater the amount of microwave energy received by the biomass so that the temperature increase very fast and the time required to reach the desired pyrolysis temperature (500°C) is also shorter. At the power usage of 960 W and 1120 W, the temperature profile is declivous compared to the power usage of 1280 W where the temperature of 480°C was reached in 10 and 8 minutes, respectively.

Referring to the fact that pyrolysis temperature profile can greatly affect the morphological structure of the biochar produced, this study also carried out a micro-hybrid heating system (Figure 2) as a comparison. In the micro-hybrid system (Figure 3), the temperature rise is unstable, especially at low power and it requires

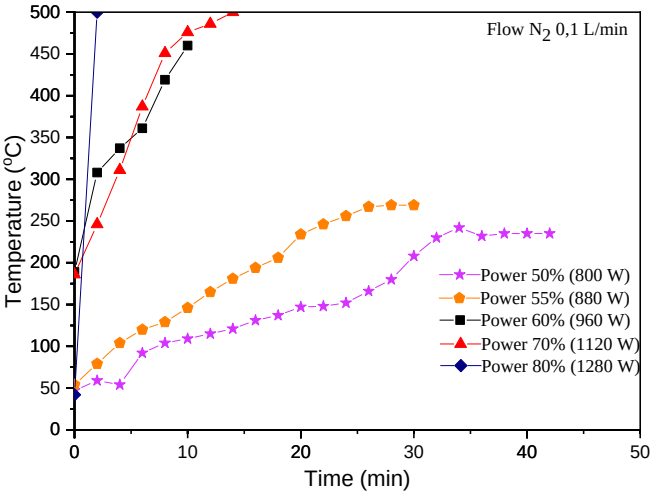

Figure 1. Temperature Profile at Various Microwave Powers.

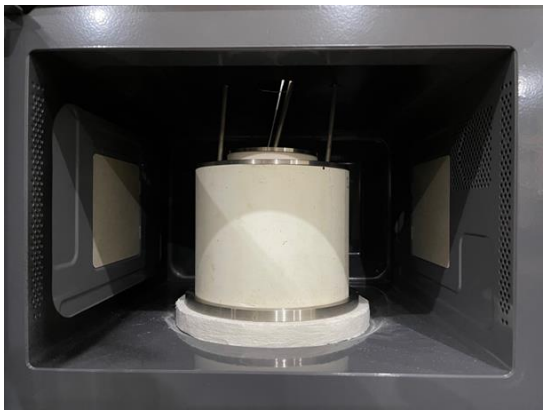

Figure 2. Alumina Reactors for Micro-Hybrid Heating System. (Larger reactor containing coconut shell charcoal, smaller reactor containing biomass sample).

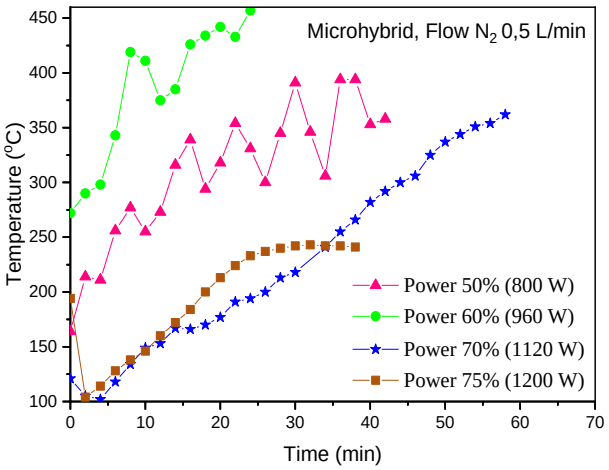

Figure 3. Temperature Profile at Various Power for Microhybrid System.

longer time than microwave heating. In addition, the desired final pyrolysis temperature (500°C) cannot be achieved at all the power used, in which the highest temperature is only 450°C at 60% output power (i.e., 960 W). Temperature instability in the micro-hybrid system may be due to the presence of two heating mechanisms that occur simultaneously but both have different time intervals. Some microwave radiation is absorbed by coconut shell charcoal, converted to heat, and then transmitted to the biomass by a conduction mechanism through reactor walls. While some other microwave radiation can be directly absorbed by the biomass and converted to heat. Therefore, at low power usage (50 and 60%), the temperature instability is very obvious because the low heating rate causes the conduction process slower. The temperature instability diminished with higher power usage, but the achievable temperature is lower. As a result, the biomass degradation process is incomplete, as shown in Figure 4(h)-(i). At 960W, the maximum achievable temperature is 450°C. As is known, biomass composed of hemicellulose, cellulose, and lignin is degraded at temperatures of 220-300°C, 300-340°C, and 300-900°C, respectively. Therefore, at 450°C all the biomass should have been degraded. The imperfection of the pyrolysis process at a temperature of 450°C (Figure 4.3(f)) may be caused by temperature instability. Therefore the temperature profile is a very important parameter to consider in the pyrolysis process. Meanwhile, Figure 4(e) shows that biomass degradation has not occurred yet. This is probably due to the very short pyrolysis time (<2 minutes) even though the pyrolysis temperature of 500°C has been reached.

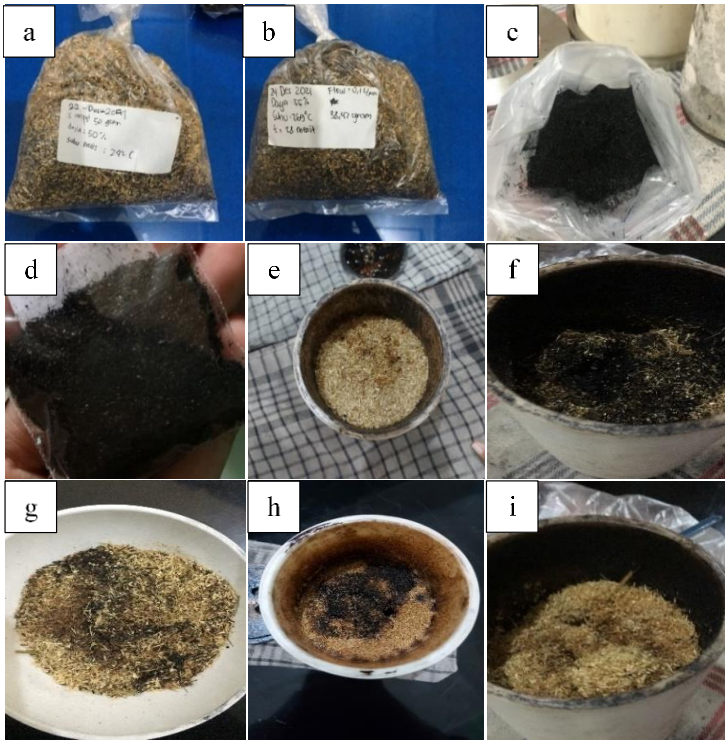

Figure 4. Pyrolysis Results at a certain Power (a) microwave, 50% power output (800 W); (b) microwave, 55% power output (880 W); (c) microwave, 60% power output (960 W); (d) microwave, 70% power output (1120 W); (e) microwave, 80% power output (1280 W); (f) micro-hybrid, 50% power output (800 W); (g) micro-hybrid, 60% power output (960 W); (h) micro-hybrid, 70% power output (1120 W); (i) micro-hybrid, 75% output (1200 W).

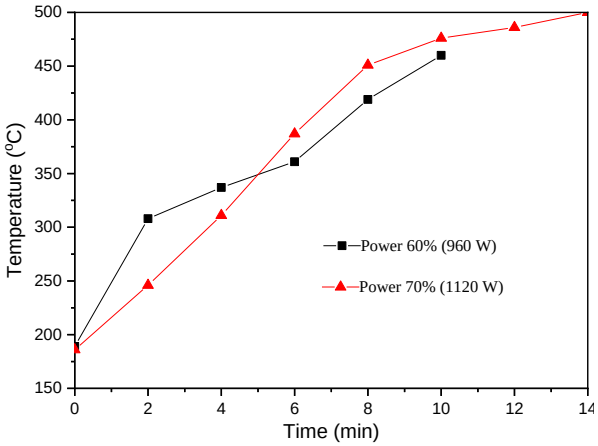

Figure 5. Temperature Profiles at 960W and 1120W.

Bamboo stem powder can be completely degraded using a microwave heating system with 60% output power (960 W) and 70% output power (1120 W), as shown in Figures 4(c) and (d). Under these conditions, the temperature rise is stable and the final temperature reaches 500°C (Figure 5). Therefore, this study only focuses on the power usage of 960W and 1120W.

Effect of Microwave Power on The Biochar Yield

Figure 6 shows that increasing microwave power decreases biochar yield due to the intensified interaction between biomass and microwave (Lam et al., 2017). After the degradation process of bamboo powder is complete, further heating causes some carbon atoms in biochar react with CO_2 and H_2O resulting from pyrolysis, according to reactions (4) and (5), thereby reducing the yield of biochar. The increase in power from 960 W to 1120 W reduced the yield by 1.24% (from 35.32 to 34.08%).

$$C + CO_2 \rightarrow 2CO \quad (4)$$
$$C + H_2O \rightarrow CO + H_2 \quad (5)$$

Although yield of biochar produced at 1120 W (namely B1120) is lower than yield of biochar produced at 960 W (namely B960), the purity of

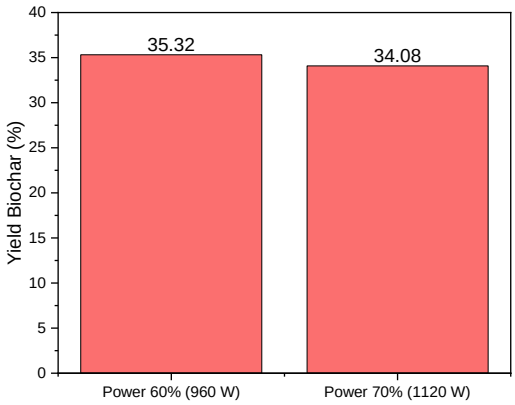

Figure 6. Graph of Effect of Microwave with Yield Biochar Pyrolysis Results.

B1120 is higher (carbon content of 82.98%) than B960 (carbon content of 72.22%). It may be due to some impurities such as K_2O being lost on high-intensity heating thereby the carbon content increases. K_2O can react with H_2, CO_2, and C according to Eq. (6)-(8). As a result, K_2O content in B960 is higher (14.33%) than in B1120 (7.89%).

$$K_2O + H_2 \rightarrow 2K + H_2O \quad (6)$$
$$K_2O + CO_2 \rightarrow K_2CO_3 \quad (7)$$
$$K_2O + C \rightarrow 2K + CO \quad (8)$$

Effect of Microwave Power on The Biochar and Activated Carbon Morphology

As previously explained, further heating after the biomass degradation process is completed causes some carbon atoms react with CO_2 and H_2O to CO gas. The partial cleavage of the C bonds due to this reaction causes an increase in the pore size of the biochar. Therefore, the higher microwave power used, the larger pore sizer, as shown in Figures 7(a) and (c). In addition, B1120 in Figure 7(c) has a more uniform pore size than B960 in Figure 7(a). It may be due to the stability of temperature rise, as shown in Figure 5. Significant changes in the surface morphology of biochar are clearly seen after the activation process with KOH, especially at B960. The pores become very large, much larger than the pores of B1120 after activation process. The development of porosity by KOH follows the following reaction.

$$2KOH \rightarrow K_2O + H_2O \quad (9)$$
$$C + K_2O \rightarrow 2K + CO \quad (10)$$

Diffusion of potassium (K) compounds into biochar widens the existing pores because these compounds can function as templates in the formation of pores. In addition, reaction (10) also contributes to the formation of new pores. As previously explained, B960 contains more K_2O from biomass impurities, in which K_2O also contributes to the activation process according to Eq. (10). Therefore, activated carbon resulting from activation of B960 (namely AC960) has a larger pore size than that of B1120 (namely AC1120). As previously explained, the

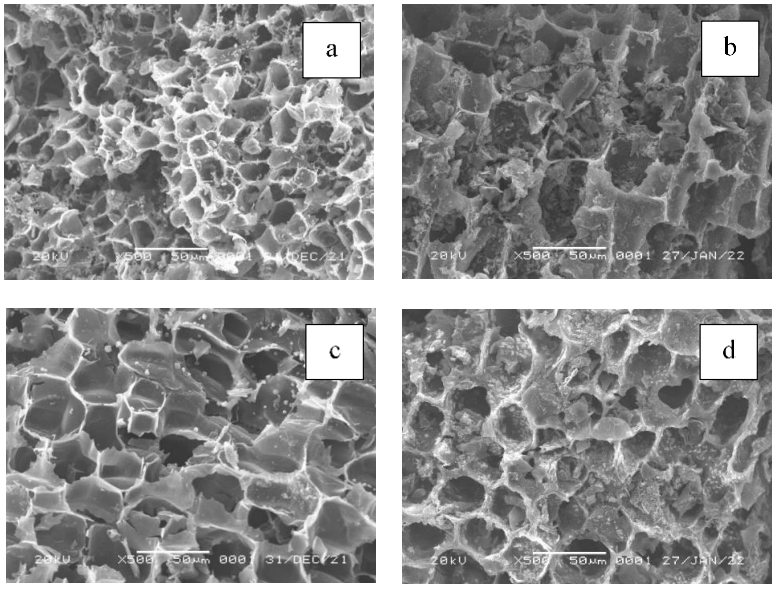

Figure 7. Morphology of (a) Biochar at 60% power output (B960), (b) Activated Carbon at 60% power output (AC960), (c) Biochar at 70% power output (B1120), (d) Activated Carbon at 70% power output (AC1120) (Magnification: 500x).

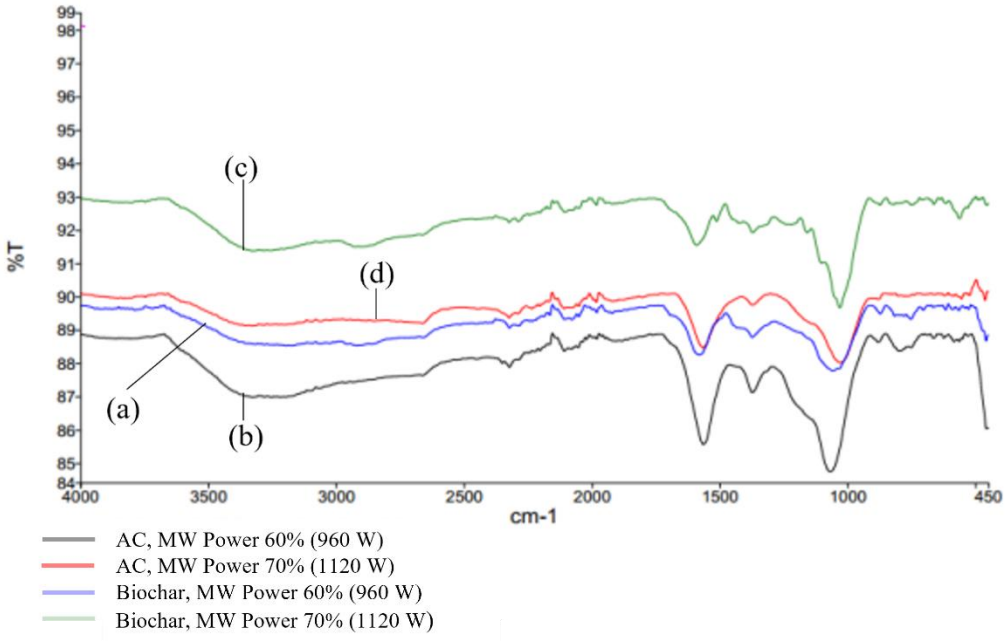

Figure 8. FTIR Spectrum on (a) Biochar (b) 60% Power Activated Carbon (c) Biochar (d) 70% Power Activated Carbon.

activation process according to Eq. (10) causes a partial loss of C, thereby the C content after the activation process decreased from 72.22% to 66.35% for AC960 and from 82.93% to 67.83% for AC1120. Figure 6 also shows that AC960 is more brittle than AC1120. AC960 pore walls are thinner and some pores are destroyed. It is because the higher power leads to an increase in carbon content and a decrease in O and H content, or in other words the H/C ratio decreases. The smaller H/C ratio leads to a higher aromatization and a more stable biochar structure, as shown in AC1120 (X. Zhang et al., 2022).

Effect of Microwave Power on The Surface Functional Groups

To confirm the presence of surface functional groups in biochars and ACs, FTIR analysis was conducted. Figure 8(a) shows biochar B960 has an absorption peak at 3198.53 cm^{-1} indicating the presence of a hydroxyl (O-H) group (Saad et al., 2019). The peak at 1373.22 cm^{-1} is assigned to the aliphatic deformation of CH_2 or CH_3 groups or O-H bending of phenolic. The existence of an absorption peak around 1580.14 cm^{-1} is attributed to the C=C stretching vibrations of aromatic compounds (Astuti et al., 2018), while a peak observed at 1059.18 cm^{-1} may be attributed to the C-O group (Saafie et al., 2019). After the activation process with KOH (Figure 8(b)), the peak of B960 at 1373.22 cm^{-1} shifts to 1372.86 cm^{-1}, indicating aromatization and dehydration occurred as a result of the decomposition and condensation of volatile matters (Saad et al., 2019). Meanwhile, the band at 3198.53 cm^{-1} for OH stretching deepens and shifts to 3330.28 cm^{-1}. It is due to ion exchange between K^+ on -OK group and H^+ on H_2O during the washing process, forming the -OH functional group (Oginni et al., 2019; Saad et al., 2019). Meanwhile, the C=C group as indicated by an absorption peak at 1580.14 cm^{-1} shifts to 1564.89 cm^{-1} and deepens. It may be due to the decomposition of the C-H bond to produce aromatic C=C bonds which is more stable at high temperatures (Saad et al., 2019).

Figure 8(c) shows that biochar B1120 has an absorption peak at 3330.99 cm^{-1} indicating the presence of a hydroxyl group (O-H) (Saad et al., 2019). The peak observed around 1591.23 cm^{-1} may be attributed to the C=C stretching vibration of aromatic compounds (Astuti et al., 2018), while the band at 1030.69 cm^{-1} reflects C-O group (Saad et al., 2019). After activation with KOH (Figure 8(d)), the absorption peak at 3300-3700 cm^{-1} indicates the existence of the -OH group is shallower. It is in contrast to biochar B960 which is deeper after the activation process. The decrease in the number of -OH groups in AC1120 may be due to the larger pore size of B1120, thereby more -OH groups can be released as H_2O during the activation process. Meanwhile, the C=C group indicated by an absorption peak at 1591.23 cm^{-1} shifts to 1564.89

cm^{-1} and deepens. It may be due to the decomposition of the C-H bond to produce aromatic C=C bonds which is more stable at high temperatures (Saad et al., 2019) and create new pores (Astuti et al., 2018).

Based on the FTIR results, it can be seen that AC1120 is better than AC960 because it contains fewer functional groups. As is known, the higher number of functional groups leads to the gas physisorption process is disturbed (Kuang et al., 2020).

CONCLUSION

The higher power used in microwave-assisted pyrolysis (MAP) leads to a more stable heating temperature profile indicated by no significant increase or decrease in temperature. In the power range studied (power output of 60 and 70%), a greater power used leads to a lower biochar yield. The character of activated carbon produced using 70% power output (AC1120) is better than activated carbon produced using 60% power output (AC1120), i.e., better surface morphology and fewer functional groups.

REFERENCES

Ahmed, M. J. 2016. Application of agricultural based activated carbons by microwave and conventional activations for basic dye adsorption: Review. Journal of Environmental Chemical Engineering. 4(1): 89–99.

Ao, W., Fu, J., Mao, X., Kang, Q., Ran, C., Liu, Y., Zhang, H., Gao, Z., Li, J., Liu, G., Dai, J. 2018. Microwave assisted preparation of activated carbon from biomass: A review. Renewable and Sustainable Energy Reviews. 92(July 2017): 958–979.

Astuti, W., Dwi Handayani, A., Wulandari, D. A. 2018. Adsorpsi Methyl Violet oleh Karbon Aktif dari Limbah Tempurung Kelapa dengan Aktivator ZnCl2 Menggunakan Pemanasan Gelombang Mikro. Jurnal Rekayasa Kimia & Lingkungan. 13(2): 189–199.

Astuti, W., Hermawan, R. A., Mukti, H., Sugiyono, N. R. 2017. Preparation of activated carbon from mangrove propagule waste by H_3PO_4 activation for Pb^{2+} adsorption. AIP Conference Proceedings. 1788: 1–6.

Astuti, W., Sulistyaningsih, T., Kusumastuti, E., Thomas, G. Y. R. S., Kusnadi, R. Y. 2019. Thermal conversion of pineapple crown leaf waste to magnetized activated carbon for dye removal. Bioresource Technology. 287(April). 121426.

Chafidz, A., Astuti, W., Augustia, V., Novira, D. T., Rofiah, N. 2018. Removal of methyl violet dye via adsorption using activated carbon prepared from Randu sawdust (Ceiba pentandra). IOP Conference Series: Earth and Environmental Science. 167(1).

Chang, K. L., Chen, C. C., Lin, J. H., Hsien, J. F., Wang, Y., Zhao, F., Shih, Y. H., Xing, Z. J., Chen, S. T. 2014. Rice straw-derived activated carbons for the removal of carbofuran from an aqueous solution. Xinxing Tan Cailiao/New Carbon Materials. 29(1): 47–54.

Coates, J. 2019. Interpretation of Infrared Spectra, A Practical Approach. Encyclopedia of Analytical Chemistry. 1–23.

Elmouwahidi, A., Zapata-Benabithe, Z., Carrasco-Marín, F., Moreno-Castilla, C. 2012. Activated carbons from KOH-activation of argan (Argania spinosa) seed shells as supercapacitor electrodes. Bioresource Technology. 111: 185–190.

Górniak, A., Midor, K., Kaźmierczak, J., Kaniak, W. 2018. Advantages and Disadvantages of Using Methane from CNG in Motor Vehicles in Polish Conditions. Multidisciplinary Aspects of Production Engineering. 1(1): 241–247.

Islam, M. A., Ahmed, M. J., Khanday, W. A., Asif, M., Hameed, B. H. 2017. Mesoporous activated carbon prepared from NaOH activation of rattan (Lacosperma secundiflorum) hydrochar for methylene blue removal. Ecotoxicology and Environmental Safety. 138(August 2016): 279–285.

Jiang, Y., Zong, P., Tian, B., Xu, F., Tian, Y., Qiao, Y., Zhang, J. 2019. Pyrolysis behaviors and product distribution of Shenmu coal at high heating rate: A study using TG-FTIR and Py-GC/MS. Energy Conversion and Management. 179(October 2018): 72–80.

Khurana, M., Veluswamy, H. P., Daraboina, N., Linga, P. 2019. Thermodynamic and kinetic modelling of mixed CH4-THF hydrate for methane storage application. Chemical Engineering Journal. 370(January): 760–771.

Krismayanti, N. P. A., Manurung, M., Suastuti, N. G. A. M. D. A. 2018. Sintesis Arang Aktif Dari Limbah Batang Bambu Dengan Aktivator Naoh Sebagai Adsorben Ion Krom (Iii) & Timbal (Ii). Cakra Kimia. 7(Iii): 189–197.

Kuang, Y., Zhang, X., Zhou, S. 2020. Adsorption of methylene blue in water onto activated carbon by surfactant modification. Water (Switzerland). 12(2): 1–19.

Lam, S. S., Liew, R. K., Wong, Y. M., Azwar, E., Jusoh, A., Wahi, R. 2017. Activated Carbon for Catalyst Support from Microwave Pyrolysis of Orange Peel. Waste and Biomass Valorization. 8(6): 2109–2119.

Larasati, I. A., Argo, D., Hawa, L. C., Keteknikan, J., Teknologi, P.-F., Brawijaya, P.-U., Veteran, J., Korespondensi, P. 2019. Proses Delignifikasi Kandungan Lignoselulosa Serbuk Bambu Betung dengan Variasi NaOH & Tekanan. Jurnal Keteknikan Pertanian Tropis & Biosistem. 7(3): 235–244.

Li, R., Su, M. 2017. The role of natural gas and renewable energy in curbing carbon emission: Case study of the United States. Sustainability (Switzerland). 9(4): 18–20.

Medhat, A., El-Maghrabi, H. H., Abdelghany, A., Abdel Menem, N. M., Raynaud, P., Moustafa, Y. M., Elsayed, M. A., Nada, A. A. 2021. Efficiently activated carbons from corn cob for methylene blue adsorption. Applied Surface Science Advances. 3(November 2020): 100037.

Mistar, E. M., Alfatah, T., Supar, M. D. 2020. Synthesis and characterization of activated carbon from Bambusa vulgaris striata using two-step KOH activation. Journal of Materials Research and Technology. 9(3): 6278–6286.

Oginni, O., Singh, K., Oporto, G., Dawson-Andoh, B., McDonald, L., Sabolsky, E. 2019. Influence of One-step and Two-step KOH Activation on Activated Carbon Characteristics. Bioresource Technology Reports. 7: 100266.

Ogungbenro, A. E., Quang, D. V., Al-Ali, K. A., Vega, L. F., Abu-Zahra, M. R. M. 2020. Synthesis and characterization of activated carbon from biomass date seeds for carbon dioxide adsorption. Journal of Environmental Chemical Engineering. 8(5): 104257.

Pratama, I., Martin, A., Nasruddin. 2014. Adsorption Isothermal Methane Gas With Mass Flow Rate of 10 SLPMand 20 SLPM For Adsorbed Natural Gas Storage. 3(57): 29–39.

Negara, D. N. K. P, Tirta Nindhia, T. G., Surata, I. W., Sucipta, M. 2017. Chemical, strength and microstructure characterization of Balinese bamboos as activated carbon source for adsorbed natural gas application. IOP Conference Series: Materials Science and Engineering, 201(1): 012033.

Qanytah, Syamsu, K., Fahma, F., Pari, G. 2020. Characterization of Ball-Milled Bamboo-Based Activated. Peer-Reviewed Article. 15: 8303–8322.

Rijali, A., Malik, U., Zulkarnain. 2015. Pembuatan & Karakterisasi Karbon Aktif dari Bambu Betung dengan Aktivasi Menggunakan Activating Agent H2O. JOM FMIPA. 148(1): 148–162.

Riyanto, C. A., Ampri, M. S., Martono, Y. 2020. Synthesis and Characterization of Nano Activated Carbon from Annatto Peels (Bixa orellana L.) Viewed from Temperature Activation and Impregnation Ratio of H3PO4. EKSAKTA: Journal of Sciences and Data Analysis. 1(1): 44–50.

Rodrigues Teixeira, A. C., Machado, P. G., Borges, R. R., Felipe Brito, T. L., Moutinho dos Santos, E., Mouette, D. 2021. The use of liquefied natural gas as an alternative fuel in freight transport – Evidence from a driver's point of view. Energy Policy. 149(December): 112106.

S. Mestre, A., Freire, C., Pires, J., P. Carvalho, A., L. Pinto, M. 2014. High performance microspherical activated carbons for methane storage and landfill gas or biogas upgrade. Journal of Materials Chemistry. 1–30.

Saad, M. J., Chia, C. H., Zakaria, S., Sajab, M. S., Misran, S., Rahman, M. H. A., Chin, S. X. 2019. Physical and chemical properties of the rice straw activated carbon produced from carbonization and KOH activation processes. Sains Malaysiana. 48(2): 385–391.

Saafie, N., Samsudin, M. F. R., Sufian, S., Ramli, R. M. 2019. Enhancement of the activated carbon over methylene blue removal efficiency via alkali-acid treatment. AIP Conference Proceedings. 2124(July).

Sieminsky, A. 2014. International Energy Outlook. Outlook. November: 70–99.

Veluswamy, H. P., Kumar, A., Seo, Y., Lee, J. D., Linga, P. 2018. A review of solidified natural gas (SNG) technology for gas storage via clathrate hydrates. Applied Energy. 216(September 2017): 262–285.

Wirawan, I. P. S., Sutrisno, S., Seminar, K. B., Nelwan, L. O. 2018. Characteristics of Microactive Carbon from Bamboo Var. Petung as Adsorbent. IOP Conference Series: Earth and Environmental Science. 147(1).

Wu, Z., Wee, V., Ma, X., Zhao, D. 2021. Adsorbed Natural Gas Storage for Onboard Applications. Advanced Sustainable Systems. 5(4): 1–16.

Yang, K., Zhang, Y., Dong, Y., Peng, J., Kaal, J., Li, W., Ma, X., Nie, Z. 2021. Tracking variations in the abun&ce and composition of dissolved organic matter in solar ponds of oilfield-produced brine. Applied Geochemistry. 131(March): 105008.

Zhang, X., Zhao, B., Liu, H., Zhao, Y., Li, L. 2022. Effects of pyrolysis temperature on biochar's characteristics and speciation and environmental risks of heavy metals in sewage sludge biochars. Environmental Technology and Innovation. 26: 102288.

Zhang, Y., Fan, S., Liu, T., Fu, W., Li, B. 2022. A review of biochar prepared by microwave-assisted pyrolysis of organic wastes. Sustainable Energy Technologies and Assessments. 50: 101873.

Zhang, Y. J., Xing, Z. J., Duan, Z. K., Li, M., Wang, Y. 2014. Effects of steam activation on the pore structure and surface chemistry of activated carbon derived from bamboo waste. Applied Surface Science. 315(1): 279–286.

Zheng, Y., Li, Q., Yuan, C., Tao, Q., Zhao, Y., Zhang, G., Liu, J., Qi, G. 2018. Thermodynamic analysis of high-pressure methane adsorption on coal-based activated carbon. Fuel. 230(May): 172–184.